8

Initial Conditions for Star Clusters

Pavel Kroupa

Argelander-Institut für Astronomie, Auf dem Hügel 71, D-53121 Bonn, Germany
pavel@astro.uni-bonn.de

8.1 Introduction

Most stars form in dense star clusters deeply embedded in residual gas. The populations of these objects range from small groups of stars with about a dozen binaries within a volume with a typical radius of $r \approx 0.3\,\mathrm{pc}$ through to objects formed in extreme star bursts containing $N \approx 10^8$ stars within $r \approx 36\,\mathrm{pc}$. Star clusters, or more generally dense stellar systems, must therefore be seen as the fundamental building blocks of galaxies. Differentiation of the term star cluster from a spheroidal dwarf galaxy becomes blurred near $N \approx 10^6$. Both are mostly pressure-supported, that is, random stellar motions dominate any bulk streaming motions such as rotation. The physical processes that drive the formation, evolution and dissolution of star clusters have a deep impact on the appearance of galaxies. This impact has many manifestations, ranging from the properties of stellar populations, such as the binary fraction and the number of type Ia and type II supernovae, through the velocity structure in galactic discs, such as the age–velocity dispersion relation, to the existence of stellar halos around galaxies, tidal streams and the survival and properties of tidal dwarf galaxies, the existence of which challenge current cosmological perspectives. Apart from this cosmological relevance, dense stellar systems provide unique laboratories in which to test stellar evolution theory, gravitational dynamics, the interplay between stellar evolution and dynamical processes and the physics of stellar birth and stellar feedback processes during formation.

Star clusters and other pressure-supported stellar systems in the sky merely offer snap-shots from which we can glean incomplete information. Because there is no analytical solution to the equations of motion for more than two stars, these differential equations need to be integrated numerically. Thus, in order to gain an understanding of these objects in terms of the above issues, a researcher needs to resort to numerical experiments in order to test various hypotheses as to the possible physical initial conditions (to test star-formation theory) or the outcome (to quantify stellar populations in galaxies,

Kroupa, P.: *Initial Conditions for Star Clusters*. Lect. Notes Phys. **760**, 181–259 (2008)
DOI 10.1007/978-1-4020-8431-7_8

for example). The initialisation of a pressure-supported stellar system is such that the initial object is relevant for the real physical Universe, and is therefore a problem of some fundamental importance.

Here empirical constraints on the initial conditions of star clusters are discussed and some problems to which star clusters are relevant are raised. Section 8.2 contains information to set up a realistic computer model of a star cluster, including models of embedded clusters. The initial mass distribution of stars is discussed in Sect. 8.3, and Sect. 8.4 delves into the initial distribution functions of multiple stars. A brief summary is provided in Sect. 8.5.

8.1.1 Embedded Clusters

In this section an outline is given of some astrophysical aspects of dense stellar systems in order to help differentiate probable evolutionary effects from initial conditions. A simple example clarifies the meaning of this. An observer may see two young populations with comparable ages (to within 1 Myr say). They have similar observed masses but different sizes and a somewhat different stellar content and different binary fractions. Do they signify two different initial conditions derived from star-formation or can both be traced back to a $t = 0$ configuration, which is the same?

Preliminaries

Assume we observe a very young population of N stars with an age $\tau_{\rm age}$ and that we have a rough estimate of its half-mass radius, $r_{\rm h}$, and embedded stellar mass, $M_{\rm ecl}$.[1] The average mass is

$$\overline{m} = \frac{M_{\rm ecl}}{N}. \tag{8.1}$$

Also assume we can estimate the star-formation efficiency (SFE), ϵ, within a few $r_{\rm h}$. For this object,

$$\epsilon = \frac{M_{\rm ecl}}{M_{\rm ecl} + M_{\rm gas}}, \tag{8.2}$$

where $M_{\rm gas}$ is the gas left over from the star-formation process. The tidal radius of the embedded cluster can be estimated from the Jacobi limit ((Eq. (7-84) in Binney & Tremaine 1987) as determined by the host galaxy when any contributions by surrounding molecular clouds are ignored,

$$r_{\rm tid} = \left(\frac{M_{\rm ecl} + M_{\rm gas}}{3\, M_{\rm gal}} \right)^{\frac{1}{3}} D, \tag{8.3}$$

[1] Throughout all masses, m, M, etc. are in units of $M_\odot$, unless noted otherwise. "Embedded stellar mass" refers to the man in stars at the time before residual gas expulsion and when star-formation has ceased.

where $M_{\rm gal}$ is the mass of the spherically distributed galaxy within the distance D of the cluster from the centre of the galaxy. This radius is a rough estimate of that distance from the cluster at which stellar motions begin to be significantly influenced by the host galaxy.

The following quantities that allow us to judge the formal dynamical state of the system, the formal crossing time of the stars through the object, can be defined as

$$t_{\rm cr} \equiv \frac{2\,r_{\rm h}}{\sigma}, \tag{8.4}$$

where[2]

$$\sigma = \sqrt{\frac{G\,M_{\rm ecl}}{\epsilon\,r_{\rm h}}} \tag{8.5}$$

is, up to a factor of order unity, the three-dimensional velocity dispersion of the stars in the embedded cluster. Note that these equations serve to estimate the possible amount of mixing of the population. If $\tau_{\rm age} < t_{\rm cr}$, the object cannot be mixed and we are seeing it close to its initial state. It takes a few $t_{\rm cr}$ for a dynamical system out of dynamical equilibrium to return back to it. This is not to be mistaken for a relaxation process.

Once the stars orbit within the object, they exchange orbital energy through weak gravitational encounters and rare strong encounters. The system evolves towards a state of energy equipartition. The energy equipartition time-scale, $t_{\rm ms}$, between massive and average stars (Spitzer 1987, p. 74), which is an estimate of the time massive stars need to sink to the centre of the system through dynamical friction on the lighter stars, is

$$t_{\rm ms} = \frac{\overline{m}}{m_{\rm max}}\,t_{\rm relax}. \tag{8.6}$$

Here, $m_{\rm max}$ is the massive-star mass and the characteristic two-body relaxation time (e.g. Eq. (4–9) in Binney & Tremaine 1987) is

$$t_{\rm relax} = 0.1\,\frac{N}{\ln N}\,t_{\rm cr}. \tag{8.7}$$

This formula refers to a pure N-body system without embedded gas. A rough estimate of $t_{\rm relax,emb}$ for an embedded cluster can be found in Eq. (8) of Adams & Myers (2001). The above (8.7) is a measure for the time a star needs to change its orbit significantly from its initial trajectory. We often estimate it by calculating the amount of time that is required to change the velocity, v, of a star by an amount $\Delta v \approx v$.

Thus, if for example, $\tau_{\rm age} > t_{\rm cr}$ and $\tau_{\rm age} < t_{\rm relax}$, the system is probably mixed and close to dynamical equilibrium, but it is not yet relaxed. That is, it has not had sufficient time for the stars to exchange a significant amount of orbital energy. Such a cluster may have erased its sub-structures.

[2] As an aside, note that $G = 0.0045\,{\rm pc}^3/M_\odot\,{\rm Myr}^2$ and that $1\,{\rm km\,s}^{-1} = 1.02\,{\rm pc/Myr}$.

Fragmentation and Size

The very early stages of cluster evolution on a scale of a few parsecs are dominated by gravitational fragmentation of a turbulent magnetised contracting molecular cloud core (Clarke, Bonnell & Hillenbrand 2000; Mac Low & Klessen 2004; Tilley & Pudritz 2007). Gas-dynamical simulations show the formation of contracting filaments, which fragment into denser cloud cores, that form subclusters of accreting protostars. As soon as the protostars radiate or lose mass with sufficient energy and momentum to affect the cloud core, these computations become expensive because radiative transport and deposition of momentum and mechanical energy by non-isotropic outflows are difficult to handle with present computational means (Stamatellos et al. 2007; Dale, Ercolano & Clarke 2007).

Observations of the very early stages at times less than a few hundreds of thousands of years suggest that protoclusters have a hierarchical protostellar distribution: a number of subclusters with radii less than 0.2 pc and separated in velocity space are often seen embedded within a region less than a pc across (Testi et al. 2000). Many of these subclusters may merge to form a more massive embedded cluster (Scally & Clarke 2002; Fellhauer & Kroupa 2005). It is unclear though if subclusters typically merge before residual gas blow-out or if the residual gas is removed before the sub-clumps can interact significantly, nor is it clear if there is a systematic mass dependence of any such possible behaviour.

Mass Segregation

Whether or not star clusters or subclusters form mass-segregated remains an open issue. Mass segregation at birth is a natural expectation because protostars near the density maximum of the cluster have more material to accrete. For these, the ambient gas is at a higher pressure allowing protostars to accrete longer before feedback termination stops further substantial gas inflow and the coagulation of protostars is more likely there (Zinnecker & Yorke 2007; Bonnell, Larson & Zinnecker 2007). Initially mass-segregated subclusters preserve mass segregation upon merging (McMillan, Vesperini & Portegies Zwart 2007). However, for $\overline{m}/m_{\rm max} = 0.5/100$ and $N \leq 5 \times 10^3$ stars, it follows from (8.6) that

$$t_{\rm ms} \leq t_{\rm cr}. \tag{8.8}$$

That is, a $100\,M_\odot$ star sinks to the cluster centre within roughly a crossing time (see Table 8.1 below for typical values of $t_{\rm cr}$).

Currently, we cannot say conclusively if mass segregation is a birth phenomenon (e.g. Gouliermis et al. 2004), or whether the more massive stars form anywhere throughout the protocluster volume. Star clusters that have already blown out their gas at ages of one to a few million years are typically mass-segregated (e.g. R136, Orion Nebula Cluster).

Table 8.1. Notes: the Y in the O stars column indicates that the maximum stellar mass in the cluster surpasses $8\,M_\odot$ (Fig. 8.1). The average stellar mass is taken to be $\overline{m} = 0.4\,M_\odot$ in all clusters. A star-formation efficiency of $\epsilon = 0.3$ is assumed. The crossing time, $t_{\rm cr}$, is (8.4). The pre-supernova gas evacuation time-scale is $\tau_{\rm gas} = r/v_{\rm th}$, where $v_{\rm th} = 10\,{\rm km\,s^{-1}}$ is the approximate sound velocity of the ionised gas and $\tau_{\rm gas} = 0.05\,{\rm Myr}$ for $r = 0.5\,{\rm pc}$, while $\tau_{\rm gas} = 0.1\,{\rm Myr}$ for $r = 1\,{\rm pc}$

$M_{\rm ecl}/M_\odot$	N	O stars? ($r_{\rm h}=$	$t_{\rm cr}$/Myr 0.5 pc	$\tau_{\rm gas}/t_{\rm cr}$ 0.5 pc	$t_{\rm cr}$/Myr 1 pc	$\tau_{\rm gas}/t_{\rm cr}$ 1 pc)
40	100	N	0.9	–	2.6	–
100	250	Y/N	0.6	0.08	1.6	0.2
500	1250	Y	0.3	0.2	0.7	0.1
10^3	2.5×10^3	Y	0.2	0.25	0.5	0.2
10^4	2.5×10^4	Y	0.06	0.8	0.2	0.5
10^5	2.5×10^5	Y	0.02	2.5	0.05	2
10^6	2.5×10^6	Y	0.006	8.3	0.02	5

To affirm, natal mass segregation would impact positively on the notion that massive stars (more than about $10\,M_\odot$) only form in rich clusters and negatively on the suggestion that they can also form in isolation. For recent work on this topic see Li, Klessen & Mac Low (2003) and Parker & Goodwin (2007).

Feedback Termination

The observationally estimated SFE (8.2) is (Lada & Lada 2003)

$$0.2 \leq \epsilon \leq 0.4, \tag{8.9}$$

which implies that the physics dominating the star-formation process on scales less than a few parsecs is stellar feedback. Within this volume, the pre-cluster cloud core contracts under self-gravity and so forms stars ever more vigorously, until feedback energy suffices to halt the process (feedback termination).

Dynamical State at Feedback Termination

Each protostar needs about $t_{\rm ps} \approx 10^5\,{\rm yr}$ to accumulate about 95% of its mass (Wuchterl & Tscharnuter 2003). The protostars form throughout the pre-cluster volume as the protocluster cloud core contracts. The overall pre-cluster cloud-core contraction until feedback termination takes (8.4, 8.5)

$$t_{\rm cl,form} \approx {\rm few} \times \frac{2}{\sqrt{G}} \left(\frac{M_{\rm ecl}}{\epsilon}\right)^{-\frac{1}{2}} r_{\rm h}^{\frac{3}{2}}, \tag{8.10}$$

(a few times the crossing time), which is about the time over which the cluster forms. Once a protostar condenses out of the hydro-dynamical flow, it becomes

a ballistic particle moving in the time-evolving cluster potential. Because many generations of protostars can form over the cluster-formation time-scale, and if the crossing time through the cluster is a few times shorter than $t_{\rm cl,form}$, the very young cluster is mostly in virial equilibrium when star-formation stops when any residual gas has been lost.[3] It is noteworthy that for $r_{\rm h} = 1\,{\rm pc}$

$$t_{\rm ps} \geq t_{\rm cl,form} \quad \text{for} \quad \frac{M_{\rm ecl}}{\epsilon} \geq 10^{4.9}\,M_\odot \tag{8.11}$$

(the protostar-formation time formally surpasses the cluster formation time), which is near the turnover mass in the old-star cluster mass function (eg. Baumgardt 1998).

A critical parameter is thus the ratio

$$\tau = \frac{t_{\rm cl,form}}{t_{\rm cr}}. \tag{8.12}$$

If it is less than unity, protostars condense from the gas and cannot reach virial equilibrium in the potential before the residual gas is removed. Such embedded clusters may be kinematically cold if the pre-cluster cloud core was contracting, or hot if the pre-cluster cloud core was pressure confined, because the young stars do not feel the gas pressure.

In those cases where $\tau > 1$, the embedded cluster is approximately in virial equilibrium because generations of protostars that drop out of the hydrodynamic flow have time to orbit the potential. The pre-gas-expulsion stellar velocity dispersion in the embedded cluster (8.5) may reach $\sigma = 40\,{\rm pc\,Myr^{-1}}$ if $M_{\rm ecl} = 10^{5.5}\,M_\odot$, which is the case for $\epsilon\, r_{\rm h} < 1\,{\rm pc}$. This is easily achieved because the radius of one-Myr old clusters is $r_{0.5} \approx 0.8\,{\rm pc}$ with no dependence on mass. Some observationally explored cases are discussed by Kroupa (2005). Notably, using K-band number counts, Gutermuth et al. (2005) appear to find evidence for expansion after gas removal.

Interestingly, recent Spitzer results suggest a scaling of the characteristic projected radius R with mass,[4]

$$M_{\rm ecl} \propto R^2 \tag{8.13}$$

(Allen et al. 2007), so the question of how compact embedded clusters form and whether there is a mass–radius relation needs further clarification. Note though that such a scaling is obtained for a stellar population that expands freely with a velocity given by the velocity dispersion in the embedded cluster (8.5),

[3] A brief transition time $t_{\rm tr} \ll t_{\rm cl,form}$ exists during which the star-formation rate decreases in the cluster while the gas is being blown out. However, for the purpose of the present discussion this time may be neglected.

[4] Throughout this text, projected radii are denoted by R, while the 3D radius is r.

$$r(t) \approx r_{\rm o} + \sigma\, t \quad \Rightarrow \quad M_{\rm ecl} = \frac{1}{G}\left(\frac{r(t) - r_o}{t}\right)^2, \tag{8.14}$$

where $r_{\rm o} \leq 1\,{\rm pc}$ is the birth radius of the cluster. Is the observed scaling then a result of expansion from a compact birth configuration after gas expulsion? If so, it would require a more massive system to be dynamically older, which is at least qualitatively in-line with the dynamical time-scales decreasing with mass. Note also that the observed scaling (8.13) cannot carry through to $M_{\rm ecl} \geq 10^4\,M_\odot$ because the resulting objects would not resemble clusters.

There are two broad camps suggesting on one hand that molecular clouds and star clusters form on a free-fall time-scale (Elmegreen 2000; Hartmann 2003; Elmegreen 2007), and on the other hand that many free-fall times are needed (Krumholz & Tan 2007). The former implies $\tau \approx 1$ while the latter implies $\tau > 1$.

Thus, currently unclear issues concerning the initialisation of N-body models of embedded clusters are the ratio τ and whether a mass–radius relation exists for embedded clusters before the development of HII regions. To make progress, I assume for now that the embedded clusters are in virial equilibrium at feedback termination ($\tau > 1$) and that they form highly concentrated with $r \leq 1\,{\rm pc}$ independently of mass.

The Mass of the Most Massive Star

Young clusters show a well-defined correlation between the mass of the most massive star, $m_{\rm max}$, and the stellar mass of the embedded cluster, $M_{\rm ecl}$. This appears to saturate at $m_{\rm max*} \approx 150\,M_\odot$ (Weidner & Kroupa 2004, 2006). This is shown in Fig. 8.1. This correlation may indicate feedback termination of star-formation within the protocluster volume coupled to the most massive stars forming latest, or turning-on at the final stage of cluster formation (Elmegreen 1983).

The evidence for a universal upper mass cutoff near

$$m_{\rm max*} \approx 150\,M_\odot \tag{8.15}$$

(Weidner & Kroupa 2004; Figer 2005; Oey & Clarke 2005; Koen 2006; Maíz Apellániz et al. 2007; Zinnecker & Yorke 2007) seems to be rather well established in populations with metallicities ranging from the LMC ($Z \approx 0.008$) to the super-solar Galactic centre ($Z \geq 0.02$) so that the stellar mass function (MF) simply stops at that mass. This mass needs to be understood theoretically (see discussion by Kroupa & Weidner 2005; Zinnecker & Yorke 2007). It is probably a result of stellar structure stability, but may be near $80\,M_\odot$ as predicted by theory if the most massive stars reside in near-equal component-mass binary systems (Kroupa & Weidner 2005). It may also be that the calculated stellar masses are significantly overestimated (Martins, Schaerer & Hillier 2005).

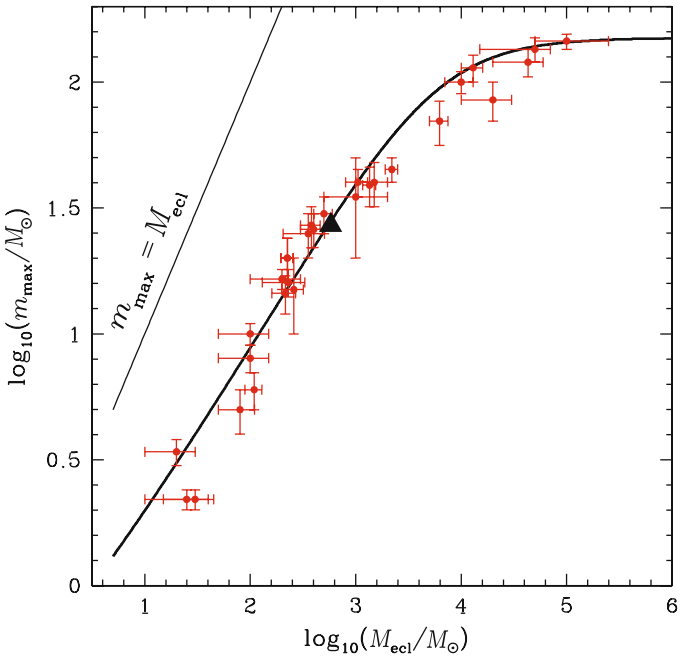

Fig. 8.1. The maximum stellar mass, $m_{\rm max}$, as a function of the stellar mass of the embedded cluster, $M_{\rm ecl}$ (Weidner, private communication, an updated version of the data presented by Weidner & Kroupa 2006). The *solid triangle* is an SPH model of star-cluster formation by Bonnell, Bate & Vine (2003), while the *solid curve* stems from stating that there is exactly one most massive star in the cluster, $1 = \int_{m_{\rm max}}^{150} \xi(m)\,{\rm d}m$ with the condition $M_{\rm ecl} = \int_{0.08}^{m_{\rm max}} m\,\xi(m)\,{\rm d}m$, where $\xi(m)$ is the stellar IMF. The solution can only be obtained numerically, but an easy-to-use, well-fitting function has been derived by Pflamm-Altenburg, Weidner & Kroupa (2007)

The Cluster Core of Massive Stars

Irrespective of whether the massive stars (more than about $10\,M_\odot$) form at the cluster centre or whether they segregate there owing to energy equipartition (8.6), they ultimately form a compact sub-population that is dynamically highly unstable. Massive stars are ejected from such cores very efficiently on a core-crossing time-scale and, for example, the well-studied Orion Nebula cluster (ONC) has probably already shot out 70% of its stars more massive than $5\,M_\odot$ (Pflamm-Altenburg & Kroupa 2006). The properties of O and B runaway stars have been used by Clarke & Pringle (1992) to deduce the typical birth configuration of massive stars. They find them to form in binaries with similar-mass components in compact small-N groups devoid of low-mass stars. Among others, the core of the Orion Nebula Cluster (ONC) is just such a system.

The Star-Formation History in a Cluster

The detailed star-formation history in a cluster contains information about the events that build up the cluster. Intriguing is the recent evidence for some clusters that while the bulk of the stars have ages that differ by less than a few 10^5 yr, a small fraction of older stars are often encountered (Palla & Stahler 2000 for the ONC, Sacco et al. 2007 for the σ Orionis cluster). This may be interpreted to mean that clusters form over about 10 Myr with a final highly accelerated phase, in support of the notion that turbulence of a magnetised gas determines the early cloud-contraction phase (Krumholz & Tan 2007).

A different interpretation would be that as a pre-cluster cloud core contracts on a free-fall time-scale, it traps surrounding field stars which then become formal cluster members. Most clusters form in regions of a galaxy that has seen previous star-formation. The velocity dispersion of the previous stellar generation, such as an expanding OB association, is usually rather low, around a few $\mathrm{km\,s^{-1}}$ to $10\,\mathrm{km\,s^{-1}}$. The deepening potential of a newly contracting pre-cluster cloud core is able to capture some of the preceding generation of stars so that these older stars become formal cluster members although they did not form in the cluster. Pflamm-Altenburg & Kroupa (2007) study this problem for the ONC and show that the age spread reported by Palla et al. (2007) can be accounted for in this way. This suggests that the star-formation history of the ONC may in fact not have started about 10 Myr ago, supporting the argument by Elmegreen (2000), Elmegreen (2007) and Hartmann (2003) that clusters form on a time-scale comparable to the crossing time of the pre-cluster cloud core. Additionally, the sample of cluster stars may be contaminated by enhanced fore- and back-ground densities of field stars by focussing of stellar orbits during cluster formation (Pflamm-Altenburg & Kroupa 2007).

For very massive clusters such as ω Cen, Fellhauer, Kroupa & Evans (2006) show that the potential is sufficiently deep that the pre-cluster cloud core may capture the field stars of a previously existing dwarf galaxy. Up to 30% or more of the stars in ω Cen may be captured field stars. This would explain an age spread of a few Gyr in the cluster and is consistent with the notion that ω Cen formed in a dwarf galaxy that was captured by the Milky Way. The attractive aspect of this scenario is that ω Cen need not have been located at the centre of the incoming dwarf galaxy as a nucleus but within its disc, because it opens a larger range of allowed orbital parameters for the putative dwarf galaxy moving about the Milky Way. The currently preferred scenario in which ω Cen was the nucleus of the dwarf galaxy implies that the galaxy was completely stripped while falling into the Milky Way leaving only its nucleus on its current retrograde orbit (Zhao 2004). The new scenario allows the dwarf galaxy to be absorbed into the bulge of the Milky Way with ω Cen being stripped from it on its way in.

Another possibility for obtaining an age spread of a few Gyr in a massive cluster such as ω Cen is gas accretion from a co-moving inter-stellar medium (Pflamm-Altenburg & Kroupa 2008). This could only have worked for ω Cen before it became unbound from its mother galaxy, though. That is, the cluster must have spent about 2–3 Gyr in its mother galaxy before it was captured by the Milky Way.

This demonstrates beautifully how an improved understanding of dynamical processes on scales of a few pc impinges on problems related to the formation of galaxies and cosmology (through the sub-structure problem). Finally, the increasingly well-documented evidence for stellar populations in massive clusters with different metallicities and ages, and in some cases even significant He enrichment, may also suggest secondary star-formation occurring from material that has been pre-enriched from a previous generation of stars in the cluster. Different IMFs need to be invoked for the populations of different ages (see Piotto 2008 for a review).

Expulsion of Residual Gas

When the most massive stars are O stars, they destroy the protocluster nebula and quench further star-formation by first ionising most of it (feedback termination). The ionised gas, at a temperature near 10^4 K and in serious over-pressure, pushes out and escapes the confines of the cluster volume at the sound speed (near $10\,\mathrm{km\,s^{-1}}$) or faster if the winds blow off O stars with velocities of thousands of $\mathrm{km\,s^{-1}}$ and impart sufficient momentum.

There are two analytically tractable regimes of behaviour, instantaneous gas removal and slow gas expulsion over many crossing times.

- First consider instantaneous gas expulsion, $\tau_{\rm gas} = 0$. The binding energy of the object of mass M and radius r is

$$E_{\rm cl,bind} = -\frac{G\,M^2}{r} + \frac{1}{2}\,M\,\sigma^2 \ < 0. \tag{8.16}$$

  Before gas expulsion, $M = M_{\rm init} = M_{\rm gas} + M_{\rm ecl} \ \rightarrow M$ and

$$\sigma^2_{\rm init} = \frac{G\,M_{\rm init}}{r_{\rm init}} \ \longrightarrow \ \sigma. \tag{8.17}$$

  After instantaneous gas expulsion, $M_{\rm after} = M_{\rm ecl} \ \rightarrow M$, but $\sigma_{\rm after} = \sigma_{\rm init} \rightarrow \sigma$, and the new binding energy is

$$E_{\rm cl,bind,after} = -\frac{G\,M^2_{\rm after}}{r_{\rm init}} + \frac{1}{2}\,M_{\rm after}\,\sigma^2_{\rm init}. \tag{8.18}$$

  But the cluster relaxes into a new equilibrium, so that, by the scalar virial theorem[5]

[5]The scalar virial theorem states that $2\,K + W = 0 \ \Rightarrow \ E = K + W = (1/2)\,W$, where K, W are the kinetic and potential energy and E is the total energy of the system.

$$E_{\rm cl,bind,after} = -\frac{1}{2}\,\frac{G\,M_{\rm after}}{r_{\rm after}}, \tag{8.19}$$

and on equating these two expressions for the final energy and using (8.17) we find that

$$\frac{r_{\rm after}}{r_{\rm init}} = \frac{M_{\rm ecl}}{M_{\rm ecl} - M_{\rm gas}}. \tag{8.20}$$

Thus, as $M_{\rm gas} \rightarrow M_{\rm ecl}$, then $\epsilon \rightarrow 0.5$ from above, $r_{\rm after} \rightarrow \infty$. This means that as the SFE approaches 50% from above, the cluster unbinds itself. But by (8.9), this result would imply either (see Kroupa, Aarseth & Hurley 2001, and references therein)

- all clusters with OB stars (and thus $\tau_{\rm gas} \ll t_{\rm cr}$) do not survive gas expulsion, or
- the clusters expel their gas slowly, $\tau_{\rm gas} \gg t_{\rm cr}$. This may be the case if surviving clusters such as the Pleiades or Hyades formed without OB stars.

- Now consider slow gas removal, $\tau_{\rm gas} \gg t_{\rm cr}$, $\tau_{\rm gas} \rightarrow \infty$. By (8.20) and the assumption that an infinitesimal mass of gas is removed instantaneously,

$$\frac{r_{\rm init} - \delta r}{r_{\rm init}} = \frac{M_{\rm init} - \delta M_{\rm gas}}{M_{\rm init} - \delta M_{\rm gas} - \delta M_{\rm gas}}. \tag{8.21}$$

For infinitesimal steps and, for convenience, $\mathrm{d}M < 0$ but $\mathrm{d}r > 0$,

$$\frac{r - \mathrm{d}r}{r} = \frac{M + \mathrm{d}M}{M + 2\,\mathrm{d}M}. \tag{8.22}$$

Re-arranging this, we find

$$\frac{\mathrm{d}r}{r} = \frac{\mathrm{d}M}{M}\,\left(1 - 2\,\frac{\mathrm{d}M}{M}\,\ldots\right), \tag{8.23}$$

so that

$$\frac{\mathrm{d}r}{r} = \frac{\mathrm{d}M}{M} \;\Rightarrow\; \ln\frac{r_{\rm after}}{r_{\rm init}} = \ln\frac{M_{\rm init}}{M_{\rm after}}, \tag{8.24}$$

upon integration of the differential equation. Thus,

$$\frac{r_{\rm after}}{r_{\rm init}} = \frac{M_{\rm ecl} + M_{\rm gas}}{M_{\rm ecl}} = \frac{1}{\epsilon}, \tag{8.25}$$

and for example, for a SFE of 20%, the cluster expands by a factor of 5, $r_{\rm after} = 5\,r_{\rm init}$, without dissolving.

Table 8.1 gives an overview of the type of behaviour one might expect for clusters with increasing number of stars, N, and stellar mass, $M_{\rm ecl}$, for two characteristic radii of the embedded stellar distribution, $r_{\rm h}$. It can be seen that the gas-evacuation time-scale becomes longer than the crossing time through

the cluster for $M_{\rm ecl} \geq 10^5\,M_\odot$. Such clusters would thus undergo adiabatic expansion as a result of gas blow out. Less-massive clusters are more likely to undergo an evolution that is highly dynamic and that can be described as an explosion (the cluster pops). For clusters without O and massive B stars, nebula disruption probably occurs on the cluster-formation time-scale of about a million years and the evolution is again adiabatic. A simple calculation of the amount of energy deposited by an O star into its surrounding cluster-nebula suggests it is larger than the nebula binding energy (Kroupa 2005). This, however, only gives, at best, a rough estimate of the rapidity with which gas can be expelled. An inhomogeneous distribution of gas leads to the gas removal preferentially along channels and asymmetrically, so that the overall gas-excavation process is highly non-uniform and variable (Dale et al. 2005).

The reaction of clusters to gas expulsion is best studied numerically with N-body codes. Pioneering experiments were performed by Tutukov (1978) and then Lada, Margulis & Dearborn (1984). Goodwin (1997a,b, 1998) studied gas expulsion by supernovae from young globular clusters. Figure 8.2 shows the evolution of an ONC-type initial cluster with a stellar mass $M_{\rm ecl} \approx 4000\,M_\odot$ and a canonical IMF (8.124) and stellar evolution, a 100% initial binary population (Sect. 8.4.2) in a solar-neighbourhood tidal field, $\epsilon = 1/3$ and spherical gas blow-out on a thermal time-scale ($v_{\rm th} = 10\,{\rm km\,s^{-1}}$). The figure demonstrates that the evolution is far more complex than the simple analytical estimates above suggest, and in fact a substantial Pleiades-type cluster emerges after losing about two-thirds of its initial stellar population (see also p. 195). Subsequent theoretical work based on an iterative scheme according to which the mass of unbound stars at each radius is removed successively shows that

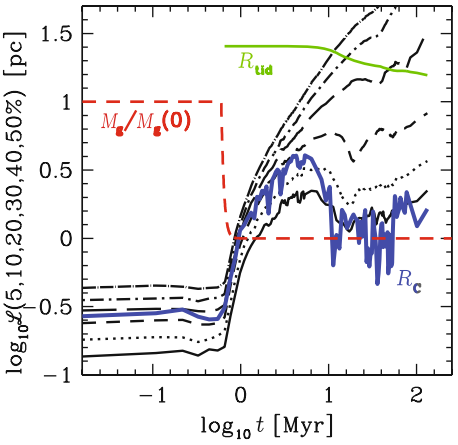

Fig. 8.2. The evolution of 5, 10, 20, ..., 50% of the Lagrangian radius and the core radius ($R_{\rm c} = r_{\rm c}$, *thick lower curve*) of the ONC-type cluster discussed in the text. The gas mass is shown as the *dashed line*. The cluster spends 0.6 Myr in an embedded phase before the gas is blown out on a thermal time-scale. The tidal radius (8.3) is shown by the *upper thick solid curve* (Kroupa, Aarseth & Hurley 2001)

the survival of a cluster depends not only on $\epsilon, \tau_{\rm gas}/t_{\rm cr}$ and $r_{\rm tid}$ but also on the detailed shape of the stellar distribution function (Boily & Kroupa 2003). For instantaneous gas removal, $\epsilon \approx 0.3$ is a lower limit for the SFE below which clusters cannot survive rapid gas blow-out. This is significantly smaller than the critical value of $\epsilon = 0.5$ below which the stellar system becomes formally unbound (8.20). However, if clusters form as complexes of subclusters, each of which pop in this way, then overall cluster survival is enhanced to even smaller values of $\epsilon \approx 0.2$ (Fellhauer & Kroupa 2005).

Whether clusters pop and what fraction of stars remain in a post-gas expulsion cluster depend critically on the ratio between the gas-removal time-scale and the cluster crossing time. This ratio thus mostly defines which clusters succumb to infant mortality and which clusters merely suffer cluster infant weight loss. The well-studied observational cases do indicate that the removal of most of the residual gas does occur within a cluster-dynamical time, $\tau_{\rm gas}/t_{\rm cr} \leq 1$. Examples noted (Kroupa 2005) are the ONC and R136 in the LMC both of which have significant super-virial velocity dispersions. Other examples are the Treasure-Chest cluster and the very young star-bursting clusters in the massively interacting Antennae galaxy that appear to have HII regions expanding at velocities so that the cluster volume may be evacuated within a cluster dynamical time. However, improved empirical constraints are needed to develop further an understanding of cluster survival. Such observations would best be the velocities of stars in very young star clusters, as they should show a radially expanding stellar population.

Indeed, Bastian & Goodwin (2006) note that many young clusters have the radial-density profile signature expected if they are expanding rapidly. This supports the notion of fast gas blow out. For example, the 0.5–2 Myr old ONC, which is known to be super-virial with a virial mass about twice the observed mass (Hillenbrand & Hartmann 1998), has already expelled its residual gas and is expanding rapidly. It has therefore probably lost its outer stars (Kroupa, Aarseth & Hurley 2001). The super-virial state of young clusters makes measurements of their mass-to-light ratio a bad estimate of the stellar mass within them (Goodwin & Bastian 2006) and rapid dynamical mass-segregation likewise makes naive measurements of the M/L ratio wrong (Boily et al. 2005; Fleck et al. 2006). Goodwin & Bastian (2006) and de Grijs & Parmentier (2007) find the dynamical mass-to-light ratios of young clusters to be too large, strongly implying they are in the process of expanding after gas expulsion.

Weidner et al. (2007) attempted to measure infant weight loss with a sample of young but exposed Galactic clusters. They applied the maximal-star-mass to cluster mass relation from above to estimate the birth mass of the clusters. The uncertainties are large, but the data firmly suggest that the typical cluster loses at least about 50% of its stars.

Binary Stars

Most stars form as binaries with, as far as can be stated today, universal orbital distribution functions (Sect. 8.4). Once a binary system is born in a dense environment, it is perturbed. This changes its eccentricity and semi-major axis. Or it undergoes a relatively strong encounter that disrupts the binary or hardens it perhaps with exchanged companions. The initial binary population therefore evolves on a cluster crossing time-scale and most soft binaries are disrupted. It has been shown that the properties of the Galactic field binary population can be explained in terms of the binary properties observed for very young populations if these go through a dense cluster environment (dynamical population synthesis, Kroupa 1995d). A dense cluster environment hardens existing binaries (p. 240). This increases the SN Ia rate in a galaxy with many dense clusters (Shara & Hurley 2002).

Binaries are significant energy sources (see also Sect. 8.4). A hard binary that interacts via a resonance with a cluster field star occasionally ejects one star with a terminal velocity $v_{\rm ej} \gg \sigma$. The ejected star either leaves the cluster causing cluster expansion so that σ drops, or it shares some of its kinetic energy with the other cluster field stars through gravitational encounters causing cluster expansion. Binaries in a cluster core can thus halt and reverse core collapse (Meylan & Heggie 1997; Heggie & Hut 2003).

Mass Loss from Evolving Stars

An old globular cluster with a turn-off mass near $0.8\,M_\odot$ has lost 30% of the mass that remained in it after gas expulsion by stellar evolution (Baumgardt & Makino 2003). Because the mass loss is most rapid during the earliest times after the cluster returned to virial equilibrium once the gas was expelled, the cluster expands further during this time. This is nicely seen in the Lagrangian radii of realistic cluster-formation models (Kroupa, Aarseth & Hurley 2001).

8.1.2 Some Implications for the Astrophysics of Galaxies

In general, the above have a multitude of implications for galactic and stellar astrophysics.

1. The heaviest-star–star-cluster-mass correlation constrains feedback models of star cluster formation (Elmegreen 1983). It also implies that the sum of all IMFs in all young clusters in a galaxy, the integrated galaxy initial mass function (IGIMF), is steeper than the invariant stellar IMF observed in star clusters. This has important effects on the mass–metallicity relation of galaxies (Koeppen, Weidner & Kroupa 2007). Additionally, star-formation rates (SFRs) of dwarf galaxies can be underestimated by up to three orders of magnitude because Hα-dark star-formation becomes possible (Pflamm-Altenburg, Weidner & Kroupa 2007). This indeed constitutes an

important example of how sub-pc processes influence the physics on cosmological scales.
2. The deduction that type-II clusters probably pop (p. 190) implies that young clusters will appear to an observer to be super-virial, i.e. to have a dynamical mass larger than their luminous mass (Bastian & Goodwin 2006; de Grijs & Parmentier 2007).
3. It further implies that galactic fields can be heated and may also lead to galactic thick discs and stellar halos around dwarf galaxies (Kroupa 2002b).
4. The variation of the gas expulsion time-scale among clusters of different type implies that the star-cluster mass function (CMF) is re-shaped rapidly, on a time-scale of a few tens of Myr (Kroupa & Boily 2002).
5. Associated with this re-shaping of the CMF is the natural production of population II stellar halos during cosmologically early star-formation bursts (Kroupa & Boily 2002; Parmentier & Gilmore 2007; Baumgardt, Kroupa & Parmentier 2008).
6. The properties of the binary-star population observed in Galactic fields are shaped by dynamical encounters in star clusters before the stars leave their cluster (Sect. 8.4).

Points 2–5 are considered in more detail in the rest of Sect. 8.1.

Stellar Associations, Open Clusters and Moving Groups

As one of the important implications of point 2, a cluster in the age range 1–50 Myr has an unphysical M/L ratio because it is out of dynamical equilibrium rather than because it has an abnormal stellar IMF (Bastian & Goodwin 2006; de Grijs & Parmentier 2007).

Another implication is that a Pleiades-like open cluster would have been born in a very dense ONC-type configuration and that, as it evolves, a moving-group-I is established during the first few dozen Myr. This comprises roughly two-thirds of the initial stellar population and the cluster is expanding with a velocity dispersion that is a function of the pre-gas-expulsion configuration (Kroupa, Aarseth & Hurley 2001). These computations were among the first to demonstrate, with high-precision N-body modelling, that the redistribution of energy within the cluster during the embedded phase and during the expansion phase leads to the formation of a substantial remnant cluster despite the inclusion of all physical effects that are disadvantageous for this to happen (explosive gas expulsion, low SFE $\epsilon = 0.33$, galactic tidal field and mass loss from stellar evolution and an initial binary-star fraction of 100%, see Fig. 8.2). Thus, expanding OB associations may be related to star-cluster birth and many OB associations ought to have remnant star clusters as nuclei (see also Clark et al. 2005).

As the cluster expands becoming part of an OB association, the radiation from its massive stars produce expanding HII regions that may trigger further star-formation in the vicinity (e.g. Gouliermis, Quanz & Henning 2007).

A moving-group-II establishes later – the classical moving group made up of stars that slowly diffuse or evaporate out of the readjusted cluster remnant with relative kinetic energy close to zero. The velocity dispersion of moving-group-I is thus comparable to the pre-gas-expulsion velocity dispersion of the cluster, while moving-group-II has a velocity dispersion close to zero.

The Velocity Dispersion of Galactic-Field Populations and Galactic Thick Discs

Thus, the moving-group-I would be populated by stars that carry the initial kinematic state of the birth configuration into the field of a galaxy. Each generation of star clusters would, according to this picture, produce overlapping moving-groups-I (and II) and the overall velocity dispersion of the new field population can be estimated by adding the squared velocities for all expanding populations. This involves an integral over the embedded-cluster mass function, $\xi_{\rm ecl}(M_{\rm ecl})$, which describes the distribution of the stellar mass content of clusters when they are born. Because the embedded cluster mass function is known to be a power-law, this integral can be calculated for a first estimate (Kroupa 2002b, 2005). The result is that, for reasonable upper cluster mass limits in the integral, $M_{\rm ecl} \leq 10^5\,M_\odot$, the observed age–velocity dispersion relation of Galactic field stars can be reproduced.

This idea can thus explain the much debated energy deficit: namely that the observed kinematic heating of field stars with age could not, until now, be explained by the diffusion of orbits in the Galactic disc as a result of scattering by molecular clouds, spiral arms and the bar (Jenkins 1992). Because the velocity-dispersion for Galactic-field stars increases with stellar age, this notion can also be used to map the star-formation history of the Milky Way disc by resorting to the observed correlation between the star-formation rate in a galaxy and the maximum star-cluster mass born in the population of young clusters (Weidner, Kroupa & Larsen 2004).

An interesting possibility emerges concerning the origin of thick discs. If the star-formation rate was sufficiently high about 11 Gyr ago, star clusters in the disc with masses up to $10^{5.5}\,M_\odot$ would have been born. If they popped a thick disc with a velocity dispersion near $40\,{\rm km\,s^{-1}}$ would result naturally (Kroupa 2002b). This notion for the origin of thick discs appears to be qualitatively supported by the observations of Elmegreen, Elmegreen & Sheets (2004) who find galactic discs at a red shift between 0.5 and 2 to show massive star-forming clumps.

Structuring the Initial Cluster Mass Function

Another potentially important implication from this picture of the evolution of young clusters is that if the ratio of the gas expulsion time to the crossing time or the SFE varies with initial (embedded) cluster mass, an initially featureless power-law mass function of embedded clusters rapidly evolves to one with

peaks, dips and turnovers at cluster masses that characterise changes in the broad physics involved.

As an example, Adams (2000) and Kroupa & Boily (2002) assumed that the function

$$M_{\rm icl} = f_{\rm st}(M_{\rm ecl}) M_{\rm ecl} \tag{8.26}$$

exists, where $M_{\rm ecl}$ is as above and $M_{\rm icl}$ is the classical initial cluster mass and $f_{\rm st} = f_{\rm st}(M_{\rm ecl})$. According to Kroupa & Boily (2002), the classical initial cluster mass is that mass which is inferred by standard N-body computations without gas expulsion (in effect this assumes $\epsilon = 1$, which is however, unphysical). Thus, for example, for the Pleiades, $M_{\rm cl} \approx 1000\,M_\odot$ at the present time (age about 100 Myr). A classical initial model would place the initial cluster mass near $M_{\rm icl} \approx 1500\,M_\odot$ by standard N-body calculations to quantify the secular evaporation of stars from an initially bound and relaxed cluster (Portegies Zwart et al. 2001). If, however, the SFE was 33% and the gas-expulsion time-scale were comparable to or shorter than the cluster dynamical time, the Pleiades would have been born in a compact configuration resembling the ONC and with a mass of embedded stars of $M_{\rm ecl} \approx 4000\,M_\odot$ (Kroupa, Aarseth & Hurley 2001). Thus, $f_{\rm st}(4000\,M_\odot) = 0.38\,(= 1500/4000)$.

By postulating that there exist three basic types of embedded clusters (Kroupa & Boily 2002), namely

Type I: clusters without O stars ($M_{\rm ecl} \leq 10^{2.5}\,M_\odot$, e.g. Taurus-Auriga pre-main sequence stellar groups, ρ Oph),
Type II: clusters with a few O stars ($10^{2.5} \leq M_{\rm ecl}/M_\odot \leq 10^{5.5}$, e.g. the ONC),
Type III: clusters with many O stars and with a velocity dispersion comparable to or higher than the sound velocity of ionized gas ($M_{\rm ecl} \geq 10^{5.5}\,M_\odot$),

it can be argued that $f_{\rm st} \approx 0.5$ for type I, $f_{\rm st} < 0.5$ for type II and $f_{\rm st} \approx 0.5$ for type III. The reason for the high $f_{\rm st}$ values for types I and III is that gas expulsion from these clusters may last longer than the cluster dynamical time because there is no sufficient ionizing radiation for type I clusters, or the potential well is too deep for the ionized gas to leave (type III clusters). The evolution is therefore adiabatic ((8.25) above). Type II clusters undergo a disruptive evolution and witness a high infant mortality rate (Lada & Lada 2003). They are the pre-cursors of OB associations and Galactic clusters. This broad categorisation has easy-to-understand implications for the star-cluster mass function.

Under these conditions and an assumed functional form for $f_{\rm st} = f_{\rm st}(M_{\rm ecl})$, the power-law embedded cluster mass function transforms into a cluster mass function with a turnover near $10^5\,M_\odot$ and a sharp peak near $10^3\,M_\odot$ (Kroupa & Boily 2002). This form is strongly reminiscent of the initial globular cluster mass function, which is inferred by, for example, Vesperini (1998, 2001), Parmentier & Gilmore (2005) and Baumgardt (1998) to be required for a

match with the evolved cluster mass function that is seen to have a universal turnover near $10^5\,M_\odot$. By the reasoning given above, this "initial" CMF is, however, unphysical, being a power-law instead.

This analytical formulation of the problem has been verified nicely with N-body simulations combined with a realistic treatment of residual gas expulsion by Baumgardt, Kroupa & Parmentier (2008), who show the Milky Way globular cluster mass function to emerge from a power-law embedded-cluster mass function. Parmentier et al. (2008) expand on this by studying the effect that different assumptions on the physics of gas removal have on shaping the star-cluster mass function within about 50 Myr. The general ansatz that residual gas expulsion plays a dominant role in early cluster evolution may thus solve the long-standing problem that the deduced initial cluster mass function needs to have this turnover, while the observed mass functions of young clusters are featureless power-law distributions.

The Origin of Population II Stellar Halos

The above view implies naturally that a major field-star component is generated whenever a population of star clusters forms. About 12 Gyr ago, the Milky Way began its assembly by an initial burst of star-formation throughout a volume spanning about 10 kpc in radius. In this volume, the star-formation rate must have reached $10\,M_\odot\,\mathrm{yr}^{-1}$ so that star clusters with masses up to $\approx 10^6\,M_\odot$ formed (Weidner, Kroupa & Larsen 2004), probably in a chaotic, turbulent early interstellar medium. The vast majority of embedded clusters suffered infant weight loss or mortality. The surviving long-lived clusters evolved to globular clusters. The so-generated field population is the spheroidal population-II halo, which has the same chemical properties as the surviving (globular) star clusters, apart from enrichment effects evident in the most massive clusters. All of these characteristics emerge naturally in the above model, as pointed out by Kroupa & Boily (2002), Parmentier & Gilmore (2007) and most recently by Baumgardt, Kroupa & Parmentier (2008).

8.1.3 Long-Term, or Classical, Cluster Evolution

The long-term evolution of star clusters that survive infant weight loss and the mass loss from evolving stars is characterised by three physical processes, the drive of the self-gravitating system towards energy equipartition, stellar evolution processes and the heating or forcing of the system through external tides. One emphasis of star-cluster work in this context is to test the theory of stellar evolution and to investigate the interrelation of stellar astrophysics with stellar dynamics. The stellar-evolution and the dynamical-evolution timescales are comparable. The reader is directed to Meylan & Heggie (1997) and Heggie & Hut (2003) for further details.

Tidal Tails

Tidal tails contain the stars evaporating from long-lived star clusters (the moving-group-II above). The typical S-shaped structure of tidal tails close to the cluster are easily understood: stars that leave the cluster with a slightly higher galactic velocity than the cluster are on slightly outward-directed galactic orbits and therefore fall behind the cluster as the angular velocity about the galactic centre decreases with distance. The outward-directed trailing arm develops. Stars that leave the cluster with slower galactic velocities than the cluster fall towards the galaxy and overtake the cluster.

Given that energy equipartition leads to a filtering in energy space of the stars that escape at a particular time, one expects a gradient in the stellar mass function progressing along a tidal tail towards the cluster so that the mass function becomes flatter, richer in more massive stars. This effect is difficult to detect but, for example, the long tidal tails found emanating from Pal 5 (Odenkirchen et al. 2003) may show evidence for it.

As emphasised by Odenkirchen et al. (2003), tidal tails have another very interesting use: they probe the gravitational potential of the Milky Way if the differential motions along the tidal tail can be measured. They are thus important future tests of gravitational physics.

Death and Hierarchical Multiple Stellar Systems

Nothing lasts forever and star clusters that survive initial relaxation to virial equilibrium after residual gas expulsion and mass loss from stellar evolution ultimately cease to exist after all member stars evaporate to leave a binary or a long-lived hierarchical multiple system composed of near-equal mass components (de la Fuente Marcos 1997, 1998). Note that these need not be single stars. These cluster remnants are interesting, because they may account for most of the hierarchical multiple stellar systems in the Galactic field (Goodwin & Kroupa 2005), with the implication that these are not a product of star-formation but rather of star-cluster dynamics.

8.1.4 What is a Galaxy?

Star clusters, dwarf-spheroidal (dSph) and dwarf-elliptical (dE) galaxies as well as galactic bulges and giant elliptical (E) galaxies are all stellar-dynamical systems that are supported by random stellar motions, i.e. they are pressure-supported. But why is one class of these pressure-supported systems referred to as star clusters, while the others are galaxies? Is there some fundamental physical difference between these two classes of systems?

Considering the radius as a function of mass, we notice that systems with $M \leq 10^6\,M_\odot$ do not show a mass–radius relation (MRR) and have $r \approx 4\,\mathrm{pc}$. More massive objects, however, show a well-defined MRR. In fact, Dabringhausen, Hilker & Kroupa (2008) find that massive compact objects (MCOs),

which have $10^6 \leq M/M_\odot \leq 10^8$, lie on the MRR of giant E galaxies (about $10^{13}\,M_\odot$) down to normal E galaxies ($10^{11}\,M_\odot$), as is evident in Fig. 8.3:

$$R/\mathrm{pc} = 10^{-3.15}\left(\frac{M}{M_\odot}\right)^{0.60\pm0.02}. \qquad (8.27)$$

Noteworthy is that systems with $M \geq 10^6\,M_\odot$ also exhibit complex stellar populations, while less massive systems have single-age, single-metallicity populations. Remarkably, Pflamm-Altenburg & Kroupa (2008) show that a stellar system with $M \geq 10^6\,M_\odot$ and a radius as observed for globular clusters can accrete gas from a co-moving warm inter-stellar medium and may re-start star-formation. The median two-body relaxation time is longer than a Hubble time for $M \geq 3\times10^6\,M_\odot$ and only for these systems is there evidence for a slight increase in the dynamical mass-to-light ratio. Intriguingly, $(M/L)_V \approx 2$ for $M < 10^6\,M_\odot$, while $(M/L)_V \approx 5$ for $M > 10^6\,M_\odot$ with a possible decrease for $M > 10^8\,M_\odot$ (Fig. 8.4). Finally, the average stellar density maximises at $M = 10^6\,M_\odot$ with about $3\times10^3\,M_\odot/\mathrm{pc}^3$ (Dabringhausen, Hilker & Kroupa 2008).

Thus,

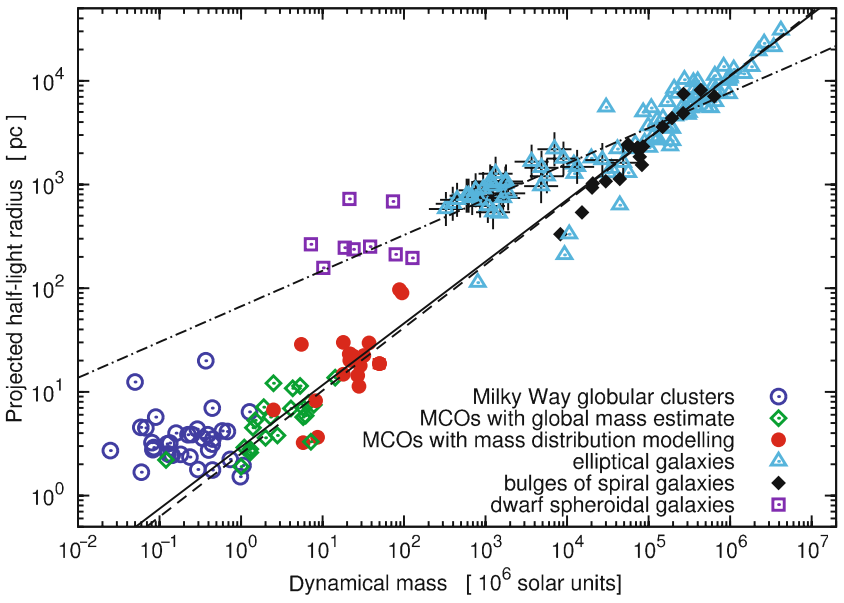

Fig. 8.3. Mass–radius data plotted against the dynamical mass of pressure-supported stellar systems (Dabringhausen, Hilker & Kroupa 2008). MCOs are massive compact objects (also referred to as ultra compact dwarf galaxies). The solid and dashed lines refer to (8.27), while the *dash-dotted line* is a fit to dSph and dE galaxies

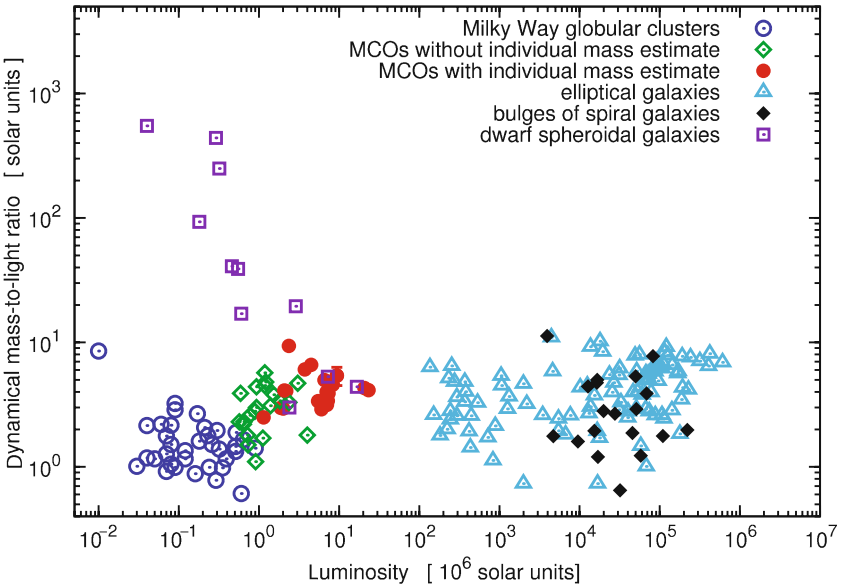

Fig. 8.4. Dynamical M/L values in dependence of the V-band luminosity of pressure-supported stellar systems (Dabringhausen, Hilker & Kroupa 2008). MCOs are massive compact objects (also referred to as ultra compact dwarf galaxies)

- the mass $10^6\,M_\odot$ appears to be special,
- stellar populations become complex above this mass,
- evidence for some dark matter only appears in systems that have a median two-body relaxation time longer than a Hubble time,
- dSph galaxies are the only stellar-dynamical systems with $10 < (M/L)_V < 1000$ and as such are total outliers and
- $10^6\,M_\odot$ is a lower accretion limit for massive star clusters immersed in a warm inter-stellar medium.

$M \approx 10^6\,M_\odot$ therefore appears to be a critical mass scale so that less-massive objects show characteristics of star clusters that are described well by Newtonian dynamics, while more massive objects show behaviour more typical of galaxies. Defining a galaxy as a stellar-dynamical object which has a median two-body relaxation time longer than a Hubble time, i.e. essentially a system with a smooth potential, may be an objective and useful way to define a galaxy (Kroupa 1998). Why only smooth systems show evidence for dark matter remains at best a striking coincidence, at worst it may be symptomatic of a problem in understanding dynamics in such systems.

8.2 Initial 6D Conditions

The previous section gave an outline of some of the issues at stake in the realm of pressure-supported stellar systems. In order to attack these and other problems, we need to know how to set up such systems in the computer. Indeed, as much as analytical solutions may be preferred, the mathematical and physical complexities of dense stellar systems leave no alternatives other than to resort to full-scale numerical integration of the $6N$ coupled first-order differential equations that describe the motion of the system through $6N$-dimensional phase space. There are three related questions to ponder. Given a well-developed cluster, how is one to set it up in order to evolve it forward in time? How does a cluster form and how does the formation process affect its later properties? How do we describe a realistic stellar population (IMF, binaries)? Each of these questions is dealt with in the following sections.

8.2.1 6D Structure of Classical Clusters

Because the state of a star cluster is never known exactly, it is necessary to perform numerical experiments with conditions that are, statistically, consistent with the cluster snap-shot. To ensure meaningful statistical results for systems with few stars, say $N < 5000$, many numerical renditions of the same object are thus necessary. For example, systems with $N = 100$ stars evolve erratically and numerical experiments are required to map out the range of possible states at a particular time: the range of half-mass radii at an age of 20 Myr in 1000 numerical experiments of a cluster, initially with $N = 100$ stars and with an initial half-mass radius $r_{0.5} = 0.5\,\mathrm{pc}$, can be compared with an actually observed object for testing consistency with the initial conditions. Excellent recent examples of this approach can be found in Hurley et al. (2005) and Portegies Zwart, McMillan & Makino (2007), with a recent review available by Hut et al. (2007) and two text books have been written dealing with computational and more general aspects of the physics of dense stellar systems (Aarseth 2003; Heggie & Hut 2003).

The six-dimensional structure of a pressure-supported stellar system at time t is conveniently described by the phase-space distribution function, $f(\boldsymbol{r}, \boldsymbol{v}; t)$, where $\boldsymbol{r}$ and $\boldsymbol{v}$ are the phase-space variables and

$$\mathrm{d}N = f(\boldsymbol{r}, \boldsymbol{v}; t)\, d^3x\, d^3v \tag{8.28}$$

is the number of stars in 6D phase-space volume element $d^3x\, d^3v$. In the case of a steady state, the Jeans theorem (Binney & Tremaine 1987, their Sect. 4.4) allows us to express f in terms of the integrals of motion, i.e. the energy and angular momentum. The phase-space distribution function can then be written as

$$f = f(\boldsymbol{r}, \boldsymbol{v}) = f(\epsilon_e, l), \tag{8.29}$$

where

$$\epsilon_e = \frac{1}{2}\, v^2 + \Phi(\boldsymbol{r}) \tag{8.30}$$

is the specific energy of a star and

$$l = |\boldsymbol{r} \times \boldsymbol{v}| \tag{8.31}$$

is the specific orbital angular momentum of a star. The Poisson equation is

$$\nabla^2 \Phi(\boldsymbol{r}) = 4\,\pi\, G\, \rho_m(\boldsymbol{r}) = 4\,\pi\, G \int_{\text{allspace}} m\, f\, d^3 v, \tag{8.32}$$

or in spherical symmetry,

$$\frac{1}{r^2}\frac{\mathrm{d}}{\mathrm{d}r}\left(r^2\,\frac{\mathrm{d}\Phi}{\mathrm{d}r}\right) = 4\,\pi\, G \int_{\text{allspace}} f_m \left(\frac{1}{2}v^2 + \Phi, |\boldsymbol{r} \times \boldsymbol{v}|\right) d^3 v, \tag{8.33}$$

where f_m is the phase-space mass-density of all matter and is equal to $m\, f$ for a system with equal-mass stars. Most pressure-supported systems have a near-spherical shape and so in most numerical work it is convenient to assume spherical symmetry.

For convenience it is useful to introduce the relative potential,[6]

$$\Psi \equiv -\Phi + \Phi_0 \tag{8.34}$$

and the relative energy

$$\mathcal{E} \equiv -\epsilon_e + \Phi_0 = \Psi - \frac{1}{2}v^2, \tag{8.35}$$

where Φ_0 is a constant so that $f > 0$ for $\mathcal{E} > 0$ and $f = 0$ for $\mathcal{E} \leq 0$. The Poisson equation becomes $\nabla^2 \Psi = -4\,\pi\, G\, \rho_m$ subject to the boundary condition $\Psi \to \Phi_0$ as $\boldsymbol{r} \to \infty$.

One important property of stellar systems is the anisotropy of their velocity distribution function. We define the anisotropy parameter

$$\beta(r) \equiv 1 - \frac{\overline{v_\theta^2}}{\overline{v_r^2}}, \tag{8.36}$$

where $\overline{v_\theta^2}, \overline{v_r^2}$ are the mean squared tangential and radial velocities at a particular location $\boldsymbol{r}$, respectively. It follows that systems with $\beta = 0$ everywhere have an isotropic velocity distribution function.

If f only depends on the energy the mean squared radial and tangential velocities are, respectively,

$$\overline{v_r^2} = \frac{1}{\rho} \int_{\text{all vel.}} v_r^2\, f \left[\Psi - \frac{1}{2}\left(v_r^2 + v_\theta^2 + v_\phi^2\right)\right]\, \mathrm{d}v_r\, \mathrm{d}v_\theta\, \mathrm{d}v_\phi \tag{8.37}$$

[6]The following discussion is based on Binney & Tremaine (1987).

and

$$\overline{v_\theta^2} = \frac{1}{\rho}\int_{\rm all\ vel.} v_\theta^2\, f\left[\Psi - \frac{1}{2}\left(v_r^2+v_\theta^2+v_\phi^2\right)\right]\,{\rm d}v_r\,{\rm d}v_\theta\,{\rm d}v_\phi. \tag{8.38}$$

If the labels θ and r are exchanged in (8.38), it can be seen that one arrives at (8.37). Equations (8.37) and (8.38) are thus identical, apart from the labelling. Thus if $f = f(\mathcal{E})$, $\beta = 0$ and the velocity distribution function is isotropic.

If f depends on the energy and the orbital angular momentum of the stars ($|\boldsymbol{l}| = |\boldsymbol{r}\times\boldsymbol{v}|$), then the mean squared radial and tangential velocities are, respectively,

$$\overline{v_r^2} = \frac{1}{\rho}\int_{\rm all\ vel.} v_r^2\, f\left[\Psi - \frac{1}{2}\left(v_r^2+v_\theta^2+v_\phi^2\right), r\sqrt{v_\theta^2+v_\phi^2}\right]\,{\rm d}v_r\,{\rm d}v_\theta\,{\rm d}v_\phi \tag{8.39}$$

and

$$\overline{v_\theta^2} = \frac{1}{\rho}\int_{\rm all\ vel.} v_\theta^2\, f\left[\Psi - \frac{1}{2}\left(v_r^2+v_\theta^2+v_\phi^2\right), r\sqrt{v_\theta^2+v_\phi^2}\right]\,{\rm d}v_r\,{\rm d}v_\theta\,{\rm d}v_\phi. \tag{8.40}$$

If the labels θ and r are exchanged in (8.40), it can be seen that this time one does not arrive at (8.39). Thus if $f = f(\mathcal{E}, l)$, then $\beta \neq 0$ and the velocity distribution function is not isotropic. This serves to demonstrate an elementary but useful property of the phase-space distribution function.

A very useful series of distribution functions can be arrived at from the simple form

$$f_m(\mathcal{E}) = \begin{cases} F\,\mathcal{E}^{n-\frac{3}{2}} & : \quad \mathcal{E} > 0, \\ 0 & : \quad \mathcal{E} \leq 0. \end{cases} \tag{8.41}$$

The mass density,

$$\rho_m(r) = 4\,\pi\,F\int_0^{\sqrt{2\,\Psi}}\left(\Psi - \frac{1}{2}v^2\right)^{n-\frac{3}{2}}\,v^2\,{\rm d}v, \tag{8.42}$$

where the upper integration bound is given by the escape condition, $\mathcal{E} = \Psi - (1/2)v^2 = 0$. Substituting $v^2 = 2\,\Psi\cos^2\theta$ for some θ leads to

$$\rho_m(r) = \begin{cases} c_n\,\Psi^n & : \quad \Psi > 0, \\ 0 & : \quad \Psi \leq 0. \end{cases} \tag{8.43}$$

For c_n to be finite, $n > 1/2$, i.e. homogeneous ($n = 0$) systems are excluded.

The Lane–Emden equation follows from the spherically symmetric Poisson equation after introducing dimensionless variables $s = r/b, \psi = \Psi/\Psi_0$, where $b = (4\,\pi\,G\,\Psi_0^{n-1}\,c_n)^{-1/2}$ and $\Psi_0 = \Psi(0)$,

$$\frac{1}{s^2}\frac{\rm d}{{\rm d}s}\left(s^2\frac{{\rm d}\psi}{{\rm d}s}\right) = \begin{cases} -\psi^n & : \quad \psi > 0, \\ 0 & : \quad \psi \leq 0. \end{cases} \tag{8.44}$$

H. Lane and R. Emden worked with this equation in the context of self-gravitating polytropic gas spheres, which have an equation of state

$$p = K\,\rho_m^{\gamma}, \tag{8.45}$$

where K is a constant and p the pressure. It can be shown that $\gamma = 1 + 1/n$. That is, the density distribution of a stellar polytrope of index n is the same as that of a polytropic gas sphere with index γ.

The natural boundary conditions to be imposed on (8.44) are at $s = 0$,

1. $\psi = 1$, because $\Psi(0) = \Psi_0$ and
2. $\mathrm{d}\psi/\mathrm{d}s = 0$ because the gravitational force must vanish at the centre.

Analytical solutions to the Lane–Emden equation are possible only for a few values of n, and we remember that a homogeneous ($n = 0$) stellar density distribution has already been excluded as a viable solutions of the general power-law phase-space distribution function.

The Plummer Model

A particularly useful case is

$$\psi = \frac{1}{\sqrt{1 + \frac{1}{3}\,s^2}}. \tag{8.46}$$

It follows immediately that this is a solution of the Lane–Emden equation for $n = 5$ and it also satisfies the two boundary conditions above and so constitutes a physically sensible potential. By integrating the Poisson equation, it can be shown that the total mass of this distribution function is finite,

$$M_\infty = \sqrt{3}\,\Psi_0\,b/G, \tag{8.47}$$

although the density distribution has no boundary. The distribution function is

$$f_m(\mathcal{E}) = \begin{cases} F\,\left(\Psi - \frac{1}{2}\,v^2\right)^{\frac{7}{2}} & , \quad v^2 < 2\Psi, \\ 0 & , \quad v^2 \geq 2\Psi, \end{cases} \tag{8.48}$$

with the relative potential

$$\Psi = \frac{\Psi_0}{\sqrt{1 + \frac{1}{3}\left(\frac{r}{b}\right)^2}} \tag{8.49}$$

and density law

$$\rho_m = \frac{\rho_{m,0}}{\left(1 + \frac{1}{3}\left(\frac{r}{b}\right)^2\right)^{\frac{5}{2}}} \tag{8.50}$$

with the above total mass. This density distribution is known as the Plummer model, named after Plummer (1911) who showed that the density distribution that results from this model provides a reasonable and, in particular, very simple analytical description of globular clusters. The Plummer model is, in

fact, a work-horse for many applications in stellar dynamics because many of its properties such as the projected velocity dispersion profile can be calculated analytically. Such formulae are useful for checking numerical codes used to set up models of stellar systems.

Properties of the Plummer Model

Some useful analytical results can be derived for the Plummer density law (see also Heggie & Hut 2003, their p. 73 for another compilation). For the Plummer law of mass $M_{\rm ecl}$, the mass-density profile (8.50) can be written as

$$\rho_m(r) = \frac{3\,M_{\rm ecl}}{4\,\pi\,r_{\rm pl}^3}\,\frac{1}{\left[1+\left(\frac{r}{r_{\rm pl}}\right)^2\right]^{\frac{5}{2}}}, \tag{8.51}$$

where $r_{\rm pl}$ is the Plummer scale length. The central number density is thus

$$\rho_{\rm c} = \frac{3\,N}{4\,\pi\,r_{\rm pl}^3}. \tag{8.52}$$

The mass within radius r follows from $M(r) = 4\,\pi\,\int_0^r \rho_m(r')\,r'^2\,{\rm d}r'$,

$$M(r) = M_{\rm ecl}\,\frac{\left(\frac{r}{r_{\rm pl}}\right)^3}{\left[1+\left(\frac{r}{r_{\rm pl}}\right)^2\right]^{\frac{3}{2}}}. \tag{8.53}$$

Thus,

$r_{\rm pl}$ contains 35.4% of the mass,
$2\,r_{\rm pl}$ contain 71.6%,
$5\,r_{\rm pl}$ contain 94.3% and
$10\,r_{\rm pl}$ contain 98.5% of the total mass.

For the half-mass radius we have

$$r_{\rm h} = (2^{\frac{2}{3}}-1)^{-\frac{1}{2}}\,r_{\rm pl} \approx 1.305\,r_{\rm pl}. \tag{8.54}$$

The projected surface mass density, $\Sigma_M(R) = 2\,\int_0^\infty \rho_m(r)\,{\rm d}z$, where R is the projected radial distance from the cluster centre and Z is the integration variable along the line-of-sight ($r^2 = R^2 + Z^2$) is

$$\Sigma_\rho(R) = \frac{M_{\rm ecl}}{\pi\,r_{\rm pl}^2}\,\frac{1}{\left[1+\left(\frac{R}{r_{\rm pl}}\right)^2\right]^2}. \tag{8.55}$$

We assume there is no mass segregation so that the mass-to-light ratio, $\Upsilon \equiv (M/L)$, measured in some photometric system is independent of radius. The integrated light within projected radius R is

$$I(R) = (1/\Upsilon) \int_0^R \Sigma_\rho(R')\, 2\,\pi\, R'\, \mathrm{d}R', \tag{8.56}$$

$$I(R) = \frac{M_{\rm ecl}\, r_{\rm pl}^2}{\Upsilon} \left[\frac{1}{r_{\rm pl}^2} - \frac{1}{R^2 + r_{\rm pl}^2} \right]. \tag{8.57}$$

Thus, $r_{\rm pl}$ is the half-light radius of the projected star cluster, $I(r_{\rm pl}) = 0.5\, I(\infty)$.

In the above equations $\rho(r) = \rho_m(r)/\overline{m}$, $N(r) = M(r)/\overline{m}$ and $\Sigma_n = \Sigma_\rho/\overline{m}$ are, respectively, the stellar number density, the number of stars within radius r and the projected surface number density profile if there is no mass segregation within the cluster. Thus the average stellar mass, $\overline{m}$, is constant.

The velocity dispersion can be calculated at any radius from the Jeans equation (8.120). For an isotropic velocity distribution ($\sigma_\theta^2 = \sigma_\phi^2 = \sigma_r^2$), such as the Plummer model, the Jeans equation yields

$$\sigma_r^2(r) = \frac{1}{\rho(r)} \int_r^\infty \rho(r')\, \frac{G\, M(r')}{r^2}\, \mathrm{d}r', \tag{8.58}$$

because $\mathrm{d}\phi(r)/\mathrm{d}r = GM(r)/r^2$ and the integration bounds have been chosen to make use of the vanishing $\rho_m(r)$ as $r \to \infty$. Note that the above equation is also valid if $M(r)$ consists of more than one spherical component such as a distinct core plus an extended halo. Combining (8.51), (8.53) and (8.58) we are led to

$$\sigma^2(r) = \left(\frac{G\, M_{\rm ecl}}{2\, r_{\rm pl}} \right) \frac{1}{\left[1 + \left(\frac{r}{r_{\rm pl}} \right)^2 \right]^{\frac{1}{2}}}, \tag{8.59}$$

where $\sigma(r)$ is the three-dimensional velocity dispersion of the Plummer sphere at radius r, $\sigma^2(r) = \sum_{k=r,\theta,\phi} \sigma_k^3(r)$ or $\sigma^2(r) = 3\,\sigma_{\rm 1D}^2(r)$ because isotropy is assumed.

A star with mass m positioned at r and with speed $v = \left(\sum_{k=1}^3 v_k^2 \right)^{1/2}$ can escape from the cluster if it has a total energy $e_{\rm bind} = e_{\rm kin} + e_{\rm pot} = 0.5\, m\, v^2 + m\, \phi(r) \geq 0$ so that $v \geq v_{\rm esc}(r)$. So the escape speed at radius r is $v_{\rm esc}(r) = \sqrt{2\,|\phi(r)|}$. The potential at r is given by the mass within r plus the potential contributed by the surrounding matter. It is calculated by integrating the contributions from each radial mass shell,

$$\begin{aligned} \phi(r) &= -\left[G\, \frac{M(r)}{r} + \int_r^\infty G\, \frac{1}{r'}\, \rho(r')\, 4\,\pi\, r'^2\, \mathrm{d}r' \right], \\ &= -\left(\frac{G\, M_{\rm ecl}}{r_{\rm pl}} \right) \frac{1}{[1 + (r/r_{\rm pl})^2]^{1/2}}. \end{aligned} \tag{8.60}$$

so that

$$v_{\rm esc}(r) = \left(\frac{2\, G\, M_{\rm ecl}}{r_{\rm pl}} \right)^{1/2} \frac{1}{[1 + (r/r_{\rm pl})^2]^{1/4}}. \tag{8.61}$$

The circular speed, v_c, of a star moving on a circular orbit at a distance r from the cluster centre is obtained from centrifugal acceleration, $v_c^2/r = \mathrm{d}\phi(r)/\mathrm{d}r = G\,M(r)/r^2$,

$$v_c^2 = \left(\frac{G\,M_{\rm ecl}}{r_{\rm pl}}\right)\frac{(r/r_{\rm pl})^2}{[1+(r/r_{\rm pl})^2]^{3/2}}. \tag{8.62}$$

In many but not all instances of interest, the initial cluster model is chosen to be in the state of virial equilibrium. That is, the kinetic and potential energies of each star balance so that the whole cluster is stationary. The scalar virial theorem,

$$2\,K + W = 0, \tag{8.63}$$

where K and W are the total kinetic and potential energy of the cluster,[7]

$$\begin{aligned} K &= \frac{1}{2}\int_0^\infty \rho(r)\,\sigma^2(r)\,4\pi r^2\mathrm{d}r, \\ &= \frac{3\pi}{64}\,\frac{G\,M_{\rm ecl}^2}{r_{\rm pl}}, \quad \text{for the Plummer sphere,} \qquad (8.64) \\ W &= \frac{1}{2}\int_0^\infty \phi(r)\,\rho(r)\,4\pi r^2\mathrm{d}r, \\ &= -\frac{3\pi}{32}\,\frac{G\,M_{\rm ecl}^2}{r_{\rm pl}} \quad \text{for the Plummer sphere.} \qquad (8.65) \end{aligned}$$

The total, or binding, energy of the cluster, $E_{\rm tot} = W + K$, is

$$E_{\rm tot} = -K = \frac{1}{2}\,W. \tag{8.66}$$

The characteristic three-dimensional velocity dispersion of a cluster can be defined as $\sigma_{\rm cl}^2 \equiv 2\,K/M_{\rm ecl}$ so that

$$\begin{aligned} \sigma_{\rm cl}^2 &= \frac{3\,\pi}{32}\,\frac{G\,M_{\rm ecl}}{r_{\rm pl}}, \qquad (8.67) \\ &\equiv \frac{G\,M_{\rm ecl}}{r_{\rm grav}}, \qquad (8.68) \\ &\equiv s^2\,\left(\frac{G\,M_{\rm ecl}}{2\,r_{\rm h}}\right), \qquad (8.69) \end{aligned}$$

which introduces the gravitational radius of the cluster, $r_{\rm grav} \equiv G\,M_{\rm ecl}^2/|W|$. For the Plummer sphere $r_{\rm grav} = (32/3\,\pi)r_{\rm pl} = 3.4\,r_{\rm pl}$ and the structure factor

$$\begin{aligned} s &= \left(\frac{6\times 1.305\,\pi}{32}\right)^{\frac{1}{2}}, \\ &\approx 0.88. \qquad (8.70) \end{aligned}$$

[7] Equation (3.251.4) on p. 295 of Gradshteyn & Ryzhik (1980) is useful to solve the integrals for the Plummer sphere.

We define the virial ratio by

$$Q = \frac{K}{|W|}, \tag{8.71}$$

so that a cluster can initially be in three possible states

$$Q \begin{cases} = \frac{1}{2} & , \text{ virial equilibrium,} \\ > \frac{1}{2} & , \text{ expanding,} \\ < \frac{1}{2} & , \text{ collapsing.} \end{cases} \tag{8.72}$$

Note that if initially $Q < 1/2$, the value $Q = 1/2$ will be reached temporarily during collapse, after which Q increases further until the cluster settles in virial equilibrium after this violent relaxation phase (Binney & Tremaine 1987, p. 271).

The characteristic crossing time through the Plummer cluster,

$$t_{\rm cr} \equiv \frac{2\,r_{\rm pl}}{\sigma_{\rm 1D,cl}}, \tag{8.73}$$

$$= \left(\frac{128}{\pi\,G}\right)^{\frac{1}{2}}\, M_{\rm ecl}^{-\frac{1}{2}}\, r_{\rm pl}^{\frac{3}{2}}, \tag{8.74}$$

with the characteristic one-dimensional velocity dispersion, $\sigma_{\rm 1D,cl} = \sigma_{\rm cl}/\sqrt{3}$.

Observationally, the core radius is that radius where the projected surface density falls to half its central value. For a real cluster it is much easier to determine than the other characteristic radii. For the Plummer sphere,

$$R_{\rm core} = \left(\sqrt{2} - 1\right)^{\frac{1}{2}}\, r_{\rm pl} = 0.64\, r_{\rm pl}, \tag{8.75}$$

from (8.55), with the assumption that the mass-to-light ratio, Υ, is independent of radius. For a King model

$$R_{\rm core}^{king} = \left(\frac{9}{4\pi\,G}\,\frac{\sigma^2}{\rho_m(0)}\right)^{\frac{1}{2}}, \tag{8.76}$$

is the King radius. From (8.59), $\sigma^2(0) = G\,M_{\rm ecl}/(2\,r_{\rm pl})$ and from (8.51), $\rho_m(0) = 3\,M_{\rm ecl}/(4\pi\,r_{\rm pl}^3)$ so that

$$r_{\rm pl} = \left(\frac{6}{4\pi\,G}\,\frac{\sigma(0)^2}{\rho_m(0)}\right)^{\frac{1}{2}} = 0.82\; R_{\rm core}^{\rm king}. \tag{8.77}$$

The Singular Isothermal Model

Another useful set of distribution functions can be arrived at by considering $n = \infty$. The Lane–Emden equation is not well defined in this limit, but for a

polytropic gas sphere (8.45) implies $\gamma \to 1$ as $n \to \infty$. Thus $p = K\,\rho_m$, which is the equation of state of an isothermal ideal gas with $K = k_{\rm B}\,T/m_{\rm p}$, where $k_{\rm B}$ is Boltzmann's constant, T the temperature and $m_{\rm P}$ the mass of a gas particle. From the equation of hydrostatic support, $\mathrm{d}p/\mathrm{d}r = -\rho_m(G\,M(r)/r^2)$, where $M(r)$ is the mass within r, the following equation can be derived

$$\frac{\mathrm{d}}{\mathrm{d}r}\left(r^2\frac{\mathrm{d}\ln\rho_m}{\mathrm{d}r}\right) = -\frac{G\,m_{\rm p}}{k_{\rm B}\,T}\,4\,\pi\,r^2\,\rho_m. \tag{8.78}$$

For a distribution function (our ansatz)

$$f_m(\mathcal{E}) = \frac{\rho_{m,1}}{(2\,\pi\,\sigma^2)^{\frac{3}{2}}}\,e^{\frac{\mathcal{E}}{\sigma^2}}, \tag{8.79}$$

where σ^2 is a new quantity related to a velocity dispersion and $\mathcal{E} = \Psi - v^2/2$, one obtains, from $\rho_m = \int f_m(\mathcal{E})\,4\,\pi\,v^2\,\mathrm{d}v$,

$$\Psi(r) = \ln\left(\frac{\rho_m(r)}{\rho_{m,1}}\right)\sigma^2. \tag{8.80}$$

From the Poisson equation it then follows that

$$\sigma = \mathrm{const} = \frac{k_{\rm B}\,T}{m_p} \tag{8.81}$$

for consistency with (8.78).

Therefore, the structure of an isothermal, self-gravitating sphere of ideal gas is identical to the structure of a collisionless system of stars whose phase-space mass-density distribution function is given by (8.79). Note that $f(\mathcal{E})$ is non-zero at all $\mathcal{E}$ (cf. King's models below).

The number-distribution function of velocities is $F(v) = \int_{\mathrm{all}\,\boldsymbol{x}} f(\mathcal{E})\,d^3x$, i.e.

$$F(v) = F_0\,e^{-\frac{v^2}{2\,\sigma^2}}. \tag{8.82}$$

This is the Maxwell–Boltzmann distribution, which results from the kinetic theory of atoms in a gas at temperature T that are allowed to bounce off each other elastically. This exact correspondence between a stellar-dynamical system and a gaseous polytrope holds only for an isothermal case ($n = \infty$).

The total number of stars in the system is $N_{\rm tot} = N_{\rm tot}\int_0^\infty F(v)\,4\,\pi\,v^2\,\mathrm{d}v$ and the number of stars in the speed interval v to $v + \mathrm{d}v$ is

$$dN = F(v)\,4\,\pi\,v^2\,\mathrm{d}v = N_{\rm tot}\frac{1}{(2\,\pi\sigma^2)^{\frac{3}{2}}}e^{-\frac{v^2}{2\,\sigma^2}}\,4\,\pi\,v^2\,\mathrm{d}v, \tag{8.83}$$

which is the Maxwell–Boltzmann distribution of speeds. The mean-square speed of stars at a point in the isothermal sphere is

$$\overline{v^2} = \frac{4\,\pi\,\int_0^\infty \sigma^2\,F(v)\,\mathrm{d}v}{4\,\pi\,\int_0^\infty F(v)\,\mathrm{d}v} = 3\sigma^2 \tag{8.84}$$

and the 1D velocity dispersion is $\sigma_{1\mathrm{D}} = \sigma_\alpha = \sigma$, where $\alpha = r, \theta, \phi, x, y, z, ...$

To obtain the radial mass-density of this model, the ansatz $\rho_m = C\,r^{-b}$ together with the Poisson equation (8.78) implies

$$\rho_m(r) = \frac{\sigma^2}{2\,\pi\,G}\,\frac{1}{r^2}. \tag{8.85}$$

That is, a singular isothermal sphere.

The Isothermal Model

The above model has a singularity at the origin. This is unphysical. In order to remove this problem, it is possible to force the central density to be finite. To this end new dimensionless variables are introduced, $\tilde{\rho_m} \equiv \rho_m/\rho_{m,0}$, $\tilde{r} \equiv r/r_0$. The density $\tilde{\rho_m}$ is the finite central density, while $r_0 = R_{\mathrm{core}}^{\mathrm{King}}$ is the King radius (8.76) at which the projected density falls to 0.5013 (i.e. about half) its central value. The radius r_0 is also sometimes called the core radius (but see further below for King models on p. 211). The Poisson equation (8.78) then becomes

$$\frac{\mathrm{d}}{\mathrm{d}\tilde{r}}\left(\tilde{r}^2\,\frac{\mathrm{d}\ln\tilde{\rho_m}}{\mathrm{d}\tilde{r}}\right) = -9\,\tilde{\rho_m}\,\tilde{r}^2. \tag{8.86}$$

This differential equation must be solved numerically for $\tilde{\rho_m}(\tilde{r})$ subject to the boundary conditions (as before),

$$\tilde{\rho_m}(\tilde{r}=0) = 1, \quad \left.\frac{\mathrm{d}\tilde{\rho_m}}{\mathrm{d}\tilde{r}}\right|_{\tilde{r}=0} = 0. \tag{8.87}$$

The solution is the isothermal sphere.

By imposing physical reality (central non-singularity) on our mathematical ansatz, we end up with a density profile that cannot be arrived at analytically but only numerically. The isothermal density sphere must be tabulated in the computer with entries such as

$$r/r_0, \quad \log_{10}\left(\frac{\rho}{\rho_0}\right) \quad \text{and} \quad \log_{10}\left(\frac{\Sigma}{r_0\,\rho_0}\right), \tag{8.88}$$

where Σ is the projected density (Binney & Tremaine 1987, for example see their Table 4.1 and Fig. 4.7 of). The circular velocity, $v_c(r) = G\,M(r)/r$ of the isothermal sphere is obtained by integrating Poisson's equation (8.78) from $r = 0$ to $r = r'$ with $r^2(\mathrm{d}\ln\rho_m/\mathrm{d}r) = -(G/\sigma^2)\,M(r)$ and

$$v_c^2(r) = -\sigma^2\,\frac{\mathrm{d}\ln\rho_m(r)}{\mathrm{d}\ln r}. \tag{8.89}$$

Numerical solution of differential (8.86) shows that $v_c \to \sqrt{2}\,\sigma$ (constant) for large r.

The isothermal sphere is a useful model for describing elliptical galaxies, within a few core radii, and disc galaxies because of the constant rotation curve. However, combining the two equations for v_c^2 above, one finds that $M(r) \approx (2\,\sigma^2/G)\,r$ for large r, i.e. the isothermal sphere has an infinite mass as it is not bounded.

The Lowered Isothermal or King Model

We have thus seen that the class of models with $n = \infty$ contain as the simplest case the singular isothermal sphere. By forcing the central density to be finite, we are led to the isothermal sphere which, however, has an infinite mass. The final model considered here within this class is the lowered isothermal model, or the King model,[8] which forces not only a finite central density but also a cutoff in radius. These have a distribution function similar to that of the isothermal model, except for a cutoff in energy,

$$f_m(\mathcal{E}) = \begin{cases} \frac{\rho_{m,1}}{(2\,\pi\,\sigma^2)^{\frac{3}{2}}}\,\left(e^{\frac{\mathcal{E}}{\sigma^2}} - 1\right) & : \quad \mathcal{E} > 0, \\ 0 & : \quad \mathcal{E} \leq 0. \end{cases} \tag{8.90}$$

The density distribution becomes

$$\rho_m = \rho_{m,1}\,\left[e^{\frac{\Psi}{\sigma^2}}\,\mathrm{erf}\left(\frac{\sqrt{\Psi}}{\sigma}\right) - \sqrt{\frac{4\,\Psi}{\pi\,\sigma^2}}\,\left(1 + \frac{2\,\Psi}{3\sigma^2}\right)\right] \tag{8.91}$$

with integration only to $\mathcal{E} = 0$ as before. The Poisson (8.78) becomes

$$\frac{\mathrm{d}}{\mathrm{d}\tilde{r}}\,\left(\tilde{r}^2\,\frac{\mathrm{d}\ln\tilde{\rho_m}}{\mathrm{d}\tilde{r}}\right) = -4\,\pi\,G\,\rho_{m,1}\,r^2\,\left[e^{\frac{\Psi}{\sigma^2}}\,\mathrm{erf}\left(\frac{\sqrt{\Psi}}{\sigma}\right) - \sqrt{\frac{4\,\Psi}{\pi\,\sigma^2}}\,\left(1 + \frac{2\,\Psi}{3\sigma^2}\right)\right]. \tag{8.92}$$

Again, this differential equation must be solved numerically for $\Psi(r)$ subject to the boundary conditions,

$$\Psi(0), \quad \frac{\mathrm{d}\Psi}{\mathrm{d}r}\,|_{r=0} = 0. \tag{8.93}$$

The density vanishes at $r = r_{\rm tid}$ (the tidal radius), where $\Psi(r = r_{\rm tid}) = 0$ also. A King model is thus limited in mass and has a finite central density,

[8] Note that King (1962) suggested a three-parameter (mass, core radius and cut-off/tidal radius), empirical, projected (2D) density law that fits globular clusters very well. These do not have information on the velocity structure of the clusters. The King (non-analytical) 6D models, which are solutions of the Jeans equation ((8.120) below) and discussed here, are published by King (1966).

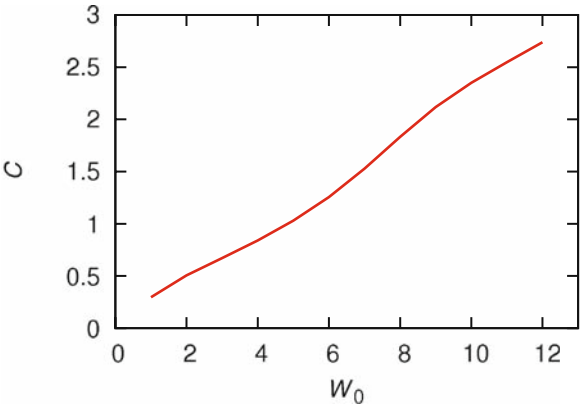

Fig. 8.5. The King concentration parameter W_0 as a function of c (cf. with Fig. 4–10 of Binney & Tremaine 1987). This figure has been produced by Andreas Küpper

but the parameter σ is not the velocity dispersion. It is rather related to the depth of the potential via the concentration parameter

$$W_o \equiv \frac{\Psi(0)}{\sigma^2}. \tag{8.94}$$

The concentration is defined as

$$c \equiv \log_{10}\left(\frac{r_{\rm tid}}{r_o}\right). \tag{8.95}$$

For globular clusters, $3 < W_o < 9,\ 0.75 < c < 1.75$ and the relation between W_o and c is plotted in Fig. 8.5. Note also that the true core radius defined as $\Sigma(R_c) = (1/2)\,\Sigma(0)$, where $\Sigma(R)$ is the projected density profile and R is the projected radius, is unequal in general to the King radius, r_0 (8.76). Finally, it should be emphasised that it is not physical to use an arbitrary $r_{\rm tid}$. The tidal radius must always match the value dictated by the cluster mass and the host galaxy (e.g. (8.3)).

8.2.2 Comparison: Plummer vs King Models

The above discussion has served to show how various popular models can be followed through from a power-law distribution function (8.41) with different indices n. The Plummer model (p. 205) and the King model (p. 212) are particularly useful for describing star clusters. The Plummer model is determined by two parameters, the mass, M, and the scale radius, $r_{\rm h} \approx 1.305\, r_{\rm pl}$. The King model requires three parameters, M, a scale radius, $r_{\rm h}$, and a concentration parameter, W_0 or c. Which subset of parameters yield models that are similar in terms of the overall density profile?

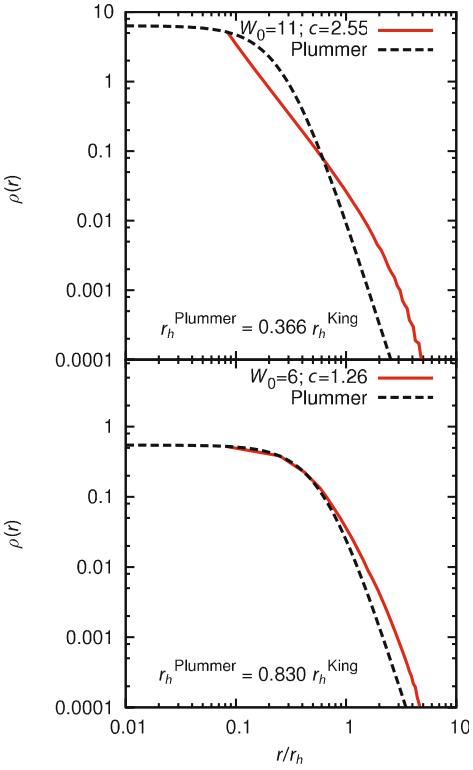

Fig. 8.6. Comparison of a King model (*solid curve*) with a Plummer model (*dashed curve*). Both have the same mass and that Plummer model is sought, which minimises the unweighted reduced chi-squared between the two models. The *upper panel* shows a high-concentration King model with $c = 2.55$ and $W_0 = 11$ and the best-fit Plummer model has $r_h^{\rm Plummer} = 0.366\, r_h^{King}$ ($r_h \equiv r_h$), as stated in the panel. The *lower panel* compares the two best matching models for the case of an intermediate-concentration King model. This figure was produced by Andreas Küpper

To answer this, the mass is set to be constant. King models with different W_0 and $r_{\rm h}$ are computed and Plummer models are sought, which minimise the reduced chi-squared value between the two density profiles. Figure 8.6 shows two examples of best-matching density profiles, and Fig. 8.7 reveals the family of Plummer profiles that best match King models with different concentrations. Note that a good match between the two is only obtained for intermediate-concentration King models ($2.5 \leq W_0 \leq 7.5$).

8.2.3 Discretisation

To set up a computer model of a stellar system with N particles (e.g. stars), the distribution functions need to be sampled N times. The relevant distribution

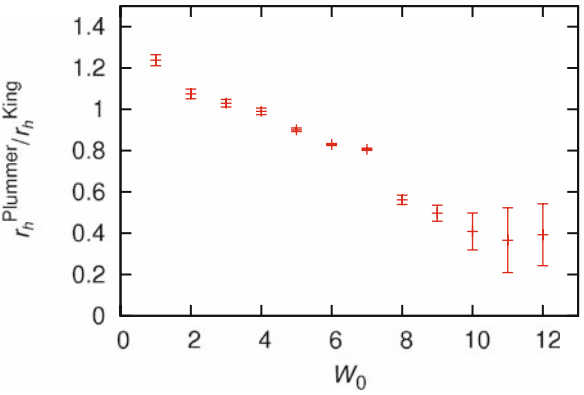

Fig. 8.7. The ratio $r_h^{\rm Plummer}/r_h^{\rm King}$ ($r_h \equiv r_h$) for the best-matching Plummer and King models (Fig. 8.6) are plotted as a function of the King concentration parameter W_0. The uncertainties are unweighted reduced chi-squared values between the two density profiles. It is evident that there are no well-matching Plummer models for low- ($c < 2.5$) and high-concentration ($c > 7.5$) King models. This figure was produced by Andreas Küpper

functions are the phase-space distribution function, the stellar initial mass function and the three distribution functions governing the properties of binary stars (periods, mass-ratios and eccentricities).

Assume the distribution function depends on the variable $\zeta_{\rm min} \leq \zeta \leq \zeta_{\rm max}$ (e.g. stellar mass, m). There are various ways of sampling from a distribution function (Press et al. 1992), but the most efficient way is to use a generating function if one exists. Consider the probability $X(\zeta)$ of encountering a value for the variable in the range $\zeta_{\rm min}$ to ζ,

$$X(\zeta) = \int_{\zeta_{\rm min}}^{\zeta} p(\zeta')\,{\rm d}\zeta', \tag{8.96}$$

with $X(\zeta_{\rm min}) = 0 \leq X(\zeta) \leq X(\zeta_{\rm max}) = 1$, and $p(\zeta)$ is the distribution function normalised so that the latter equal sign holds ($X = 1$). $p(\zeta)$ is the probability density. The inverse of (8.96), $\zeta(X)$, is the generating function. It is a one-to-one map of the uniform distribution $X \in [0,1]$ to $\zeta \in [\zeta_{\rm min}, \zeta_{\rm max}]$. If an analytical inverse does not exist, it can be found numerically in a straightforward manner, for example, by constructing a table of X, ζ and then interpolating this table to obtain a ζ for a given X.

Example: The Power-Law Stellar Mass Function

As an example, consider the distribution function

$$\xi(m) = k\,m^{-\alpha}, \quad \alpha = 2.35; \quad 0.5 \leq \frac{m}{M_\odot} \leq 150. \tag{8.97}$$

The probability density is $p(m) = k_p\, m^{-\alpha}$ and $\int_{0.5}^{150} p(m)\,\mathrm{d}m = 1 \Rightarrow k_p = 0.53$. Thus

$$X(m) = \int_{0.5}^{m} p(m)\,\mathrm{d}m = k_p\,\frac{150^{1-\alpha} - 0.5^{1-\alpha}}{1-\alpha} \tag{8.98}$$

and the generating function for stellar masses becomes

$$m(X) = \left[X\frac{1-\alpha}{k_p} + 0.5^{1-\alpha}\right]^{\frac{1}{1-\alpha}}. \tag{8.99}$$

It is easy to programme this into an algorithm. Obtain a random variate X from a random number generator and use the above generating function to get a corresponding mass, m. Repeat N times.

Generating a Plummer Model

Perhaps the most useful and simplest model of a bound stellar system is the Plummer model (p. 205). It is worth introducing the discretisation of this model in some detail, because analytical formulae go a long way, which is important for testing codes. A condensed form of this material is available in Aarseth, Hénon and Wielen (1974).

The mass within radius r is ($r_{\rm pl} = b$ here)

$$M(r) = \int_0^r \rho_m(r')\,4\,\pi\,r'^2\,\mathrm{d}r' = M_{\rm cl}\,\frac{(r/r_{\rm pl})^3}{\left[1+(r/r_{\rm pl})^2\right]^{\frac{3}{2}}}. \tag{8.100}$$

A number uniformly distributed between zero and one can then be defined,

$$X_1(r) = \frac{M(r)}{M_{\rm cl}} = \frac{\zeta^3}{[1+\zeta^2]}, \tag{8.101}$$

where $\zeta \equiv r/r_{\rm pl}$ and $X_1(r=\infty) = 1$. This function can be inverted to yield the generating function for particle distances distributed according to a Plummer density law,

$$\zeta(X_1) = \left(X_1^{-\frac{2}{3}} - 1\right)^{-\frac{1}{2}}. \tag{8.102}$$

The coordinates of the particles $x, y, z, r^2 = (\zeta\, r_{\rm pl})^2 = x^2 + y^2 + z^2$ can be obtained as follows. For a given particle we already have r. For all possible x and y, z has a uniform distribution, $p(z) = \mathrm{const} = 1/(2\,r)$ over the range $-r \le z \le +r$. Thus, for a second random variate between zero and one,

$$X_2(z) = \int_{-r}^{z} p(z')\,\mathrm{d}z' = \frac{1}{2\,r}\,(z+r)\,, \tag{8.103}$$

with $X_2(+r) = 1$. The generating function for z becomes

$$z(X_2) = 2\,r\,X_2 - r. \tag{8.104}$$

Having obtained r and z, x and y can be arrived at as follows, noting the equation for a circle, $r^2 - z^2 = x^2 + y^2$. Choose a random angle θ, which is uniformly distributed over the range $0 \leq \theta \leq 2\,\pi$. Thus $p(\theta) = 1/(2\,\pi)$ and the third random variate becomes

$$X_3(\theta) = \int_0^\theta \frac{1}{2\,\pi}\,\mathrm{d}\theta' = \frac{\theta}{2\,\pi}. \tag{8.105}$$

The corresponding generating function is

$$\theta(X_3) = 2\,\pi\,X_3. \tag{8.106}$$

Finally,

$$x = \left(r^2 - z^2\right)^{\frac{1}{2}}\,\cos\theta; \quad \text{and} \quad y = \left(r^2 - z^2\right)^{\frac{1}{2}}\,\sin\theta. \tag{8.107}$$

The velocity for each particle cannot be obtained as simply as the positions. In order for the initial stellar system to be in virial equilibrium, the potential and kinetic energy need to balance according to the scalar virial theorem. This is ensured by forcing the velocity distribution function to be that of the Plummer model,

$$f_m(\epsilon_e) = \begin{cases} \left(\frac{24\sqrt{2}}{2\,\pi^3}\,\frac{r_{\rm pl}^2}{(G\,M_{\rm cl})^5}\right)\,(-\epsilon_e)^{\frac{7}{2}} & , \quad \epsilon_e \leq 0, \\ 0 & , \quad \epsilon_e > 0, \end{cases} \tag{8.108}$$

where

$$\epsilon_e(r, v) = \Phi(r) + (1/2)\,v^2 \tag{8.109}$$

is the specific energy per star and

$$\Phi(r) = -\frac{G\,M_{\rm cl}}{r_{\rm pl}}\,\left(1 + \left(\frac{r}{r_{\rm pl}}\right)^2\right)^{-\frac{1}{2}} \tag{8.110}$$

is the potential. Now, the Plummer distribution function can be expressed in terms of r and v,

$$f(r, v) = f_o\,\left(-\Phi(r) - \frac{1}{2}\,v^2\right)^{\frac{7}{2}}, \tag{8.111}$$

for a normalisation constant f_o and dropping the mass subscript, because we assume the positions and velocities do not depend on particle mass. With the escape speed at distance r from the Plummer centre, $v_{\rm esc}(r) = \sqrt{-2\,\Phi(r)} \equiv v/\zeta$, it follows that

$$f(r, v) = f_o\,\left(\frac{1}{2}\,v_{\rm esc}\right)^7\,\left(1 - \zeta^2\right)^{\frac{7}{2}}. \tag{8.112}$$

The number of particles with speeds in the interval v to $v + \mathrm{d}v$ is

$$\mathrm{d}N = f(r, v)\, 4\,\pi\, v^2\, \mathrm{d}v \equiv g(v)\, \mathrm{d}v. \tag{8.113}$$

Thus

$$g(v) = 16\,\pi\, f_o\, \left(\frac{1}{2}\, v_{\rm esc}(r)\right)^9\, \left(1 - \zeta^2(r)\right)^{\frac{7}{2}}\, \zeta^2(r), \tag{8.114}$$

that is,

$$g(\zeta) = g_o\, \zeta^2(r)\, \left(1 - \zeta^2(r)\right)^{\frac{7}{2}}, \tag{8.115}$$

for a normalisation constant g_o determined by demanding that

$$X_4(\zeta = 1) = 1 = \int_0^1 g(\zeta')\, \mathrm{d}\zeta' \tag{8.116}$$

for a fourth random number variate $X_4(\zeta) = \int_0^\zeta g(\zeta')\, \mathrm{d}\zeta'$. It follows that

$$X_4(\zeta) = \frac{1}{2}\, \left(5\,\zeta^3 - 3\,\zeta^5\right). \tag{8.117}$$

This cannot be inverted to obtain an analytical generating function for $\zeta = \zeta(X_4)$. Therefore, numerical methods need to be used to solve (8.117). For example, one way to obtain ζ for a given random variate X_4 is to find the root of the equation $0 = (1/2)\,(5\,\zeta^3 - 3\,\zeta^5) - X_4$, or one can use the Neumann rejection method (Press et al. 1992).

The following procedure can be implemented to calculate the velocity vector of a particle for which r and ζ are already known from above. Compute $v_{\rm esc}(r)$ so that $v = \zeta\, v_{\rm esc}$. Each speed v is then split into its components v_x, v_y, v_z, assuming velocity isotropy using the same algorithm as above for x, y, z:

$$v_z(X_5) = (2\,X_5 - 1)\, v; \quad \theta(X_6) = 2\,\pi\, X_6; \tag{8.118}$$

$$v_x = \sqrt{v^2 - v_z^2}\, \cos\theta; \quad v_y = \sqrt{v^2 - v_z^2}\, \sin\theta. \tag{8.119}$$

Note that a rotating Plummer model can be generated by simply switching the signs of v_x and v_y so that all particles have the same direction of motion in the x, y plane.

As an aside, an efficient numerical method to set up triaxial ellipsoids with or without an embedded rotating disc is described by Boily, Kroupa & Peñarrubia-Garrido (2001).

Generating an Arbitrary Spherical, Non-Rotating Model

In most cases an analytical density distribution is not known (e.g. the King models above). Such numerical models can nevertheless be discretised straightforwardly as follows. Assume that the density distribution, $\rho(r)$, is known. Compute $M(r)$ and $M_{\rm cl}$. Define $X(r) = M(r)/M_{\rm cl}$, as above. We thus

have a numerical grid of numbers $r,\ M(r),\ X(r)$. For a given random variate $X \in [0,1]$, interpolate r from this grid. Compute x, y, z as above.

If the distribution function of speeds is too complex to yield an analytical generating function $X(\zeta)$ for the speeds ζ, we can resort to the following procedure. One of the Jeans equations for a spherical system is

$$\frac{\mathrm{d}}{\mathrm{d}r}\left(\rho(r)\,\sigma_r(r)^2\right) + \frac{\rho(r)}{r}\,\left[2\,\sigma_r^2(r) - \left(\sigma_\theta(r)^2 + \sigma_\phi(r)^2\right)\right] = -\rho(r)\,\frac{\mathrm{d}\Phi(r)}{\mathrm{d}r}. \tag{8.120}$$

For velocity isotropy, $\sigma_r^2 = \sigma_\theta^2 = \sigma_\phi^2$, this reduces to

$$\frac{\mathrm{d}\left(\rho\,\sigma_r^2\right)}{\mathrm{d}r} = -\rho\,\frac{\mathrm{d}\Phi}{\mathrm{d}r}. \tag{8.121}$$

Integrating this by making use of $\rho \to 0$ as $r \to \infty$ and remembering that $\mathrm{d}\Phi/\mathrm{d}r = -G\,M/r^2$,

$$\sigma_r^2(r) = \frac{1}{\rho(r)}\,\int_r^\infty \rho(r')\,\frac{G\,M(r')}{r'^2}\,\mathrm{d}r'. \tag{8.122}$$

For each particle at distance r, a one-dimensional velocity dispersion, $\sigma_r(r)$, is thus obtained. Choosing randomly from a Gaussian distribution with dispersion $\sigma_i, i = r, \theta, \phi, x, y, z$, then gives the velocity components (e.g. v_x, v_y, v_z) for this particle.

Rotating Models

Star clusters are probably born with some rotation because the pre-cluster cloud core is likely to have contracted from a cloud region with differential motions that do not cancel. How large this initial angular momentum content of an embedded cluster is remains uncertain because the dominant motions are random and chaotic owing to the turbulent velocity field of the gas. Once the star-formation process is quenched as a result of gas blow-out (Sect. 8.1.1), the cluster expands. This must imply substantial reduction in the rotational velocity. A case in point is ω Cen, which has been found to rotate with a peak velocity of about $7\,\mathrm{km\,s^{-1}}$ (Pancino et al. 2007, and references therein).

A setup for rotating cluster models is easily made, for instance, by increasing the tangential velocities of stars by a certain factor. A systematic study of relaxation-driven angular momentum re-distribution within star clusters has become available through the work of the group of Rainer Spurzem and Hyung-Mok Lee and the interested reader is directed to that body of work (Kim et al. 2008, and references therein). One important outcome of this work is that core collapse is substantially accelerated in rotating models. The primary reason for this is that increased rotational support reduces the role of support through random velocities for the same cluster dimension. Thus, the relative stellar velocities decrease and the stars exchange momentum and energy more efficiently, enhancing two-body relaxation and thence the approach towards energy equipartition.

8.2.4 Cluster Birth and Young Clusters

Some astrophysical issues related to the initial conditions of star clusters have been raised in Sect. 8.1.1. In order to address most of these issues numerical experiments are required. The very initial phase, the first 0.5 Myr, can only be treated through gas-dynamical computations that, however, lack the numerical resolution for the high-precision stellar-dynamical integrations, which are the essence of collisional dynamics during the gas-free phase of a cluster's life. This gas-free stage sets in with the blow out of residual gas at an age of about 0.5–1.5 Myr. The time 0.5–1.5 Myr is dominated by the physics of stellar feedback and radiation transport in the residual gas as well as energy and momentum transfer to it through stellar outflows. The gas-dynamical computations cannot treat all the physical details of the processes acting during this critical time, which also include early stellar-dynamical processes such as mass segregation and binary–binary encounters.

One successful procedure to investigate the dominant macroscopic physical processes of these stellar-dynamical processes, gas blow-out and the ensuing cluster expansion, through to the long-term evolution of the remnant cluster, is to approximate the residual gas component as a time-varying potential in which the young stellar population is trapped. The pioneering work using this approach has been performed by Lada, Margulis & Dearborn (1984), whereby the earlier numerical work by Tutukov (1978) on open clusters and later N-body computations by Goodwin (1997a,b, 1998) on globular clusters must also be mentioned in this context.

The physical key quantities that govern the emergence of embedded clusters from their clouds and their subsequent appearance are (Baumgardt, Kroupa & Parmentier 2008, Sect. 8.1.1):

- sub-structuring,
- initial mass segregation,
- the dynamical state at feedback termination (dynamical equilibrium?, collapsing? or expanding?),
- the star-formation efficiency, ϵ,
- the ratio of the gas-expulsion time-scale to the stellar crossing time through the embedded cluster, $\tau_{\rm gas}/t_{\rm cross}$ and
- the ratio of the embedded-cluster half-mass radius to its tidal radius, $r_{\rm h}/r_{\rm t}$.

It becomes rather apparent that the physical processes governing the emergence of star clusters from their natal clouds is terribly messy, and the research-field is clearly observationally driven. Observations have shown that star clusters suffer substantial infant weight loss and probably about 90% of all clusters disperse altogether (infant mortality). This result is consistent with the observational insight that clusters form in a compact configuration with a low star-formation efficiency ($0.2 \leq \epsilon \leq 0.4$) and that residual-gas blow-out occurs on a time-scale comparable or even faster than an embedded-cluster crossing time-scale (Kroupa 2005). Theoretical work can give a reasonable

description of these empirical findings by combining some of the above parameters, such as an effective star-formation efficiency as a measure of the amount of gas removed for a cluster of a given stellar mass if this cluster were in dynamical equilibrium at feedback termination, and that the gas and stars were distributed according to the same radial density function with the same scaling radius.

Embedded Clusters: One way to parameterise an embedded cluster is to set up a Plummer model in which the stellar positions follow a density law with the parameters $M_{\rm ecl}$ and $r_{\rm pl}$ and the residual gas is a time-varying Plummer potential initially with the parameters $M_{\rm gas}$ and $r_{\rm pl}$, i.e. modelled with the same radial density law. The effective star-formation efficiency is then given by (8.2). Stellar velocities must then be calculated from a Plummer law with total mass $M_{\rm ecl} + M_{\rm gas}$ following the recipes of Sect. 8.2.3. The gas can be removed by evolving $M_{\rm gas}$ or $r_{\rm pl}$. For example, Kroupa, Aarseth & Hurley (2001) and Baumgardt, Kroupa & Parmentier (2008) assumed the gas mass decreases exponentially after an embedded phase lasting about 0.5 Myr during which the cluster is allowed to evolve in dynamical equilibrium. Bastian & Goodwin (2006), as another example, do not include a gas potential but take the initial velocities of stars to be $1/\sqrt{\epsilon}$ times larger, $v_{\rm embedded} = (1/\sqrt{\epsilon})\, v_{\rm no\ gas}$, to model the effect of instantaneous gas removal. Many variations of these assumptions are possible and Adams (2000), for example, investigated the fraction of stars left in a cluster remnant if the radial scale length of the gas is different to that of the stars, i.e. for a radially dependent star-formation efficiency, $\epsilon(r)$.

Subclustering: Initial subclustering has been barely studied. Scally & Clarke (2002) considered the degree of sub-structuring of the ONC allowed by its current morphology, while Fellhauer & Kroupa (2005) computed the evolution of massive star-cluster complexes, assuming each member cluster in the complex undergoes its own individual gas-expulsion process. McMillan, Vesperini & Portegies Zwart (2007) showed that initially mass-segregated subclusters retain mass segregation upon merging. This is an interesting mechanism for accelerating dynamical mass segregation because it occurs faster in smaller-N systems, which have a shorter relaxation time.

The simplest initial conditions for such numerical experiments are to set up the star-cluster complex (or protoONC-type cluster, for example) as a Plummer model, where each particle is a smaller subcluster. Each subcluster is also a Plummer model, embedded in a gas potential given as a Plummer model. The gas-expulsion process from each subcluster can be treated as above.

Mass Segregation and Gas Blow-Out: The problem of how initially mass-segregated clusters react to gas blow-out has not been studied at all in the past. This is due partially to the lack of convenient algorithms to set up mass-segregated clusters that are in dynamical equilibrium and which do not go into core collapse as soon as the N-body integration begins. An interesting

consequence here is that gas blow-out will unbind mostly the low-mass stars, while the massive stars are retained. These, however, evolve rapidly so that the mass lost from the remnant cluster owing to the evolution of the massive stars can become destructive, enhancing infant mortality.

Ladislav Šubr has developed a numerically efficient method to set up initially mass-segregated clusters close to core-collapse based on a novel concept that uses the potentials of subsets of stars ordered by their mass (Šubr, Kroupa & Baumgardt 2008).[9] An alternative algorithm based on ordering the stars by increasing mass and increasing total energy that leads to total mass segregation, and also to a model that is not in core collapse and which therefore evolves towards core collapse, has been developed by Baumgardt, Kroupa & de Marchi (2008). An application concerning the effect on the observed stellar mass function in globular clusters shows that gas expulsion leads to bottom-light stellar mass functions in clusters with a low concentration, consistent with observational data (Marks, Kroupa & Baumgardt 2008).

8.3 The Stellar IMF

The stellar initial mass function (IMF), $\xi(m)\,\mathrm{d}m$, where m is the stellar mass, is the parent distribution function of the masses of stars formed in one event. Here, the number of stars in the mass interval m to $m + \mathrm{d}m$ is

$$\mathrm{d}N = \xi(m)\,\mathrm{d}m. \tag{8.123}$$

The IMF is, strictly speaking, an abstract theoretical construct because any observed system of N stars merely constitutes a particular representation of this universal distribution function, if such a function exists (Elmegreen 1997; Maíz Apellániz & Úbeda 2005). The probable existence of a unique $\xi(m)$ can be inferred from the observations of an ensemble of systems each consisting of N stars (e.g. Massey 2003). If, after corrections for (a) stellar evolution, (b) unknown multiple stellar systems and (c) stellar-dynamical biases, the individual distributions of stellar masses are similar within the expected statistical scatter, we (the community) deduce that the hypothesis that the stellar mass distributions are not the same can be excluded. That is, we make the case for a universal, standard or canonical stellar IMF within the physical conditions probed by the relevant physical parameters (metallicity, density, mass) of the populations at hand.

Related overviews of the IMF can be found in Kroupa (2002a); Chabrier (2003); Bonnell, Larson & Zinnecker (2007); Kroupa (2007a), and a review with an emphasis on the metal-rich problem is available in Kroupa (2007b). Zinnecker & Yorke (2007) provide an in-depth review of the formation and distribution of massive stars. Elmegreen (2007) discusses the possibility that star-formation occurs in different modes with different IMFs.

[9] The C-language software package *plumix* may be downloaded from the website `http://www.astro.uni-bonn.de/~webaiub/english/downloads.php`.

8.3.1 The Canonical or Standard Form of the Stellar IMF

The canonical stellar IMF is a two-part-power law (8.128). The only structure found with confidence so far is the change of index from the Salpeter/Massey value to a smaller one near $0.5\,M_\odot$[10]

$$\begin{aligned} \xi(m) &\propto m^{-\alpha_i}, \quad i = 1,2 \\ \alpha_1 &= 1.3 \pm 0.3, \quad , \quad 0.08 \le m/M_\odot \le 0.5, \\ \alpha_2 &= 2.3 \pm 0.5, \quad , \quad 0.5 \le m/M_\odot \le m_{\max}, \end{aligned} \tag{8.124}$$

where $m_{\max} \le m_{\max *} \approx 150\,M_\odot$ follows from Fig. 8.1. Brown dwarfs have been found to form a separate population with $\alpha_0 \approx 0.3 \pm 0.5$, (8.129) (Thies & Kroupa 2007).

It has been corrected for bias through unresolved multiple stellar systems in the low-mass ($m < 1\,M_\odot$) regime (Kroupa, Gilmore & Tout 1991) by a multi-dimensional optimisation technique. The general outline of this technique is as follows (Kroupa, Tout & Gilmore 1993). First, the correct form of the stellar-mass–luminosity relation is extracted using observed stellar binaries and theoretical constraints on the location, amplitude and shape of the minimum of its derivative, $\mathrm{d}m/\mathrm{d}M_V$, near $m = 0.3\,M_\odot, M_V \approx 12, M_I \approx 9$ in combination with the observed shape of the nearby and deep Galactic-field stellar luminosity function (LF)

$$\Psi(M_V) = -\left(\frac{\mathrm{d}m}{\mathrm{d}M_V}\right)^{-1} \xi(m), \tag{8.125}$$

where $\mathrm{d}N = \Psi(M_V)\,\mathrm{d}M_V$ is the number of stars in the magnitude interval M_V to $M_V + \mathrm{d}M_V$. Once the semi-empirical mass–luminosity relation of stars, which is an excellent fit to the most recent observational constraints by Delfosse et al. (2000), is established, a model of the Galactic field is calculated with the assumption that a parameterised form for the MF and different values for the scale-height of the Galactic disc and different binary fractions in it. Measurement uncertainties and age and metallicity spreads must also be considered in the theoretical stellar population. Optimisation in this multi-parameter space (MF parameters, scale-height and binary population) against observational data leads to the canonical stellar MF for $m < 1\,M_\odot$.

One important result from this work is the finding that the LF of main-sequence stars has a universal sharp peak near $M_V \approx 12, M_I \approx 9$. It results from changes in the internal constitution of stars that drive a non-linearity in the stellar mass–luminosity relation. A consistency check is then performed as follows. The above MF is used to create young populations of binary systems (Sect. 8.4.2) that are born in modest star clusters consisting of a few hundred stars. Their dissolution into the Galactic field is computed with an

[10]The uncertainties in α_i are estimated from the alpha-plot (Sect. 8.3.2), as shown in Fig. 5 of Kroupa (2002b), to be about 95% confidence limits.

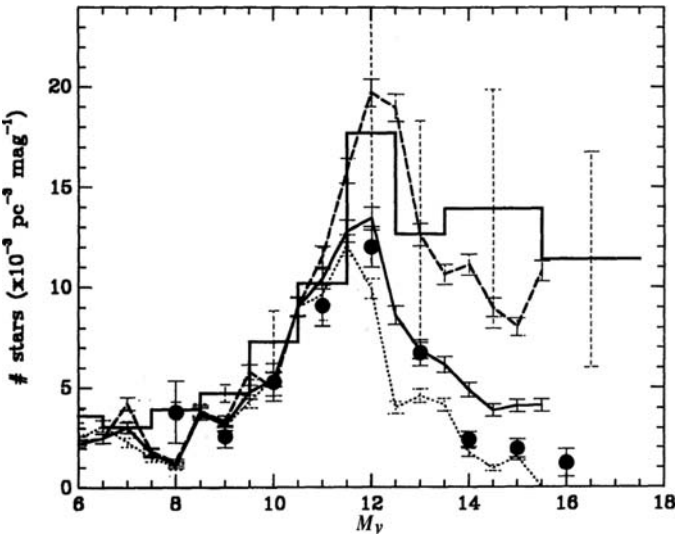

Fig. 8.8. The Galactic field population that results from disrupted star clusters, unification of both the nearby (*solid histogram*) and deep (*filled circles*) LFs with one parent MF (8.124). The theoretical nearby LF (*dashed line*) is the LF of all individual stars, while the *solid curve* is a theoretical LF with a mixture of about 50 per cent unresolved binaries and single stars from a clustered star-formation mode. According to this model, all stars are formed as binaries in modest clusters, which disperse to the field. The resulting Galactic field population has a binary fraction and a mass-ratio distribution as observed. The dotted curve is the initial system LF (100% binaries) (Kroupa 1995a,b). Note the peak in both theoretical LFs. It stems from the extremum in the derivative of the stellar-mass–luminosity relation in the mass range 0.2–0.4 $M_\odot$ (Kroupa 2002b)

N-body code and the resulting theoretical field is compared to the observed LFs (Fig. 8.8). Further confirmation of the form of the canonical IMF comes from independent sources, most notably by Reid, Gizis & Hawley (2002) and also Chabrier (2003).

In the high-mass regime, Massey (2003) reports the same slope or index $\alpha_3 = 2.3 \pm 0.1$ for $m \geq 10\,M_\odot$ in many OB associations and star clusters in the Milky Way and the Large and Small Magellanic clouds (LMC, SMC, respectively). It is therefore suggested to refer to $\alpha_2 = \alpha_3 = 2.3$ as the Salpeter/Massey slope or index, given the pioneering work of Salpeter (1955) who derived this value for stars with masses 0.4–10 $M_\odot$.

Multiplicity corrections await publication once we learn more about how the components are distributed in massive stars (cf. Preibisch et al. 1999; Zinnecker 2003). Weidner & Kroupa (private communication) are in the process of performing a very detailed study of the influence of unresolved binary and higher-order multiple stars on determinations of the high-mass IMF.

Contrary to the Salpeter/Massey index ($\alpha = 2.3$), Scalo (1986) found $\alpha_{\rm MWdisc} \approx 2.7$ ($m \geq 1\,M\odot$) from a very thorough analysis of OB star counts in the Milky Way disc. Similarly, the star-count analysis of Reid, Gizis & Hawley (2002) leads to $2.5 \leq \alpha_{\rm MWdisc} \leq 2.8$, and Tinsley (1980), Kennicutt (1983) (his extended Miller-Scalo IMF), Portinari, Sommer-Larsen & Tantalo (2004) and Romano et al. (2005) find $2.5 \leq \alpha_{\rm MWdisc} \leq 2.7$. That $\alpha_{\rm MWdisc} > \alpha_2$ follows naturally is shown in Sect. 8.3.4.

Below the hydrogen-burning limit (see also Sect. 8.3.3) there is substantial evidence that the IMF flattens further to $\alpha_0 \approx 0.3 \pm 0.5$ (Martín et al. 2000; Chabrier 2003; Moraux et al. 2004). Therefore, the canonical IMF most likely has a peak at $0.08\,M_\odot$. Brown dwarfs, however, comprise only a few per cent of the mass of a population and are therefore dynamically irrelevant (Table 8.2). The logarithmic form of the canonical IMF,

$$\xi_{\rm L}(m) = \log_{10}\, m\, \xi(m), \tag{8.126}$$

which gives the number of stars in $\log_{10}\, m$-intervals, also has a peak near $0.08\,M_\odot$. However, the system IMF (of stellar single and multiple systems combined to system masses) has a maximum in the mass range 0.4–0.6 $M_\odot$ (Kroupa et al. 2003).

The above canonical or standard form has been derived from detailed considerations of Galactic field star counts and so represents an average IMF. For low-mass stars, it is a mixture of stellar populations spanning a large range of ages (0–10 Gyr) and metallicities ([Fe/H]≥ -1). For the massive stars it constitutes a mixture of different metallicities ([Fe/H]≥ -1.5) and star-forming conditions (OB associations to very dense star-burst clusters: R136 in the LMC). Therefore, it can be taken as a canonical form and the aim is to test the

IMF UNIVERSALITY HYPOTHESIS that the canonical IMF constitutes the parent distribution of all stellar populations.

Negation of this hypothesis would imply a variable IMF. Note that the work of Massey (2003) has already established the IMF to be invariable for $m \geq 10\,M_\odot$ and for densities $\rho \leq 10^5\,{\rm stars\,pc^{-3}}$ and metallicity $Z \geq 0.002$.

Finally, Table 8.2 compiles some numbers that are useful for simple insights into stellar populations.

8.3.2 Universality of the IMF: Resolved Populations

The strongest test of the IMF UNIVERSALITY HYPOTHESIS (p. 225) is obtained by studying populations that can be resolved into individual stars. Because we also seek co-eval populations with stars at the same distance and with the same metallicity to minimise uncertainties, star clusters and stellar associations would seem to be the test objects of choice. But before contemplating such work, some lessons from stellar dynamics are useful.

Table 8.2. The number fraction $\eta_N = 100\int_{m_1}^{m_2}\xi(m)\,\mathrm{d}m/\int_{m_l}^{m_u}\xi(m)\,\mathrm{d}m$ and the mass fraction $\eta_M = 100\int_{m_1}^{m_2} m\,\xi(m)\,\mathrm{d}m/M_{\rm cl}$, $M_{\rm cl} = \int_{m_l}^{m_u} m\,\xi(m)\,\mathrm{d}m$, in per cent of BDs or main-sequence stars in the mass interval m_1 to m_2 and the stellar contribution, $\rho^{\rm st}$, to the Oort limit and to the Galactic-disc surface mass-density, $\Sigma^{\rm st} = 2\,h\rho^{\rm st}$, near to the Sun, with $m_l = 0.01\,M_\odot$, $m_u = 120\,M_\odot$ and the Galactic-disc scale-height $h = 250\,\mathrm{pc}$ ($m < 1\,M_\odot$ Kroupa, Tout & Gilmore 1993) and $h = 90\,\mathrm{pc}$ ($m > 1\,M_\odot$, Scalo 1986). Results are shown for the canonical IMF (8.124) for the high-mass-star IMF approximately corrected for unresolved companions ($\alpha_3 = 2.7, m > 1\,M_\odot$) and for the present-day mass function (PDMF, $\alpha_3 = 4.5$, Scalo 1986; Kroupa, Tout & Gilmore 1993), which describes the distribution of stellar masses now populating the Galactic disc. For gas in the disc, $\Sigma^{\rm gas} = 13 \pm 3\,M_\odot/\mathrm{pc}^2$ and remnants $\Sigma^{\rm rem} \approx 3\,M_\odot/\mathrm{pc}^2$ (Weidemann 1990). The average stellar mass is $\overline{m} = \int_{m_l}^{m_u} m\,\xi(m)\,\mathrm{d}m/\int_{m_l}^{m_u}\xi(m)\,\mathrm{d}m$. $N_{\rm cl}$ is the number of stars that have to form in a star cluster so that the most massive star in the population has the mass $m_{\rm max}$. The mass of this population is $M_{\rm cl}$ and the condition is $\int_{m_{\rm max}}^{\infty}\xi(m)\,\mathrm{d}m = 1$ with $\int_{0.01}^{m_{\rm max}}\xi(m)\,\mathrm{d}m = N_{\rm cl} - 1$. $\Delta M_{\rm cl}/M_{\rm cl}$ is the fraction of mass lost from the cluster due to stellar evolution if we assume that, for $m \geq 8\,M_\odot$, all neutron stars and black holes are kicked out by asymmetrical supernova explosions but that white dwarfs are retained (Weidemann et al. 1992) and have masses $m_{\rm WD} = 0.084\,m_{\rm ini} + 0.444\,[M_\odot]$. This is a linear fit to the data of Weidemann (2000, their Table 3) for progenitor masses $1 \leq m/M_\odot \leq 7$ and $m_{\rm WD} = 0.5\,M_\odot$ for $0.7 \leq m/M_\odot < 1$. The evolution time for a star of mass $m_{\rm to}$ to reach the turn-off age is available in Fig. 20 of Kroupa (2007a)

Mass range $[M_\odot]$	η_N [%] α_3			η_M [%] α_3			$\rho^{\rm st}$ $[M_\odot/\mathrm{pc}^3]$ α_3	$\Sigma^{\rm st}$ $[M_\odot/\mathrm{pc}^2]$ α_3
	2.3	2.7	4.5	2.3	2.7	4.5	4.5	4.5
0.01–0.08	37.2	37.7	38.6	4.1	5.4	7.4	3.2×10^{-3}	1.60
0.08–0.5	47.8	48.5	49.7	26.6	35.2	48.2	2.1×10^{-2}	10.5
0.5–1	8.9	9.1	9.3	16.1	21.3	29.2	1.3×10^{-2}	6.4
1–8	5.7	4.6	2.4	32.4	30.3	15.1	6.5×10^{-3}	1.2
8–120	0.4	0.1	0.0	20.8	7.8	0.1	3.6×10^{-5}	6.5×10^{-3}
$\overline{m}/M_\odot =$	0.38	0.29	0.22				$\rho^{\rm st}_{\rm tot} = 0.043$	$\Sigma^{\rm st}_{\rm tot} = 19.6$

	$\alpha_3 = 2.3$		$\alpha_3 = 2.7$			$\Delta M_{\rm cl}/M_{\rm cl}$ [%]	
$m_{\rm max}$ $[M_\odot]$	$N_{\rm cl}$	$M_{\rm cl}$ $[M_\odot]$	$N_{\rm cl}$	$M_{\rm cl}$ $[M_\odot]$	$m_{\rm to}$ $[M_\odot]$	$\alpha_3 = 2.3$	$\alpha_3 = 2.7$
1	16	2.9	21	3.8	80	3.2	0.7
8	245	74	725	195	60	4.9	1.1
20	806	269	3442	967	40	7.5	1.8
40	1984	703	1.1×10^4	2302	20	13	4.7
60	3361	1225	2.2×10^4	6428	8	22	8.0
80	4885	1812	3.6×10^4	1.1×10^4	3	32	15
100	6528	2451	5.3×10^4	1.5×10^4	1	44	29
120	8274	3136	7.2×10^4	2.1×10^4	0.7	47	33

Star Clusters and Associations

To access a pristine population one would consider observing star-clusters that are younger than a few Myr. However, such objects carry rather serious disadvantages. The pre-mainsequence stellar evolution tracks are unreliable (Baraffe et al. 2002; Wuchterl & Tscharnuter 2003) so that the derived masses are uncertain by at least a factor of about two. Remaining gas and dust lead to patchy obscuration. Very young clusters evolve rapidly. The dynamical crossing time is given by (8.4) where the cluster radii are typically $r_{\rm h} < 1\,{\rm pc}$ and for pre-cluster cloud-core masses $M_{\rm gas+stars} > 10^3\,M_\odot$ the velocity dispersion $\sigma_{\rm cl} > 2\,{\rm km\,s^{-1}}$ so that $t_{\rm cr} < 1\,{\rm Myr}$.

The inner regions of populous clusters have $t_{\rm cr} \approx 0.1\,{\rm Myr}$ and thus significant mixing and relaxation occurs there by the time the residual gas has been expelled by any winds and photo-ionising radiation from massive stars. This is the case in clusters with $N \geq$ few $\times$ 100 stars (Table 8.1).

Massive stars ($m > 8\,M_\odot$) are either formed at the cluster centre or get there through dynamical mass segregation, i.e. energy equipartition (Bonnell et al. 2007). The latter process is very rapid ((8.6), p. 184) and can occur within 1 Myr. A cluster core of massive stars is therefore either primordial or forms rapidly because of energy equipartition in the cluster and it is dynamically highly unstable decaying within a few $t_{\rm cr,\,core}$. The ONC, for example, should not be hosting a Trapezium because it is extremely unstable. The implication for the IMF is that the ONC and other similar clusters and the OB associations which stem from them must be very depleted in their massive star content (Pflamm-Altenburg & Kroupa 2006).

Important for measuring the IMF are corrections for the typically high multiplicity fraction of the very young population. However, these are very uncertain because the binary population is in a state of change (Fig. 8.14 below). The determination of an IMF relies on the assumption that all stars in a very young cluster formed together. However, trapping and focussing of older field or OB association stars by the forming cluster has been found to be possible (Sect. 8.1.1).

Thus, be it at the low-mass end or the high-mass end, the stellar mass function seen in very young clusters cannot be the true IMF. Statistical corrections for the above effects need to be applied and comprehensive N-body modelling is required.

Old open clusters, in which most stars are on or near the main sequence, are no better stellar samples. They are dynamically highly evolved, because they have left their previous concentrated and gas-rich state and so they contain only a small fraction of the stars originally born in the cluster (Kroupa & Boily 2002; Weidner et al. 2007; Baumgardt & Kroupa 2007). The binary fraction is typically high and comparable to the Galactic field, but does depend on the initial density and the age of the cluster as does the mass-ratio distribution of companions. So, simple corrections cannot be applied equally for all old clusters. The massive stars have died and secular evolution begins

to affect the remaining stellar population (after gas expulsion) through energy equipartition. Baumgardt & Makino (2003) have quantified the changes of the MF for clusters of various masses and on different Galactic orbits. Near the half-mass radius, the local MF resembles the global MF in the cluster but the global MF is already significantly depleted of its lower-mass stars by about 20% of the cluster disruption time.

Given that we are never likely to learn the exact dynamical history of a particular cluster, it follows that we can never ascertain the IMF for any individual cluster. This can be summarised concisely with the following conjecture.

CLUSTER IMF CONJECTURE: The IMF cannot be extracted for any individual star cluster.

JUSTIFICATION: For clusters younger than about 0.5 Myr, star-formation has not ceased and the IMF is therefore not yet assembled and the cluster cores consisting of massive stars have already dynamically ejected members (Pflamm-Altenburg & Kroupa 2006). For clusters with an age between 0.5 and a few Myr, the expulsion of residual gas has lead to loss of stars (Kroupa, Aarseth & Hurley 2001). Older clusters are either still losing stars owing to residual gas expulsion or are evolving secularly through evaporation driven by energy equipartition (Baumgardt & Makino 2003). Furthermore, the birth sample is likely to be contaminated by captured stars (Fellhauer, Kroupa & Evans 2006; Pflamm-Altenburg & Kroupa 2007). There exists no time when all stars are assembled in an observationally accessible volume (i.e. a star cluster).

Note that the CLUSTER IMF CONJECTURE implies that individual clusters cannot be used to make deductions on the similarity or not of their IMFs, unless a complete dynamical history of each cluster is available. Notwithstanding this pessimistic conjecture, it is nevertheless necessary to observe and study star clusters of any age. Combined with thorough and realistic N-body modelling the data, do lead to essential statistical constraints on the IMF UNIVERSALITY HYPOTHESIS. Such an approach is discussed in the next section.

The Alpha Plot

Scalo (1998) conveniently summarised a large part of the available observational constraints on the IMF of resolved stellar populations with the alpha plot, as used by Kroupa (2001, 2002b) for explicit tests of the IMF UNIVERSALITY HYPOTHESIS given the CLUSTER IMF CONJECTURE. One example is presented in Fig. 8.9, which demonstrates that the observed scatter in $\alpha(m)$ can be readily understood as being due to Poisson uncertainties (see also Elmegreen 1997, 1999) and dynamical effects, as well as arising from biases through unresolved multiple stars. Furthermore, there is no evident systematic change of α at a given m with metallicity or density of the star-forming cloud.

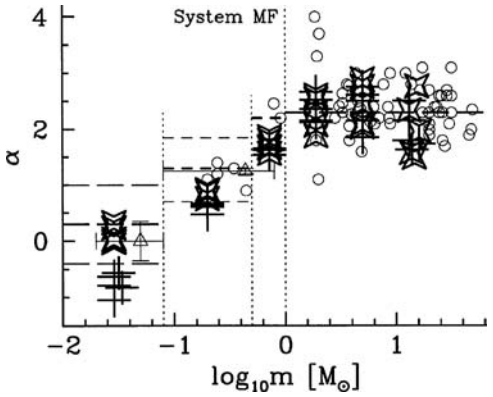

Fig. 8.9. The alpha plot. The power-law index, α, is measured over stellar mass-ranges and plotted at the mid-point of the respective mass range. The power-law indices are measured on the mass function of system masses, where stars not in binaries are counted individually. *Open circles* are the observations from open clusters and associations of the Milky Way and the Large and Small Magellanic clouds collated mostly by Scalo (1998). The open stars (*crosses*) are theoretical star clusters observed in the computer at an age of 3 (0) Myr and within a radius of 3.2 pc from the cluster centre. The 5 clusters have 3000 stars in 1500 binaries initially and the assumed IMF is the canonical one. The theoretical data nicely show a similar spread to the observational ones; note the binary-star-induced depression of α_1 in the mass range 0.1–0.5 $M_\odot$. The IMF UNIVERSALITY HYPOTHESIS can therefore not be discarded given the observed data. Models are from Kroupa (2001)

More exotic populations such as the Galactic bulge have also been found to have a low-mass MF indistinguishable from the canonical form (e.g. Zoccali et al. 2000). Thus the IMF UNIVERSALITY HYPOTHESIS cannot be falsified for known resolved stellar populations.

Very Ancient and/or Metal-Poor Resolved Populations

Witnesses of the early formation phase of the Milky Way are its globular clusters. Such 10^4–$10^6\,M_\odot$ clusters formed with individual star-formation rates of 0.1–1 $M_\odot\,\mathrm{yr}^{-1}$ and densities of about 5×10^3–$10^5\,M_\odot\,\mathrm{pc}^{-3}$. These are relatively high values, when compared with the current star-formation activity in the Milky Way disc. For example, a $5\times10^3\,M_\odot$ Galactic cluster forming in 1 Myr corresponds to a star-formation rate of $0.005\,M_\odot\,\mathrm{yr}^{-1}$. The alpha plot, however, does not support any significant systematic difference between the IMF of stars formed in globular clusters and present-day low-mass star-formation. For massive stars, it can be argued that the mass in stars more massive than $8\,M_\odot$ cannot have been larger than about half the cluster mass, because otherwise the globular clusters would not be as compact as they are today. This constrains the IMF to have been close to the canonical IMF (Kroupa 2001).

A particularly exotic star-formation mode is thought to have occurred in dwarf-spheroidal (dSph) satellite galaxies. The Milky Way has about 19 such satellites at distances from 50 to 250 kpc (Metz & Kroupa 2007). These objects have stellar masses and ages comparable to those of globular clusters, but are 10–100 times larger and are thought to have 10–1000 times more mass in dark matter than in stars. They also show evidence for complex star-formation activity and metal-enrichment histories and must therefore have formed under rather exotic conditions. Nevertheless, the MFs in two of these satellites are found to be indistinguishable from those of globular clusters in the mass range 0.5–$0.9\,M_\odot$. So again there is consistency with the canonical IMF (Grillmair et al. 1998; Feltzing, Gilmore & Wyse 1999).

The work of Yasui et al. (2006) and Yasui et al. (2008) have been pushing studies of the IMF in young star clusters to the outer, metal-poor regions of the Galactic disc. They find the IMF to be indistinguishable, within the uncertainties, from the canonical IMF.

The Galactic Bulge and Centre

For low-mass stars the Galactic bulge has been shown to have a MF indistinguishable from the canonical form (Zoccali et al. 2000). However, abundance patterns of bulge stars suggest the IMF was top-heavy (Ballero, Kroupa & Matteucci 2007). This may be a result of extreme star-burst conditions prevailing in the formation of the bulge (Zoccali et al. 2006).

Even closer to the Galactic centre, models of the Hertzsprung–Russell diagram of the stellar population within 1 pc of Sgr A* suggest the IMF was always top-heavy there (Maness et al. 2007). Perhaps, this is the long-sought after evidence for a variation of the IMF under very extreme conditions, in this case a strong tidal field and higher temperatures (but note Fig. 8.10 below).

Extreme Star Bursts

As noted on p. 199, objects with a mass $M \geq 10^6\,M_\odot$ have an increased M/L ratio. If such objects form in 1 Myr, their star-formation rates SFR $\geq 1\,M_\odot$/yr and they probably contain more than 10^4 O stars packed within a region spanning at most a few parsecs, given their observed present-day mass–radius relation. Such a star-formation environment is presently outside the reach of theoretical investigation. However, it is conceivable that the higher M/L ratios of such objects may be due to a non-canonical IMF. One possibility is that the IMF is bottom-heavy as a result of intense photo-destruction of accretion envelopes of intermediate to low-mass stars (Mieske & Kroupa 2008). Another possibility is that the IMF becomes top-heavy leaving many stellar remnants that inflate the M/L ratio (Dabringhausen & Kroupa 2008). Work is in progress to achieve observational constraints on these two possibilities.

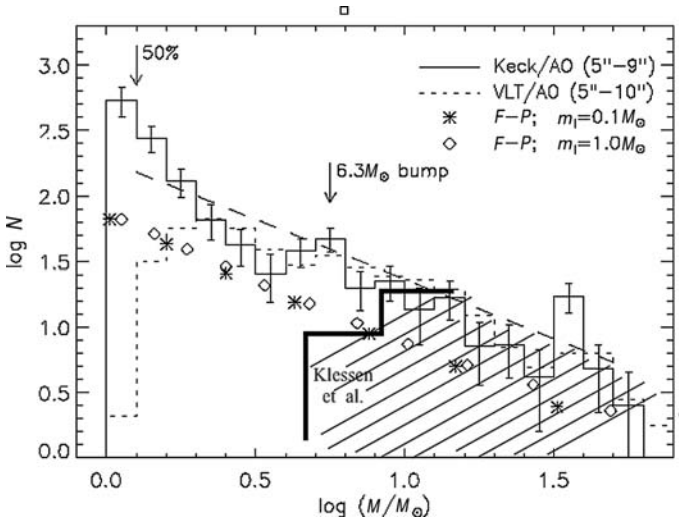

Fig. 8.10. The observed mass function of the Arches cluster near the Galactic centre by Kim et al. (2006) shown as the thin histogram is confronted with the theoretical MF for this object calculated with the SPH technique by Klessen, Spaans & Jappsen (2007), marked as the hatched histogram. The latter has a down-turn (bold steps near $10^{0.7}$) incompatible with the observations. This rules out a theoretical understanding of the stellar mass spectrum because one counter-example suffices to bring-down a theory. One possible reason for the theoretical failure may be the assumed turbulence driving. For details of the figure see Kim et al. (2006)

Population III: The Primordial IMF

Most theoretical workers agree that the primordial IMF ought to be top-heavy because the ambient temperatures were much higher and the lack of metals did not allow gas clouds to cool and to fragment into sufficiently small cores (Larson 1998). The existence of extremely metal-poor, low-mass stars with chemical peculiarities is interpreted to mean that low-mass stars could form under extremely metal-poor conditions but that their formation was suppressed in comparison to later star-formation (Tumlinson 2007). Models of the formation of stellar populations during cosmological structure formation suggest that low-mass population-III stars should be found within the Galactic halo if they formed. Their absence to-date would imply a primordial IMF depleted in low-mass stars (Brook et al. 2007).

Thus, the last three sub-sections hint at physical environments in which the IMF universality hypothesis may be violated.

8.3.3 Very Low-Mass Stars (VLMSs) and Brown Dwarfs (BDs)

The origin of BDs and some VLMSs is being debated fiercely. One camp believes these objects to form as stars, because the star-formation process does not know where the hydrogen burning mass limit is (e.g. Eislöffel & Steinacker 2008). The other camp believes that BDs cannot form exactly like stars through continued accretion because the conditions required for this to occur in molecular clouds are far too rare (e.g. Reipurth & Clarke 2001; Goodwin & Whitworth 2007).

If BDs and VLMSs form like stars, they should follow the same pairing rules. In particular, BDs and G dwarfs would pair in the same manner, i.e. according to the same mathematical rules, as M dwarfs and G dwarfs. Kroupa et al. (2003) tested this hypothesis by constructing N-body models of Taurus-Auriga-like groups and Orion-Nebula-like clusters, finding that it leads to far too many star–BD and BD–BD binaries with the wrong semi-major axis distribution. Instead, star–BD binaries are very rare (Grether & Lineweaver 2006), while BD–BD binaries are rarer than stellar binaries (BDs have a 15% binary fraction as opposed to 50% for stars) and BDs have a semi-major axis distribution significantly narrower than that of star–star binaries. The hypothesis of a star-like origin of BDs must therefore be discarded. BDs and some VLMSs form a separate population, which is however linked to that of the stars.

Thies & Kroupa (2007) re-addressed this problem with a detailed analysis of the underlying MF of stars and BDs given observed MFs of four populations: Taurus, Trapezium, IC348 and the Pleiades. By correcting for unresolved binaries in all four populations and taking into account the different pairing rules of stellar and VLMS and BD binaries, they discovered a significant discontinuity of the MF. BDs and VLMSs therefore form a truly separate population from that of the stars. It can be described by a single power-law MF (8.129), which implies that about one BD forms per five stars in all four populations.

This strong correlation between the number of stars and BDs and the similarity of the BD MF in the four populations implies that the formation of BDs is closely related to the formation of stars. Indeed, the truncation of the binary binding energy distribution of BDs at a high energy suggests that energetic processes must be operating in the production of BDs, as discussed by Thies & Kroupa (2007). Two such possible mechanisms are embryo ejection (Reipurth & Clarke 2001) and disc fragmentation (Goodwin & Whitworth 2007).

8.3.4 Composite Populations: The IGIMF

The vast majority of all stars form in embedded clusters and so the correct way to proceed to calculate a galaxy-wide stellar IMF is to add up all the IMFs of all star clusters born in one star-formation epoch. Such epochs may be identified with the Zoccali et al. (2006) star-burst events that create the Galactic

bulge. In disc galaxies they may be related to the time-scale of transforming the interstellar matter to star clusters along spiral arms. Addition of the clusters born in one epoch gives the integrated galactic initial mass function, the IGIMF (Kroupa & Weidner 2003).

IGIMF DEFINITION: The IGIMF is the IMF of a composite population, which is the integral over a complete ensemble of simple stellar populations.

Note that a simple population has a mono-metallicity and a mono-age distribution and is therefore a star cluster. Age and metallicity distributions emerge for massive populations with $M_{\rm cl} \geq 10^6\,M_\odot$ (e.g. ω Cen). This indicates that such objects, which also have relaxation times comparable to or longer than a Hubble time, are not simple (Sect. 8.1.4). A complete ensemble is a statistically complete representation of the initial cluster mass function (ICMF) in the sense that the actual mass function of $N_{\rm cl}$ clusters lies within the expected statistical variation of the ICMF.

IGIMF CONJECTURE: The IGIMF is steeper than the canonical IMF if the IMF UNIVERSALITY HYPOTHESIS holds.

JUSTIFICATION: Weidner & Kroupa (2006) calculate that the IGIMF is steeper than the canonical IMF for $m \geq 1\,M_\odot$ if the IMF UNIVERSALITY HYPOTHESIS holds. The steepening becomes negligible if the power-law mass function of embedded star clusters,

$$\xi_{\rm ecl}(M_{\rm ecl}) \propto M_{\rm ecl}^{-\beta}, \tag{8.127}$$

is flatter than $\beta = 1.8$.

It may be argued that IGIMF = IMF (e.g. Elmegreen 2006) because, when a star cluster is born, its stars are randomly sampled from the IMF up to the most massive star possible. On the other hand, the physically motivated ansatz of Weidner & Kroupa (2005, 2006) to take the mass of a cluster as the constraint and to include the observed correlation between the maximal star mass and the cluster mass (Fig. 8.1) yields an IGIMF which is equal to the canonical IMF for $m \leq 1.5\,M_\odot$ but which is systematically steeper above this mass. By incorporating the observed maximal-cluster-mass vs star-formation rate of galaxies, $M_{\rm ecl,max} = M_{\rm ecl,max}(SFR)$, for the youngest clusters (Weidner, Kroupa & Larsen 2004) it follows for $m \geq 1.5\,M_\odot$ that low-surface-brightness (LSB) galaxies ought to have very steep IGIMFs, while normal or L_* galaxies have Scalo-type IGIMFs, i.e. $\alpha_{\rm IGIMF} = \alpha_{\rm MWdisc} > \alpha_2$ (Sect. 8.3.1) follows naturally. This systematic shift of $\alpha_{\rm IGIMF}$ ($m \geq 1.5\,M_\odot$) with galaxy type implies that less massive galaxies have a significantly suppressed supernova II rate per low-mass star. They also show a slower chemical enrichment so that the observed metallicity–galaxy-mass relation can be nicely accounted

for (Koeppen, Weidner & Kroupa 2007). Another very important implication is that the SFR–Hα-luminosity relation for galaxies flattens so that the SFR becomes greater by up to three orders of magnitude for dwarf galaxies than the value calculated from the standard (linear) Kennicutt relation (Pflamm-Altenburg, Weidner & Kroupa 2007).

Strikingly, the IGIMF variation has now been directly measured by Hoversten & Glazebrook (2008) using galaxies in the Sloan Digital Sky Survey. Lee et al. (2004) have indeed found LSBs to have bottom-heavy IMFs, while Portinari, Sommer-Larsen & Tantalo (2004) and Romano et al. (2005) find the Milky Way disc to have a an IMF steeper than Salpeter's for massive stars which is, in comparison with Lee et al. (2004), much flatter than the IMF of LSBs, as required by the IGIMF CONJECTURE.

8.3.5 Origin of the IMF: Theory vs Observations

General physical concepts such as coalescence of protostellar cores, mass-dependent focussing of gas accretion on to protostars, stellar feedback and fragmentation of molecular clouds lead to predictions of systematic variations of the IMF with changes of the physical conditions of star-formation (Murray & Lin 1996; Elmegreen 2004). (But see Casuso & Beckman 2007 for a simple cloud coagulation/dispersal model that leads to an invariant mass distribution.) Thus, the thermal Jeans mass of a molecular cloud decreases with temperature and increasing density. This implies that for higher metallicity (stronger cooling) and density the IMF should shift on average to smaller stellar masses (e.g. Larson 1998; Bonnell et al. 2007). The entirely different notion that stars regulate their own masses through a balance between feedback and accretion also implies smaller stellar masses for higher metallicity due, in part, to more dust and thus more efficient radiation pressure on the gas through the dust grains. Also, a higher metallicity allows more efficient cooling and thus a lower gas temperature, a lower sound speed and therefore a lower accretion rate (Adams & Fatuzzo 1996; Adams & Laughlin 1996). As discussed above, a systematic IMF variation with physical conditions has not been detected. Thus, theoretical reasoning, even at its most elementary level, fails to account for the observations.

A dramatic case in point has emerged recently: Klessen, Spaans & Jappsen (2007) report state-of-the art calculations of star-formation under physical conditions as found in molecular clouds near the Sun and they are able to reproduce the canonical IMF. Applying the same computational technology to the conditions near the Galactic centre, they obtain a theoretical IMF in agreement with the previously reported apparent decline of the stellar MF in the Arches cluster below about $6\,M_\odot$. Kim et al. (2006) published their observations of the Arches cluster on the astrophysics preprint archive shortly after Klessen, Spaans & Jappsen (2007) and performed N-body calculations of the dynamical evolution of this young cluster, revising our knowledge significantly. In contradiction to the theoretical prediction, they find that the MF continues

to increase down to their 50% completeness limit ($1.3\,M_\odot$) with a power-law exponent only slightly shallower than the canonical Massey/Salpeter value once mass-segregation has been corrected for. This situation is demonstrated in Fig. 8.10. It therefore emerges that there does not seem to exist any solid theoretical understanding of the IMF.

Observations of cloud cores appear to suggest that the canonical IMF is already frozen in at the pre-stellar cloud-core level (Motte, Andre & Neri 1998; Motte et al. 2001). Nutter & Ward-Thompson (2007) and Alves, Lombardi & Lada (2007) find, however, the pre-stellar cloud cores are distributed according to the same shape as the canonical IMF but shifted to larger masses by a factor of about three or more. This is taken to perhaps mean a star-formation efficiency per star of 30% or less independently of stellar mass. The interpretation of such observations in view of multiple star-formation in each cloud-core is being studied by Goodwin et al. (2008), while Krumholz (2008) outlines current theoretical understanding of how massive stars form out of massive pre-stellar cores.

8.3.6 Conclusions: IMF

The IMF UNIVERSALITY HYPOTHESIS, the CLUSTER IMF CONJECTURE and the IGIMF CONJECTURE have been stated. In addition, we may make the following assertions.

1. The stellar luminosity function has a pronounced maximum at $M_V \approx 12$, $M_I \approx 9$, which is universal and well understood as a result of stellar physics. Thus by counting stars in the sky we can look into their interiors.
2. Unresolved multiple systems must be accounted for when the MFs of different stellar populations are compared.
3. BDs and some VLMSs form a separate population that correlates with the stellar content. There is a discontinuity in the MF near the star/BD mass transition.
4. The canonical IMF (8.124) fits the star counts in the solar neighbourhood and all resolved stellar populations available to-date. Recent data at the Galactic centre suggest a top-heavy IMF, perhaps hinting at a possible variation with conditions (tidal shear, temperature).
5. Simple stellar populations are found in individual star clusters with $M_{\rm cl} \leq 10^6\ M_\odot$. These have the canonical IMF.
6. Composite populations describe entire galaxies. They are a result of many epochs of star-cluster formation and are described by the IGIMF CONJECTURE.
7. The IGIMF above about $1\,M_\odot$ is steep for LSB galaxies and flattens to the Scalo slope ($\alpha_{\rm IGIMF} \approx 2.7$) for L_* disc galaxies. This is nicely consistent with the IMF UNIVERSALITY HYPOTHESIS in the context of the IGIMF CONJECTURE.

8. Therefore, the IMF UNIVERSALITY HYPOTHESIS cannot be excluded despite the CLUSTER IMF CONJECTURE for conditions $\rho \leq 10^5\,\mathrm{stars\,pc^{-3}}$, $Z \geq 0.002$ and non-extreme tidal fields.
9. Modern star-formation computations and elementary theory give wrong results concerning the variation and shape of the stellar IMF, as well as the stellar multiplicity (Goodwin & Kroupa 2005).
10. The stellar IMF appears to be frozen-in at the pre-stellar cloud-core stage. So it is probably a result of the processes that lead to the formation of self-gravitating molecular clouds.

8.3.7 Discretisation

As discussed above, a theoretically motivated form of the IMF that passes observational tests does not exist. Star-formation theory gets the rough shape of the IMF right. There are fewer massive stars than low-mass stars. However, other than this, it fails to make any reliable predictions whatsoever as to how the IMF should look in detail under different physical conditions. In particular, the overall change of the IMF with metallicity, density or temperature predicted by theory is not evident. An empirical multi-power-law form description of the IMF is therefore perfectly adequate and has important advantages over other formulations. A general formulation of the stellar IMF in terms of multiple power-law segments is

$$\xi(m) = k \begin{cases} \left(\frac{m}{m_{\rm H}}\right)^{-\alpha_0} & , m_{\rm low} \leq m \leq m_{\rm H} \\ \left(\frac{m}{m_{\rm H}}\right)^{-\alpha_1} & , m_{\rm H} \leq m \leq m_0 \\ \left(\frac{m_0}{m_{\rm H}}\right)^{-\alpha_1} \left(\frac{m}{m_0}\right)^{-\alpha_2} & , m_0 \leq m \leq m_1 \\ \left(\frac{m_0}{m_{\rm H}}\right)^{-\alpha_1} \left(\frac{m_1}{m_0}\right)^{-\alpha_2} \left(\frac{m}{m_1}\right)^{-\alpha_3} & , m_1 \leq m \leq m_{\rm max} \end{cases} , \qquad (8.128)$$

where $m_{\rm max} \leq m_{\rm max*} \approx 150\,M_\odot$ depends on the stellar mass of the embedded cluster (Fig. 8.1). The empirically determined stellar IMF is a two-part-form (8.124), with a third power-law for BDs, whereby BDs and VLMSs form a separate population from that of the stars (p. 232),

$$\xi_{\rm BD} \propto m^{-\alpha_0}, \quad \alpha_0 \approx 0.3, \qquad (8.129)$$

(Martín et al. 2000; Chabrier 2003; Moraux, Bouvier & Clarke 2004) and

$$\xi_{\rm BD}(0.075\,M_\odot) \approx 0.25 \pm 0.05\,\xi(0.075\,M_\odot),$$

(Thies & Kroupa 2007) where ξ is the canonical stellar IMF (8.124). This implies that about one BD forms per five stars.

One advantage of the power-law formulation is that analytical generating functions and other quantities can be readily derived. Another important advantage is that with a multi-power-law form, different parts of the IMF

can be varied in numerical experiments without affecting the other parts. A practical numerical formulation of the IMF is prescribed in Pflamm-Altenburg & Kroupa (2006). Thus, for example, the canonical two-part power-law IMF can be changed by adding a third power-law above $1\,M_\odot$ and making the IMF top-heavy ($\alpha_{m>1\,M_\odot} < \alpha_2$), without affecting the shape of the late-type stellar luminosity function as evident in Fig. 8.8. The KTG93 (Kroupa, Tout & Gilmore 1993) IMF is such a three-part power-law form relevant to the overall young population in the Milky Way disc. This is top-light ($\alpha_{m>1\,M_\odot} > \alpha_2$, Kroupa & Weidner 2003).

A log-normal formulation does not offer these advantages and requires power-law tails above about $1\,M_\odot$ and for brown dwarfs, for consistency with the observations discussed above. However, while not as mathematically convenient, the popular Chabrier log-normal plus power-law IMF (Table 1 of Chabrier 2003) formulation leads to an indistinguishable stellar mass distribution to the two-part power-law IMF (Fig. 8.11). Various analytical forms for the IMF are compiled in Table 3 of Kroupa (2007a).

A generating function for the two-part power-law form of the canonical IMF (8.124) can be written down by following the steps taken in Sect. 8.2.3. The corresponding probability density is

$$\begin{array}{ll} p_1 = k_{p,1}\, m^{-\alpha_1}, & 0.08 \leq m \leq 0.5\,M_\odot \\ p_2 = k_{p,2}\, m^{-\alpha_2}, & 0.5 < m \leq m_{\max}, \end{array} \tag{8.130}$$

where $k_{p,i}$ are normalisation constants ensuring continuity at $0.5\,M_\odot$ and

$$\int_{0.08}^{0.5} p_1\,\mathrm{d}m + \int_{0.5}^{m_{\max}} p_2\,\mathrm{d}m = 1, \tag{8.131}$$

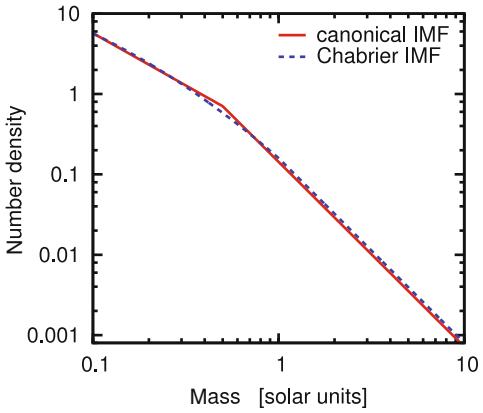

Fig. 8.11. Comparison between the popular Chabrier IMF (log-normal plus power-law extension above $1\,M_\odot$, *dashed curve*, Table 1 in Chabrier 2003) with the canonical two-part power-law IMF (*solid line*, (8.124)). The figure is from Dabringhausen, Hilker & Kroupa (2008)

whereby $m_{\rm max}$ follows from Fig. 8.1. Defining

$$X_1' = \int_{0.08}^{0.5} p_1(m)\,{\rm d}m, \tag{8.132}$$

it follows that

$$X_1(m) = \int_{0.08}^{m} p_1(m)\,{\rm d}m, \quad \text{if } m \leq 0.5\,M_\odot, \tag{8.133}$$

or

$$X_2(m) = X_1' + \int_{0.5}^{m} p_2(m)\,{\rm d}m, \quad \text{if } m > 0.5\,M_\odot. \tag{8.134}$$

The generating function for stellar masses follows from inversion of the above two equations $X_i(m)$. The procedure is then to choose a random variate $X \in [0,1]$ and to select the generating function $m(X_1 = X)$ if $0 \leq X \leq X_1$, or $m(X_2 = X)$ if $X_1 < X \leq 1$.

This algorithm is readily generalised to any number of power-law segments (8.128), such as including a third segment for brown dwarfs and allowing the IMF to be discontinuous near $0.08\,M_\odot$ (Thies & Kroupa 2007). Such a form has been incorporated into the NBODY4/6/7 programmes, but hitherto without the discontinuity. However, Jan Pflamm-Altenburg has developed a more powerful and general method of generating stellar masses (or any other quantities) given an arbitrary distribution function (Pflamm-Altenburg & Kroupa 2006).[11]

8.4 The Initial Binary Population

It has already been demonstrated that corrections for unresolved multiple stars are of much importance to derive correctly the shape of the stellar MF given an observed LF (Fig. 8.8). Binary stars are also of significant importance for the dynamics of star clusters because a binary has intrinsic dynamical degrees of freedom that a single star does not possess. A binary can therefore exchange energy and angular momentum with the cluster. Indeed, binaries are very significant energy sources, as for example, a binary composed of two $1\,M_\odot$ main-sequence stars and with a semi-major axis of 0.1 AU has a binding energy comparable to that of a $1000\,M_\odot$ cluster of size 1 pc. Such a binary can interact with cluster-field star accelerating them to higher velocities and thereby heating the cluster.

The dynamical properties describing a multiple system are

- the period P (in days throughout this text) or semi-major axis a (in AU),
- the system mass $m_{\rm sys} = m_1 + m_2$,

[11] The C-language software package, libimf, can be downloaded from the website `http://www.astro.uni-bonn.de/~webaiub/english/downloads.php`.

- the mass ratio $q \equiv \frac{m_2}{m_1} \leq 1$, where m_1, m_2 are, respectively, the primary and secondary-star masses and
- the eccentricity $e = (r_{\rm apo} - r_{\rm peri})/(r_{\rm apo} + r_{\rm peri})$, where $r_{\rm apo}, r_{\rm peri}$ are, respectively, the apocentric and pericentric distances.

Given a snapshot of a binary, the above quantities can be computed from the relative position, $\boldsymbol{r}_{\rm rel}$ and velocity, $\boldsymbol{v}_{\rm rel}$, vectors and the masses of the two companion stars by first calculating the binding energy,

$$E_{\rm b} = \frac{1}{2}\,\mu\,v_{\rm rel}^2 - \frac{G\,m_1\,m_2}{r_{\rm rel}} = -\frac{G\,m_1\,m_2}{2\,a} \Rightarrow a, \tag{8.135}$$

where $\mu = m_1\,m_2\,/(m_1 + m_2)$ is the reduced mass. From Kepler's third law we have

$$m_{\rm sys} = \frac{a_{AU}^3}{P_{\rm yr}^2} \Rightarrow P = P_{\rm yr} \times 365.25 \text{ days}, \tag{8.136}$$

where $P_{\rm yr}$ is the period in years and a_{AU} is in AU. Finally, the instantaneous eccentricity can be calculated using

$$e = \left[\left(1 - \frac{r_{\rm rel}}{a}\right)^2 + \frac{\left(\boldsymbol{r}_{\rm rel} \cdot \boldsymbol{v}_{\rm rel}\right)^2}{a\,G\,m_{\rm sys}}\right]^{\frac{1}{2}}, \tag{8.137}$$

which can be derived from the orbital angular momentum too,

$$\boldsymbol{L} = \mu\,\boldsymbol{v}_{\mathbf{rel}} \times \boldsymbol{r}_{\mathbf{rel}}, \tag{8.138}$$

with

$$L = \left[\frac{G}{m_{\rm sys}}\,a\,(1 - e^2)\right]^{\frac{1}{2}}\,m_1\,m_2. \tag{8.139}$$

The relative equation of motion is

$$\frac{{\rm d}^2\boldsymbol{r}_{\rm rel}}{{\rm d}t^2} = -G\frac{m_{\rm sys}}{r_{\rm rel}^3}\boldsymbol{r}_{\rm rel} + \boldsymbol{a}_{\rm pert}(t), \tag{8.140}$$

where $\boldsymbol{a}_{\rm pert}(t)$ is the time-dependent perturbation from other cluster members. It follows that the orbital elements of a binary in a cluster are functions of time, $P = P(t)$ and $e = e(t)$. Also, $q = q(t)$ during strong encounters when partners are exchanged. Because most stars form in embedded clusters, the binary-star properties of a given population cannot be taken to represent the initial or primordial values.

The following conjecture can be proposed.

DYNAMICAL POPULATION SYNTHESIS CONJECTURE: if initial binary populations are invariant, a dynamical birth configuration of a stellar population can be inferred from its observed binary population. This birth configuration is not unique, however, but defines a class of dynamically equivalent solutions.

The proof is simple. Set up initially identical binary populations in clusters with different radii and masses and calculate the dynamical evolution with an N-body programme. For a given snapshot of a population, there is a scalable starting configuration in terms of size and mass (Kroupa 1995c,d).

Binaries can absorb energy and thus cool a cluster. They can also heat a cluster. There are two extreme regimes that can be understood with a Gedanken experiment. Define

$$\begin{array}{c} E_{\rm bin} \equiv -E_{\rm b} > 0, \\ E_{\rm k} \equiv (1/2)\,\overline{m}\,\sigma^2 \approx (1/N) \times \text{ kinetic energy of cluster.} \end{array} \tag{8.141}$$

Soft binaries have $E_{\rm bin} \ll E_{\rm k}$, while hard binaries have $E_{\rm bin} \gg E_{\rm k}$. A useful equation in this context is the relation between the orbital period and circular velocity of the reduced particle,

$$\log_{10} P[\text{days}] = 6.986 + \log_{10} m_{\rm sys}[M_\odot] - 3\,\log_{10} v_{\rm orb}[\text{km s}^{-1}]. \tag{8.142}$$

Consider now the case of a soft binary, a reduced-mass particle with $v_{\rm orb} \ll \sigma$. By the principle of energy equipartition, $v_{\rm orb} \to \sigma$ (8.5) as time progresses. This implies $a \uparrow, P \uparrow$. A hard binary has $v_{\rm orb} \gg \sigma$. Invoking energy equipartition, we see that $v_{\rm orb} \downarrow$, $a \downarrow, P \downarrow$. Furthermore, the amount of energy needed to ionise a soft binary is negligible compared to the amount of energy required to ionise a hard binary. And the cross section for suffering an encounter scales with the semi-major axis. This implies that a soft binary becomes ever more likely to suffer an additional encounter as its semi-major axis increases. Therefore, it is much more probable for soft binaries to be disrupted rapidly, than for hard binaries to do so. Thus follows (Heggie 1975; Hills 1975) a law.

HEGGIE–HILLS LAW: soft binaries soften and cool a cluster while hard binaries harden and heat a cluster.

Numerical scattering experiments by Hills (1975) have shown that hardening of binaries often involves partner exchanges. Heggie (1975) derived the above law analytically. Binaries in the energy range $10^{-2}\,E_{\rm k} \le E_{\rm bin} \le 10^2\,E_{\rm k}$, $33^{-1}\,\sigma \le v_{\rm orb} \le 33\,\sigma$ cannot be treated analytically owing to the complex resonances that are created between the binary and the incoming star or binary. It is these binaries that may be important for the early cluster evolution, depending on its velocity dispersion, $\sigma = \sigma(M_{\rm ecl})$. Cooling of a cluster is energetically not significant but has been seen for the first time by Kroupa, Petr & McCaughrean (1999).

Figure 8.12 shows the broad evolution of the initial period distribution in a star cluster. At any time, binaries near the hard/soft boundary, with energies $E_{\rm bin} \approx E_{\rm k}$ and periods $P \approx P_{\rm th}$ ($v_{\rm orb} = \sigma$) (8.5), the thermal period, are most active in the energy exchange between the cluster field and the binary population. The cluster expands as a result of binary heating and

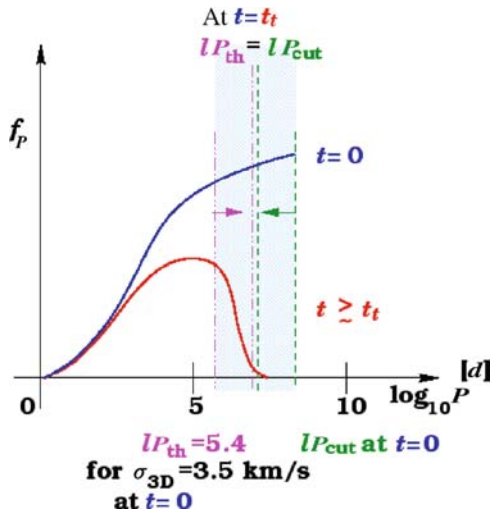

Fig. 8.12. Illustration of the evolution of the distribution of binary star periods in a cluster ($l\mathrm{P} = \log_{10} P$). A binary has orbital period $P_{\rm th}$ when $\sigma_{\rm 3D}$ ($= \sigma$) equals its circular orbital velocity (8.142). The initial or birth distribution (8.164) evolves to the form seen at time $t > t_t$

mass segregation and the hard/soft boundary, $P_{\rm th}$, shifts to longer periods. Meanwhile, binaries with $P > P_{\rm th}$ continue to be disrupted while $P_{\rm th}$ keeps shifting to longer periods. This process ends when

$$P_{\rm th} \geq P_{\rm cut}, \tag{8.143}$$

which is the cutoff or maximum period in the surviving period distribution. At this critical time, t_t, further cluster expansion is slowed because the population of heating sources, the binaries with $P \approx P_{\rm th}$, is significantly reduced. The details strongly depend on the initial value of $P_{\rm th}$, which determines the amount of binding energy in soft binaries which can cool the cluster if significant enough.

After the critical time, $t_{\rm t}$, the expanded cluster reaches a temporary state of thermal equilibrium with the remaining binary population. Further evolution of the binary population occurs with a significantly reduced rate determined by the velocity dispersion in the cluster, the cross section given by the semi-major axis of the binaries and their number density and that of single stars in the cluster. The evolution of the binary star population during this slow phase usually involves partner exchanges and unstable but also long-lived hierarchical systems. The IMF is critically important for this stage, as the initial number of massive stars determines the cluster density at $t \geq 5\,$Myr owing to mass loss from evolving stars. Further binary depletion occurs once the cluster goes into core-collapse and the kinetic energy in the core rises.

8.4.1 Frequency of Binaries and Higher-Order Multiples

The emphasis here is on late-type binary stars because higher-order multiples are rare as observed. The information on the multiplicity of massive stars is very limited (Goodwin et al. 2007). We define, respectively, the number of single stars, binaries, triples, quadruples, etc., by the numbers

$$(N_{\rm sing} : N_{\rm bin} : N_{\rm trip} : N_{\rm quad} : \ldots) = (\mathcal{S} : \mathcal{B} : \mathcal{T} : \mathcal{Q} : \ldots) \quad (8.144)$$

and the multiplicity fraction by

$$f_{\rm mult} = \frac{N_{\rm mult}}{N_{\rm sys}} = \frac{\mathcal{B}+\mathcal{T}+\mathcal{Q}+\ldots}{\mathcal{S}+\mathcal{B}+\mathcal{T}+\mathcal{Q}+\ldots} \quad (8.145)$$

and the binary fraction is

$$f_{\rm bin} = \frac{\mathcal{B}}{N_{\rm sys}}. \quad (8.146)$$

In the Galactic field, Duquennoy & Mayor (1991) derive from a decade-long survey for G-dwarf primary stars, ${}^{\rm G}N_{\rm mult} = (57{:}38{:}4{:}1)$ and for M-dwarfs Fischer & Marcy (1992) find ${}^{\rm M}N_{\rm mult} = (58{:}33{:}7{:}1)$. Thus,

$${}^{\rm G}f_{\rm mult} = 0.43; \quad {}^{\rm G}f_{\rm bin} = 0.38 \quad (8.147)$$

$${}^{\rm M}f_{\rm mult} = 0.41; \quad {}^{\rm M}f_{\rm bin} = 0.33. \quad (8.148)$$

It follows that most stars are indeed binary.

After correcting for incompleteness,

$${}^{\rm G}f_{\rm bin} = 0.53 \pm 0.08, \quad (8.149)$$

$${}^{\rm K}f_{\rm bin} = 0.45 \pm 0.07, \quad (8.150)$$

$${}^{\rm M}f_{\rm bin} = 0.42 \pm 0.09, \quad (8.151)$$

where the K-dwarf data have been published by Mayor et al. (1992). It follows that

$${}^{\rm G}f_{\rm bin} \approx^{\rm K} f_{\rm bin} \approx^{\rm M} f_{\rm bin} \approx 0.5 \approx f_{\rm tot} \quad (8.152)$$

in the Galactic field, perhaps with a slight decrease towards lower masses. In contrast, for brown dwarfs, ${}^{\rm BD}f_{\rm bin} \approx 0.15 \ll {}^{\rm stars}f_{\rm bin}$ (Thies & Kroupa 2007 and references therein).

An interesting problem arises because 1 Myr old stars have $f_{\rm TTauri} \approx 1$ (e.g. Duchêne 1999). Given the above information, the following conjecture can be stated:

Binary-star conjecture: nearly all stars form in binary systems.

Justification: if a substantial fraction of stars were to form in higher-order multiple systems, or as small-N systems, the typical properties of these at

birth imply their decay within typically 10^4 to 10^5 yr, leaving a predominantly single-stellar population. However, the majority of 10^6 yr old stars are observed to be in binary systems (Goodwin & Kroupa 2005).

Higher-order multiple systems do exist and can only be hierarchical to guarantee stability. Such systems are multiple stars, which are stable over many orbital times and are usually tight binaries orbited by an outer tertiary companion, or two tight binaries in orbit about each other. Stability issues are discussed in detail in Chap. 3, based on a theoretical development from first principles. In particular, a new stability criterion for the general three-body problem is derived in terms of all the orbital parameters. For comparable masses, long-term stability is typically ensured for a ratio of the outer pericentre to the inner semi-major axis of about 4. If the stability condition is not fulfilled, higher-order multiple systems usually decay on a time-scale relating to the orbital parameters. Star cluster remnants (or dead star clusters) may be the origin of most hierarchical, higher-order multiple stellar systems in the field (p. 199).

8.4.2 The Initial Binary Population – Late-Type Stars

The initial binary population is described by distribution functions that are as fundamental for a stellar population as the IMF. There are four distribution functions that define the initial dynamical state of a population,

1. the IMF, $\xi(m)$,
2. the distribution of periods (or semi-major axis), $\mathrm{d}f = f_P(\log P)\,\mathrm{d}\log P$,
3. the distribution of mass-ratios, $\mathrm{d}f = f_q(q)\,\mathrm{d}q$ and
4. the distribution of eccentricities, $\mathrm{d}f = f_e(e)\,\mathrm{d}e$,

where $\mathrm{d}f$ is the fraction of systems between f and $f + \mathrm{d}f$. Thus, for example, ${}^{\mathrm{G}}f_{\log P}(\log_{10} P = 4.5) = 0.11$, i.e. of all G-dwarfs in the sky, 11% have a companion with a period in the range 4–5 d (Fig. 8.16).

These distribution functions have been measured for late-type stars in the Galactic field and in star-forming regions (Fig. 8.13). According to Duquennoy & Mayor (1991) and Fischer & Marcy (1992), both G-dwarf and M-dwarf binary systems in the Galactic field have period distribution functions that are well described by log-normal functions,

$$f_P(\log_{10} P) = f_{\mathrm{tot}} \left(\frac{1}{\sigma_{\log_{10} P}\sqrt{2\,\pi}} \right) e^{\left[-\frac{1}{2} \frac{(\log_{10} P - \overline{\log_{10} P})^2}{\sigma^2_{\log_{10} P}} \right]}, \qquad (8.153)$$

with $\overline{\log_{10} P} \approx 4.8$ and $\sigma_{\log_{10} P} \approx 2.3$ and $\int_{\mathrm{all}\,P} f_{\log_{10} P}(\log_{10} P)\,\mathrm{d}\log_{10} P = f_{\mathrm{tot}} \approx 0.5$. K-dwarfs appear to have an indistinguishable period distribution.

From Fig. 8.13 it follows that the pre-mainsequence binary fraction is larger than that of main-sequence stars (see also Duchêne 1999). Is this an evolutionary effect?

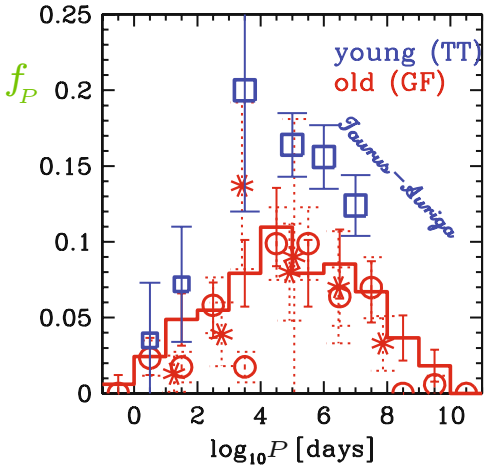

Fig. 8.13. Measured period-distribution functions for G-dwarfs in the Galactic field (*histogram*, Duquennoy & Mayor 1991), K-dwarfs (*open circles*, Mayor et al. 1992) and M-dwarfs (*asterisks*, Fischer & Marcy 1992). About 1-Myr-old T Tauri binary data (*open squares*, partially from the Taurus–Auriga stellar groups) are a compilation from various sources (see Fig. 10 in Kroupa, Aarseth & Hurley 2001). In all cases, the area under the distribution is $f_{\rm tot}$

Further, Duquennoy & Mayor (1991) derived the mass-ratio and eccentricity distributions for G-dwarfs in the Galactic field. The mass-ratio distribution of G-dwarf primaries is not consistent with random sampling from the canonical IMF (8.124), as the number of observed low-mass companions is underrepresented (Kroupa 1995c). In contrast, the pre-mainsequence mass-ratio distribution is consistent, within the uncertainties, with random sampling from the canonical IMF for $q \geq 0.2$ (Woitas, Leinert & Koehler 2001). The eccentricity distribution of Galactic-field G-dwarfs is found to be thermal for $\log_{10} P \geq 3$, while it is bell shaped with a maximum near $e = 0.25$ for $\log_{10} P \leq 3$. Not much is known about the eccentricity distribution of pre-mainsequence binaries, but numerical experiments show that f_e does not evolve much in dense clusters, i.e. the thermal distribution must be initial (Kroupa 1995d).

The thermal eccentricity distribution,

$$f_e(e) = 2\,e, \tag{8.154}$$

follows from a uniform binding-energy distribution (all energies are equally populated) as follows. The orbital angular momentum of a binary is

$$L^2 = \frac{G}{m_{\rm sys}} \frac{G\,m_1\,m_2}{2E_{\rm bin}} \left(1 - e^2\right) \left(m_1\,m_2\right)^2, \tag{8.155}$$

from which follows

$$e = \left(1 - 2\,E_{\rm bin}\,L^2\,\frac{m_{\rm sys}}{G^2\,(m_1\,m_2)^2}\right)^{\frac{1}{2}}. \tag{8.156}$$

Differentiation leads to

$$\frac{{\rm d}e}{{\rm d}E_{\rm bin}} = \left[-L^2\frac{m_{\rm sys}}{G^2\,(m_1\,m_2)^2}\right]\,e^{-1} \propto e^{-1}. \tag{8.157}$$

The number of binaries with eccentricities in the range $e, e + {\rm d}e$ is the same number of binaries with binding energy in the range $E_{\rm bin}, E_{\rm bin} + {\rm d}E_{\rm bin}$ (the same sample of binaries),

$$f(e)\,{\rm d}e = f(E_{\rm bin})\,{\rm d}E_{\rm bin} \propto f(E_{\rm bin})\,e\,{\rm d}e. \tag{8.158}$$

But

$$\int_0^1 f(e)\,{\rm d}e = 1. \tag{8.159}$$

That is,

$$f(E_{\rm bin})\int_0^1 e\,{\rm d}e \propto f(E_{\rm bin})\,\frac{1}{2}\,e^2|_0^1 = {\rm const.} \tag{8.160}$$

So

$$f(E_{\rm bin}) = {\rm const}\ \Rightarrow\ f(e)\,{\rm d}e = 2\,e\,{\rm d}e. \tag{8.161}$$

Thus, $f(e) = 2\,e$ is a thermalized distribution. All energies are equally occupied so $f(E_{\rm bin}) = {\rm const}$. N-body experiments have demonstrated that the period distribution function must span the observed range of periods at birth, because dynamical encounters in dense clusters cannot widen an initially narrow distribution (Kroupa & Burkert 2001). There are thus three discrepancies between main-sequence and pre-mainsequence late-type stellar binaries,

1. the binary fraction is higher for the latter,
2. the period distribution function is different and
3. the mass-ratio distribution is consistent with random paring for the latter, while it is deficient in low-mass companions in the former, for G-dwarf primaries.

Can these be unified? That is, are there unique initial $f_{\log P}, f_q$ and f_e consistent with the pre-mainsequence data that can be evolved to the observed main-sequence distributions?

This question can be solved by framing the following ansatz. Assume the orbital-parameter distribution function for binaries with primaries of mass m_1 can be separated,

$$\mathcal{D}(\log P, e, q\,:\,m_1) = f_{\log P}\,f_e\,f_q. \tag{8.162}$$

The stellar-dynamical operator, $\Omega^{N,r_{\rm h}}$, can now be introduced so that the initial distribution function is transformed to the final (Galactic-field) one,

$$D_{\rm fin}(\log P, e, q\,:\,m_1) = \Omega^{N,r_{\rm h}}\,\left[\mathcal{D}_{\rm in}(\log P, e, q\,:\,m_1)\right]. \tag{8.163}$$

This operator provides a dynamical environment equivalent to that of a star cluster with N stars and a half-mass radius $r_{\rm h}$ (see also the Dynamical Population Synthesis Conjecture, p. 239). Kroupa (1995c) and Kroupa (1995d) indeed show this to be the case for a cluster with $N = 200$ binaries and $r_{\rm h} = 0.77\,{\rm pc}$ and derive the initial distribution function, $\mathcal{D}_{\rm in}$, for late-type binary systems that fulfils the above requirement and also has a simple generating function (see below). It is noteworthy that such a cluster is very similar to the typical cluster from which most field stars probably originate. The full solution for Ω, so that the Galactic field is reproduced from forming and dissolving star clusters, requires full-scale inverse dynamical population synthesis for the Galactic field.

Thus, by the DYNAMICAL POPULATION SYNTHESIS CONJECTURE (p. 239), the above ansatz with $\Omega^{N,r_{\rm h}}$ leads to one solution of the inverse dynamical population synthesis problem (the 200 binary, $r_{\rm h} = 0.8\,{\rm pc}$ cluster, Fig. 8.14 i.e. most stars in the Galactic field stem from clusters dynamically similar to this one), provided the birth (or primordial) distribution functions for $\log P, e, q$ are

$$f_{\log P,{\rm birth}} = \eta\,\frac{\log P - \log P_{\rm min}}{\delta + (\log P - \log P_{\rm min})^2}. \tag{8.164}$$

This distribution function has a generating function (Sect. 8.2.3)

$$\log P(X) = \left[\delta\,\left(e^{\frac{2\,X}{\eta}} - 1\right)\right]^{\frac{1}{2}} + \log P_{\rm min}. \tag{8.165}$$

The solution obtained by Kroupa (1995d) has

$$\eta = 2.5, \quad \delta = 45, \quad \log P_{\rm min} = 1, \tag{8.166}$$

so that $\log P_{\rm max} = 8.43$ since $\int_{\log P_{\rm min}}^{\log P_{\rm max}} f_{\log P}\,{\rm d}\log P = f_{\rm tot} = 1$ is a requirement for stars at birth. Intriguingly, similar distributions can be arrived at semi-empirically if we assume isolated formation of binary stars in a turbulent molecular cloud (Fisher 2004).

The birth-eccentricity distribution is thermal (8.154) while the birth mass-ratio distribution is generated from random pairing from the canonical IMF. However, in order to reproduce (1) the observed data in the eccentricity–period diagram, (2) the observed eccentricity distribution and (3) the observed mass-ratio distribution for short-period ($\log P \leq 3$) systems, a correlation of the parameters needs to be introduced through eigenevolution. Eigenevolution is the sum of all dissipative physical processes that transfer mass, energy and angular momentum between the companions when they are still very young and accreting.

A formulation that is quite successful in reproducing the overall observed correlations between $\log P, e, q$ for short-period systems has been derived from tidal circularisation theory (Kroupa 1995d). The most effective orbital dissipation occurs when the binary is at periastron,

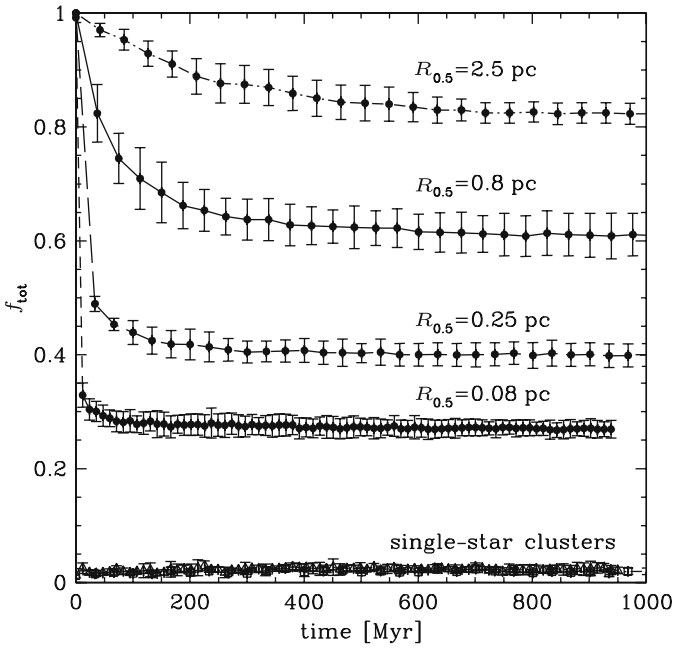

Fig. 8.14. Evolution of $f_{\rm tot}$, the total binary fraction for stellar mass $0.1 \leq m_i/M_\odot \leq 1.1$, $i = 1, 2$ with time for the four star-cluster models initially with $N = 200$ binaries computed by Kroupa (1995c) in the search for the existence of an $\Omega^{r_{\rm h},N}$. The initial half-mass radius of the clusters is denoted in this text as $r_{\rm h}$. Note that the $r_{\rm h} = 0.8\,{\rm pc}$ cluster yields the correct $f_{\rm tot} \approx 0.5$ for the Galactic field. The period-distribution function and the mass-ratio distribution function that emerge from this cluster also fit the observed Galactic-field distribution. Some binary stars form by three-body encounters in clusters that initially consist only of single stars and the proportion of such binaries is shown for the single-star clusters (with initially $N = 400$ stars). Such dynamically formed binaries are very rare and so $f_{\rm tot}$ remains negligible

$$r_{\rm peri} = (1-e)\, P_{\rm yr}^{\frac{2}{3}}\, (m_1+m_2)^{\frac{1}{3}}\,, \tag{8.167}$$

where $P_{\rm yr} = P/365.25$ is the period in years. Let the binary be born with eccentricity $e_{\rm birth}$, then the system evolves approximately, according to (Goldman & Mazeh 1994), as

$$\frac{1}{e}\,\frac{{\rm d}e}{{\rm d}t} = -\rho' \Rightarrow \log_{10} e_{\rm in} = -\rho + \log_{10} e_{\rm birth}, \tag{8.168}$$

where $1/\rho'$ is the tidal circularisation time-scale, $e_{\rm in}$ is the initial eccentricity and

$$\rho = \int_0^{\Delta t} \rho'\,{\rm d}t = \left(\frac{\lambda\, R_\odot}{r_{\rm peri}}\right)^{\chi}, \tag{8.169}$$

where $R_\odot$ is the Solar radius in AU, λ, χ are tidal circularisation parameters and $r_{\rm peri}$ (in AU) is assumed to be constant because the dissipational

force only acts tangentially at periastron. Note that a large λ implies that tidal dissipation is effective for large separations of the companions (e.g. they are puffed-up pre-mainsequence structures) and a small χ implies the dissipation is soft, i.e. weakly varying with the separation of the companions. In this integral, $\Delta t \leq 10^5\,\mathrm{yr}$ is the time-scale within which pre-mainsequence eigenevolution completes. The initial period becomes, from (8.167),

$$P_{\rm in} = P_{\rm birth}\left(\frac{m_{\rm tot,birth}}{m_{\rm tot,in}}\right)^{\frac{1}{2}}\left(\frac{1-e_{\rm birth}}{1-e_{\rm in}}\right)^{\frac{3}{2}}. \tag{8.170}$$

Kroupa (1995d) assumed the companions merge if $a_{\rm in} \leq 10\,R_\odot$ in which case $m_1 + m_2 \rightarrow m$.

In order to reproduce the observed mass-ratio distribution, given random pairing at birth and to also reproduce the fact that short-period binaries tend to have similar-mass companions, Kroupa (1995d) implemented a feeding algorithm, according to which the secondary star accretes high angular momentum gas from the circumbinary accretion disc or material, so that its mass increases while the primary mass remains constant. Thus, after generating the two birth masses randomly from the canonical IMF, the initial mass-ratio is

$$q_{\rm in} = q_{\rm birth} + (1 - q_{\rm birth})\,\rho^*, \tag{8.171}$$

where

$$\rho^* = \begin{cases} \rho & : \quad \rho \leq 1, \\ 1 & : \quad \rho > 1. \end{cases} \tag{8.172}$$

The above is a very simple algorithm which nevertheless reproduces the essence of orbital dissipation so that the correlations between the orbital parameters for short-period systems are well accounted for. The best parameters for the evolution

$$\text{birth} \;\rightarrow\; \text{initial} : \lambda = 28\,,\; \chi = 0.75. \tag{8.173}$$

Figure 8.15 shows an example of the overall model in terms of the eccentricity–period diagram. Figures 8.16 and 8.17 demonstrate that it nicely accounts for the period and mass-ratio distribution data, respectively.

Note that initial distributions are derived from birth distributions. This is to be understood in terms of these initial distributions being the initialisation of N-body experiments, while the birth distributions are more related to the theoretical distribution of orbital parameters before dissipational and accretion processes have had a major effect on them. The birth distributions are, however, mostly an algorithmic concept. Once the N-body integration is finished, e.g. when the cluster is dissolved, the remaining binaries can be evolved to the main-sequence distributions by applying the same eigenevolution algorithm above, but with parameters

$$\text{after Nbody integration} \;\rightarrow\; \text{mainsequence} : \lambda_{\rm ms} = 24.7\,,\; \chi_{\rm ms} = 8. \tag{8.174}$$

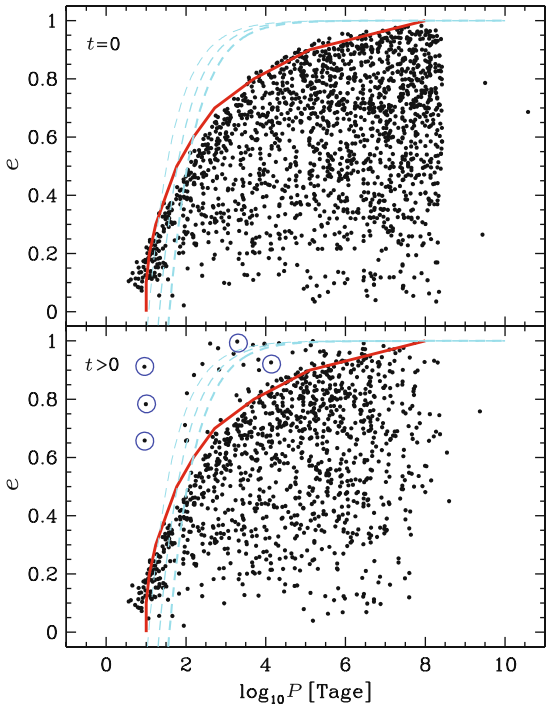

Fig. 8.15. Eccentricity–period after pre-mainsequence eigenevolution ($\lambda = 28, \chi = 0.75$) at $t = 0$ (*upper panel*) for masses $0.1 \leq m_i/M_\odot \leq 1.1$ and after cluster disintegration (*bottom panel*; note: *Tage* means days). Systems with semi-major axes, $a \leq 10\,R_\odot$ have been merged. Binaries are only observed to have $e, \log P$ below the envelope described by Duquennoy & Mayor (1991). The region above is forbidden because pre-mainsequence dissipation depopulates it within 10^5 yr. However, dynamical encounters can repopulate the eigenevolution region so that systems with forbidden parameters can be found but are short-lived. Some of these are indicated as *open circles*. Eigenevolution (tidal circularisation) on the main sequence with $\lambda_{\rm ms} = 24.7$ and $\chi_{\rm ms} = 8$, applied to the data in the *lower panel*, depopulates the eigenevolution region and circularises all orbits with periods less than about 12 d. The *dashed lines* are constant periastron distances (8.167) for $r_{\rm peri} = \lambda\,R_\odot$ and $m_{\rm sys} = 2.2, 0.64$ and $0.2\,M_\odot$ (in increasing thickness). Horizontal and vertical cuts through this diagram produce eccentricity and period distribution functions, and mass-ratio distributions that fit the observations (Kroupa 1995d)

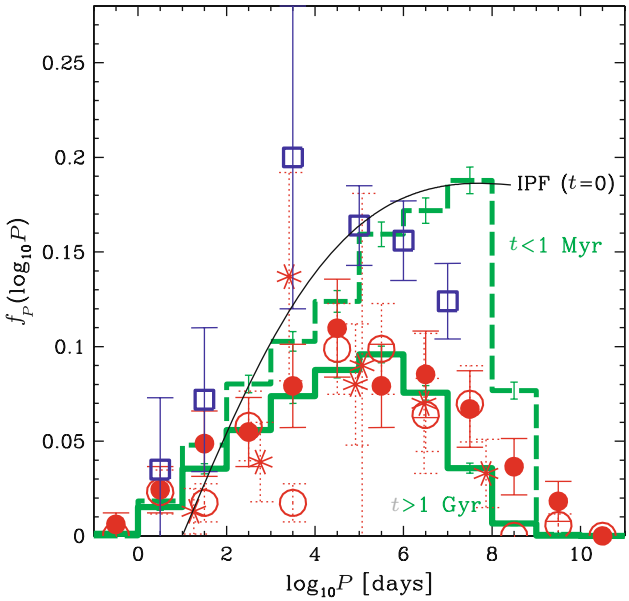

Fig. 8.16. The period distribution functions (IPF: (8.164) with (8.166) and for stellar masses $0.1 \leq m_i/M_\odot \leq 1.1$). The *dashed histogram* is derived from IPF with the eigenevolution and feeding algorithms and represents the binary population at an age of about 10^5 yr. The solid histogram follows from the dashed one after evolving a cluster with initially $N = 200$ binaries and $r_{\rm h} = 0.8$ pc. The agreement of the dashed histogram with the observational pre-mainsequence data (as in Fig. 8.13) and of the *solid histogram* with the observed main sequence (Galactic field) data (also as in Fig. 8.13) is good. A full model of the Galactic field late-type binary population has been arrived at which unifies all available, but apparently discordant, observational data (see also Figs. 8.14, 8.15, and 8.17), nothing that the longest-period TTauri binary population is expected to show some disruption

The need for $\lambda_{\rm ms} < \lambda$ and $\chi_{\rm ms} > \chi$ to ensure, for example, the tidal circularisation period of 12 days for G dwarfs (Duquennoy & Mayor 1991) is nicely qualitatively consistent with the shrinking of pre-mainsequence stars and the emergence of radiative cores that essentially reduce the coupling between the stellar surface, where the dissipational forces are most effective, and the centre of the star. The reader is also directed to Mardling & Aarseth (2001) who introduce a model of tidal circularisation to the N-body code. Finally, the above work and the application to the ONC and Pleiades (Kroupa, Aarseth & Hurley 2001) suggests the following hypothesis:

INITIAL BINARY UNIVERSALITY HYPOTHESIS: the initial period (8.166), eccentricity (8.154) and mass-ratio (random pairing from canonical IMF) distributions constitute the parent distribution of all late-type stellar populations.

Can this hypothesis be rejected?

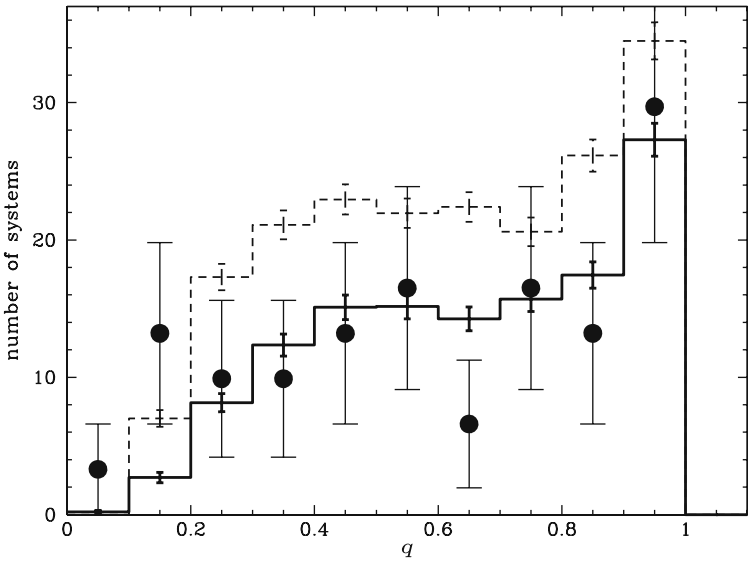

Fig. 8.17. The mass-ratio distribution for stars with $0.1 \leq m/M_{\odot} \leq 1.1$ is the solid histogram, whereas the initial mass-ratio distribution (random pairing from the canonical IMF, after eigenevolution and feeding, at an age of about 10^5 yr) is shown as the *dashed histogram*. The solid histogram follows from the dashed one after evolving a cluster with initially $N = 200$ binaries and $r_{\rm h} = 0.8$ pc. The observational data (*solid dots*, Reid & Gizis 1997) have been obtained after removing WD companions and scaling to the model. This solar neighbourhood 8 pc sample is not complete and may be biased towards $q = 1$ systems (Henry et al. 1997). Nevertheless, the agreement between model (*solid histogram*) and the data is striking. A full model of the Galactic field binary population has been arrived at which unifies all available, but apparently discordant, observational data (see also Figs. 8.14, 8.15, 8.16)

8.4.3 The Initial Binary Population – Massive Stars

The above semi-empirical distribution functions have been formulated for late-type stars (primary mass $m_1 \leq 1\,M_{\odot}$). It is for these that we have the best observations. It is not clear yet if they are also applicable to massive binaries.

An approach taken by Clarke & Pringle (1992) is to constrain the binary properties of OB stars by assuming that runaway OB stars are ejected from star-forming regions. About 10–25% of all O stars are runaway stars, while about 2% of B stars are runaways. This approach leads to the result that massive stars must form in small-N groups of binaries that are biased towards unit mass ratio. This is a potentially powerful approach but it can only constrain the properties of OB binaries when they are ejected. This occurs after many dynamical encounters in the cluster core, which typically lead to the mass-ratio evolving towards unity as the binaries harden. The true birth

properties of massive binaries therefore remain obscure and we need to resort to N-body experiments to test various hypotheses given the observations. One such hypothesis could be, for example, to assume massive stars form in binaries with birth pairing properties as for low-mass stars (Sect. 8.4.2), i.e. most massive primaries would have a low-mass companion and to investigate if this hypothesis leads to the observed number of runaway massive stars through dynamical mass segregation to the cluster core and partner exchanges through dynamical encounters there between the massive stars.

Apart from the fraction of runaway stars, direct surveys have lead to some insights into the binary properties of the observed massive stars. Thus, for example, Baines et al. (2006) report a very high ($f \approx 0.7 \pm 0.1$) binary fraction among Herbig Ae/Be stars with a binary fraction that increases with increasing primary mass. Furthermore, they find that the circumbinary discs and the binary orbits appear to be coplanar. This supports a fragmentation origin rather than collisions or capture as the origin of massive binaries. Most O stars are believed to exist as short-period binaries with $q \approx 1$ (García & Mermilliod 2001), at least in rich clusters. On the other hand, small-q appear to be favoured in smaller clusters such as the ONC, consistent with random pairing (Preibisch et al. 1999). Kouwenhoven et al. (2005) report that the A and late-type B binaries in the Scorpius OB2 association have a mass-ratio distribution inconsistent with random pairing. The lower limit on the binary fraction is 0.52, while Kouwenhoven et al. (2007) update this to a binary fraction of 72%. They also find that the semi-major axis distribution contains too many close pairs compared to a Duquennoy & Mayor (1991) log-normal distribution. These are important constraints but, again, they are derived for binaries in an OB association, which is an expanded version of a dense star cluster (Sect. 8.1.2) and therefore hosts a dynamically evolved population.

Given the above results, perhaps the massive binaries in the ONC represent the primordial population, whereas in rich clusters and in OB associations the population has already evolved dynamically through hardening and companion exchanges (f_q rising towards $q = 1$). This possibility needs to be investigated with high-precision N-body computations of young star clusters. The first simplest hypothesis to test would be to extend the pairing rules of Sect. 8.4.2 to all stellar masses, perform many (because of the small number of massive stars) N-body renditions of the same basic pre-gas expulsion cluster and to quantify the properties of the emerging stellar population at various dynamical times (Kroupa 2001).

Another approach would be to constrain a and m_2 for a given $m_1 \geq 5\,M_\odot$ so that

$$E_{\rm bin} \approx E_{\rm k} \tag{8.175}$$

(8.141). Or we can test the initial massive-star population given by

$$a < \frac{r_c}{N_{\rm OB}^{\frac{1}{3}}}, \tag{8.176}$$

which follows from stating that the density of a massive binary, $2 \times 3/(a^3\, 4\,\pi)$, be larger than the cluster-core density, $N_{\rm OB}\, 3/(r_c^3\, 4\,\pi)$. So far, none of these possibilities have been tested, apart from the Initial Binary Universality Hypothesis (p. 250) extension to massive stars (Kroupa 2001).

8.5 Summary

The above material gives an outline of how to set up an initial, birth or primordial stellar population so that it resembles observed stellar populations. In Sect. 8.4.2 a subtle differentiation was made between initial and birth populations, in the sense that an initial population is derived from a birth population through processes that act too rapidly to be treated by an N-body integration.

An N-body stellar system is generated for numerical experiments by specifying its 3D structure and velocity field (Sect. 8.2), the mass distribution of its population (Sect. 8.3) and the properties of its binary population (Sect. 8.4). Given the distribution functions discussed here and the existing numerical results based on these, it is surprising how universal the stellar and binary population turns out to be at birth. A dependence of the IMF or the birth binary properties on the physical properties of star-forming clouds cannot be detected conclusively. In fact, the theoretical proposition that there should be a dependency can be rejected, except possibly (i) in the extreme tidal field environment at the Galactic centre, or (ii) in the extreme protostellar density environment of ultra-compact dwarf galaxies, or (iii) for extreme physical environments (pp. 230–231).

The unified picture that has emerged concerning the origin of stellar populations is that stars form according to a universal IMF and mostly in binary systems. They form in very dense clusters, which expel their residual gas and rapidly evolve to T- or OB-associations. If the latter are massive enough, the dense embedded clusters evolve to populous OB associations that may be expanding rapidly and contain cluster remnants, which may reach globular cluster masses and beyond, in intense star-bursts. This unified picture explains naturally the high infant weight loss and infant mortality of clusters, the binary properties of field stars, possibly thick discs of galaxies and the existence of population II stellar halos around galaxies that have old globular cluster systems.

Many open questions remain. Why is the star-formation product so universal within current constraints? How are massive stars distributed in binaries? Do they form at the centres of their clusters? Why is the cluster mass of about $10^6\, M_\odot$ special? And which star cluster population is a full solution to the inverse dynamical population synthesis problem? (p. 246). Many more observations are required. These must not only be of topical high red-shift star-burst systems but also of the more mundane low red-shift, and preferably local, star-forming objects, globular and open star clusters.

Acknowledgement

It is a pleasure to thank Sverre Aarseth for organising a splendid and much to be remembered Cambridge N-body school in the Summer of 2006, and also Christopher Tout for editing and proof-reading this chapter. I am indebted to Jan Pflamm-Altenburg who read parts of this manuscript carefully, to Andreas Küpper for producing the Plummer vs King model comparisons and for carefully reading the whole text, and to Joerg Dabringhausen, who supplied figures from his work.

References

Aarseth S. J. 2003, Gravitational N-Body Simulations. Cambridge Univ. Press, Cambridge 202
Aarseth S. J., Hénon M., Wielen R., 1974, A&A, 37, 183 216
Adams F. C., 2000, ApJ, 542, 964 197, 221
Adams F. C., Fatuzzo M., 1996, ApJ, 464, 256 234
Adams F. C., Laughlin G., 1996, ApJ, 468, 586 234
Adams F. C., Myers P. C., 2001, ApJ, 553, 744 183
Allen L., Megeath S. T., Gutermuth R., Myers P. C., et al., 2007, in Reipurth B., Jewitt D., Keil K., eds, Protostars and Planets V. University Arizona Press, Tucson, p. 361 186
Alves J., Lombardi M., Lada C. J., 2007, A&A, 462, L17 235
Baines D., Oudmaijer R. D., Porter J. M., Pozzo M., 2006, MNRAS, 367, 737 252
Ballero S., Kroupa P., Matteucci F., 2007, MNRAS, 467, 117 230
Baraffe I., Chabrier G., Allard F., Hauschildt P. H., 2002, A&A, 382, 563 227
Bastian N., Goodwin S. P., 2006, MNRAS, 369, L9 193, 195, 221
Baumgardt H., 1998, A&A, 330, 480 197
Baumgardt H., Kroupa P., 2007, MNRAS, 380, 1589 227
Baumgardt H., Kroupa P., de Marchi G., 2008, MNRAS, in press (astroph/0806.0622) 222
Baumgardt H., Kroupa P., Parmentier G., 2008, MNRAS, 384, 1231 195, 198, 220, 221
Baumgardt H., Makino J., 2003, MNRAS, 340, 227 194, 228
Binney J., Tremaine S., 1987, Galactic Dynamics. Princeton Univ. Press, Princeton, NJ 182, 183, 202, 203, 209, 211, 213
Boily C. M., Kroupa P., 2003, MNRAS, 338, 673 193
Boily C. M., Kroupa P., Peñarrubia-Garrido J., 2001, New Astron., 6, 27 218
Boily C. M., Lançon A., Deiters S., Heggie D. C., 2005, ApJ, 620, L27 193
Bonnell I. A., Bate M. R., Vine S. G., 2003, MNRAS, 343, 413 188
Bonnell I. A., Larson R. B., Zinnecker H., 2007, in Reipurth B., Jewitt D., Keil K., eds, Protostars and Planets V. University Arizona Press, Tucson, p. 149 184, 222, 227, 234
Brook C. B., Kawata D., Scannapieco E., Martel H., Gibson B. K., 2007, ApJ, 661, 10 231
Casuso E., Beckman J. E., 2007, ApJ, 656, 897 234
Chabrier G., 2003, PASP, 115, 763 222, 224, 225, 236, 237
Clark P. C., Bonnell I. A., Zinnecker H., Bate M. R., 2005, MNRAS, 359, 809 195

Clarke C. J., Bonnell I. A., Hillenbrand L. A., 2000, in Mannings V., Boss A. P., Russell S. S., eds, Protostars and Planets IV. University Arizona Press, Tucson, p. 151 184
Clarke C. J., Pringle J. E., 1992, MNRAS, 255, 423 188, 251
Dabringhausen J., Hilker M., Kroupa P., 2008, MNRAS, 386, 864 199, 200, 201, 237
Dabringhausen J., Kroupa P., Baumgardt, H., 2008, MNRAS, submitted 230
Dale J. E., Bonnell I. A., Clarke C. J., Bate M. R., 2005, MNRAS, 358, 291 192
Dale J. E., Ercolano B., Clarke C. J., 2007, MNRAS, 1056 184
de Grijs R., Parmentier G., 2007, Chinese J. Astron. Astrophys., 7, 155 193, 195
de la Fuente Marcos R., 1997, A&A, 322, 764 199
de la Fuente Marcos R., 1998, A&A, 333, L27 199
Delfosse X., Forveille T., Ségransan D., Beuzit J.-L., Udry S., Perrier C., Mayor M., 2000, A&A, 364, 217 223
Duchêne G., 1999, A&A, 341, 547 242, 243
Duquennoy A., Mayor M., 1991, A&A, 248, 485 242, 243, 244, 249, 250, 252
Eislöffel J., Steinacker J., 2008, in The Formation of Low-Mass-Protostars and Proto-Brown Dwarfs. (in press, astro-ph/0701525), ASP conf. series Vol. 384, p. 359, ed: Gerard von Belle 232
Elmegreen B. G., 1983, MNRAS, 203, 1011 187, 194
Elmegreen B. G., 1997, ApJ, 486, 944 222, 228
Elmegreen B. G., 1999, ApJ, 515, 323 228
Elmegreen B. G., 2000, ApJ, 530, 277 187, 189
Elmegreen B. G., 2004, MNRAS, 354, 367 234
Elmegreen B. G., 2006, ApJ, 648, 572
Elmegreen B. G., 2007, ApJ, 668, 1064 187, 189, 222
Elmegreen D. M., Elmegreen B. G., Sheets C. M., 2004, ApJ, 603, 74 196
Fellhauer M., Kroupa P., 2005, ApJ, 630, 879 184, 193, 221
Fellhauer M., Kroupa P., Evans N. W., 2006, MNRAS, 372, 338 189, 228
Feltzing S., Gilmore G., Wyse R. F. G., 1999, ApJ, 516, L17 230
Figer D. F., 2005, Nature, 434, 192 187
Fischer D. A., Marcy, G. W., 1992, ApJ, 396, 178 242, 243, 244
Fisher R. T., 2004, ApJ, 600, 769 246
Fleck J.-J., Boily C. M., Lançon A., Deiters S., 2006, MNRAS, 369, 1392 193
García B., Mermilliod J. C., 2001, A&A, 368, 122 252
Goldman I., Mazeh T., 1994, ApJ, 429, 362 247
Goodwin S. P., 1997a, MNRAS, 284, 785 192, 220
Goodwin S. P., 1997b, MNRAS, 286, 669 192, 220
Goodwin S. P., 1998, MNRAS, 294, 47 192, 220
Goodwin S. P., Bastian N., 2006, MNRAS, 373, 752 193
Goodwin S. P., Kroupa, P., 2005, A&A, 439, 565 199, 236, 243
Goodwin S. P., Kroupa P., Goodman, A., Burkert, A., 2007, in Reipurth B., Jewitt D., Keil K., eds, Protostars and Planets V. University Arizona Press, Tucson, p. 133 242
Goodwin S. P., Nutter D., Kroupa P., Ward-Thompson D., Whitworth A. P., 2008, A&A, 477, 823 235
Goodwin S. P., Whitworth A., 2007, A&A, 466, 943 232
Gouliermis D., Keller S. C., Kontizas M., Kontizas E., Bellas-Velidis I., 2004, A&A, 416, 137 184
Gouliermis D. A., Quanz S. P., Henning T., 2007, ApJ, 665, 306 195

Gradshteyn I. S., Ryzhik I. M., 1980, Table of Integrals, Series, and Products. Academic Press, New York 208
Grether D., Lineweaver C. H., 2006, ApJ, 640, 1051 232
Grillmair C. J., et al., 1998, AJ, 115, 144 230
Gutermuth R. A., Megeath S. T., Pipher J. L., Williams J. P., Allen L. E., Myers P. C., Raines S. N., 2005, ApJ, 632, 397 186
Hartmann L., 2003, ApJ, 585, 398 187, 189
Heggie D. C., 1975, MNRAS, 173, 729 240
Heggie D., Hut P., 2003, The Gravitational Million-Body Problem. Cambridge Univ. Press, Cambridge 194, 198, 202, 206
Henry T. J., Ianna P. A., Kirkpatrick J. D., Jahreiss H., 1997, AJ, 114, 388 251
Hillenbrand L. A., Hartmann L. W., 1998, ApJ, 492, 540 193
Hills J. G., 1975, AJ, 80, 809 240
Hoversten E. A., Glazebrook K., 2008 ApJ, 675, 163 234
Hurley J. R., Pols O. R., Aarseth S. J., Tout C. A., 2005, MNRAS, 363, 293 202
Hut P., Mineshige S., Heggie D. C., Makino J., 2007, Progress Theor. Phys., 118, 187 202
Jenkins A., 1992, MNRAS, 257, 620 196
Kennicutt R. C., 1983, ApJ, 272, 54 225
Kim S. S., Figer D. F., Kudritzki R. P., Najarro F., 2006, ApJ, 653, L113 231, 234
Kim E., Yoon I., Lee H. M., Spurzem R., 2008, MNRAS, 383, 2 219
King I. R., 1962, AJ, 67, 471 212
King I. R., 1966, AJ, 71, 64 212
Klessen R. S., Spaans M., Jappsen A.-K., 2007, MNRAS, 374, L29 231, 234
Koen C., 2006, MNRAS, 365, 590 187
Koeppen J., Weidner C., Kroupa P., 2007, MNRAS, 375, 673 194, 234
Kouwenhoven M. B. N., Brown A. G. A., Portegies Zwart S. F., Kaper L., 2007, A&A, 474, 77 252
Kouwenhoven M. B. N., Brown A. G. A., Zinnecker H., Kaper L., Portegies Zwart S. F., 2005, A&A, 430, 137 252
Kroupa P., 1995a, ApJ, 453, 350 224
Kroupa P., 1995b, ApJ, 453, 358 224
Kroupa P., 1995c, MNRAS, 277, 1491 240, 244, 246, 247
Kroupa P., 1995d, MNRAS, 277, 1507 194, 240, 244, 246, 248, 249
Kroupa P., 1998, MNRAS, 300, 200 201
Kroupa P., 2000, New Astron., 4, 615
Kroupa P., 2001, MNRAS, 322, 231 228, 229, 252, 253
Kroupa P., 2002a, Science, 295, 82 222
Kroupa P., 2002b, MNRAS, 330, 707 195, 196, 223, 224, 228
Kroupa P., 2005, in Turon C., O'Flaherty K. S., Perryman M. A. C., eds, Proc. Gaia Symp. Vol. 576, The Three-Dimensional Universe with Gaia. ESA Publications Division, Noordwijk, p. 629 (astro-ph/0412069) 186, 192, 193, 196, 220
Kroupa P., 2007a, in Valls-Gabaud D., Chavez M., eds, Resolved Stellar Populations. (in press, astro-ph/0703124) 222, 226, 237
Kroupa P., 2007b, in Israelian G., Meynet G., eds, The Metal Rich Universe. Cambridge Univ. Press, Cambridge (astro-ph/0703282) 222
Kroupa P., Aarseth S. J., Hurley J., 2001, MNRAS, 321, 699 191, 192, 193, 194, 195, 197, 221
Kroupa P., Boily C. M., 2002, MNRAS, 336, 1188 195, 197, 198, 227
Kroupa P., Bouvier J., Duchêne G., Moraux E., 2003, MNRAS, 346, 354 225, 232

Kroupa P., Burkert A., 2001, ApJ, 555, 945 245
Kroupa P., Gilmore G., Tout C. A., 1991, MNRAS, 251, 293 223
Kroupa P., Petr M. G., McCaughrean M. J., 1999, New Astron., 4, 495 240
Kroupa P., Tout C. A., Gilmore G., 1993, MNRAS, 262, 545 223, 226, 237
Kroupa P., Weidner C., 2003, ApJ, 598, 1076 233, 237
Kroupa P., Weidner C., 2005, in Cesaroni, R., Felli M., Churchwell E., Walmsley M., eds, Proc. IAU Symp. 227, Massive Star Birth: A Crossroads of Astrophysics. Cambridge Univ. Press, Cambridge, p. 423 187
Krumholz M. R., 2008, in Knapen J., Mahoney T., Vazdekis A., eds, Pathways Through an Eclectic Universe. (astro-ph/0706.3702) ASP conference series, vol. 390 235
Krumholz M. R., Tan J. C., 2007 ApJ, 654, 304 187, 189
Lada C. J., Lada E. A., 2003, ARA&A, 41, 57 185, 197
Lada C. J., Margulis M., Dearborn D., 1984, ApJ, 285, 141 192, 220
Larson R. B., 1998, MNRAS, 301, 569 231, 234
Lee H.-C., Gibson B. K., Flynn C., Kawata D., Beasley M. A., 2004, MNRAS, 353, 113 234
Li Y., Klessen R. S., Mac Low M.-M., 2003, ApJ, 592, 975 185
Mac Low M.-M., Klessen R. S., 2004, Rev. Mod. Phys., 76, 125 184
Maíz Apellániz J., Úbeda L., 2005, ApJ, 629, 873 222
Maíz Apellániz J., Walborn N. R., Morrell N. I., Niemela V. S., Nelan E. P., 2007, ApJ, 660, 1480 187
Maness H., et al., 2007, ApJ, 669, 1024 230
Mardling R. A., Aarseth S. J., 2001, MNRAS, 321, 398 250
Marks M., Kroupa P., Baumgardt H., 2008, MNRAS, 386, 2047 222
Martín E. L., Brandner W., Bouvier J., Luhman K. L., Stauffer J., Basri G., Zapatero Osorio M. R., Barrado y Navascués, D., 2000, ApJ, 543, 299 225, 236
Martins F., Schaerer D., Hillier D. J., 2005, A&A, 436, 1049 187
Massey P., 2003, ARA&A, 41, 15 222, 224, 225
Mayor M., Duquennoy A., Halbwachs J.-L., Mermilliod J.-C., 1992, in McAlister H. A., Hartkopf W. I., eds, ASP Conf. Ser. Vol. 32, Complementary Approaches to Double and Multiple Star Research. Astron. Soc. Pacific, San Francisco, p. 73 242, 244
McMillan S. L. W., Vesperini E., Portegies Zwart S. F., 2007, ApJ655, L45 184, 221
Metz M., Kroupa P., 2007, MNRAS, 376, 387 230
Meylan G., Heggie D. C., 1997, A&AR, 8, 1 194, 198
Mieske S., Kroupa P., 2008, ApJ, 677, 276 230
Moraux E., Bouvier J., Clarke C., 2004, in Combes F., Barret D., Contini T., Meynadier F., Pagani L., eds, SF2A-2004: Semaine de l'Astrophysique Francaise. EdP-Sciences, Conference Series, p. 251 225, 236
Motte F., Andre P., Neri R., 1998, A&A, 336, 150 235
Motte F., André P., Ward-Thompson D., Bontemps S., 2001, A&A, 372, L41 235
Murray S. D., Lin D. N. C., 1996, ApJ, 467, 728 234
Nutter D., Ward-Thompson D., 2007, MNRAS, 374, 1413 235
Odenkirchen M., et al., 2003, AJ, 126, 2385 199
Oey M. S., Clarke C. J., 2005, ApJ, 620, L43 187
Palla F., Randich S., Pavlenko Y. V., Flaccomio E., Pallavicini, R., 2007, ApJ, 659, L41 189
Palla F., Stahler S. W, 2000, ApJ, 540, 255 189
Pancino E., Galfo A., Ferraro F. R., Bellazzini M., 2007, ApJ, 661, L155 219

Parker R. J., Goodwin S. P., 2007, MNRAS, 380, 1271 185
Parmentier G., Gilmore G., 2005, MNRAS, 363, 326 197
Parmentier G., Gilmore G., 2007, MNRAS, 377, 352 195, 198
Parmentier G., Goodwin S., Kroupa P., Baumgardt H., 2008, ApJ, 678, 347 198
Pflamm-Altenburg J., Kroupa P., 2006, MNRAS, 373, 295 188, 227, 228, 237, 238
Pflamm-Altenburg J., Kroupa P., 2007, MNRAS, 375, 855 189, 228
Pflamm-Altenburg J., Kroupa P., 2008, MNRAS, submitted 190, 200
Pflamm-Altenburg J., Weidner C., Kroupa P., 2007, ApJ, 671, 1550 188, 194, 234
Piotto G., 2008, in Cassisi S., Salaris M., XXI Century Challenges for Stellar Evolution. Mem. d. Soc. Astron. It., Vol. 79/2 (arXiv:0801.3175) 190
Plummer H. C., 1911, MNRAS, 71, 460 205
Portegies Zwart S. F., McMillan S. L. W., Hut P., Makino J., 2001, MNRAS, 321, 199 197
Portegies Zwart S. F., McMillan S. L. W., Makino J., 2007, MNRAS, 374, 95 202
Portinari L., Sommer-Larsen J., Tantalo, R., 2004, MNRAS, 347, 691 225, 234
Preibisch T., Balega Y., Hofmann K., Weigelt G., Zinnecker H., 1999, New Astron., 4, 531 224, 252
Press W. H., Teukolsky S. A., Vetterling W. T., Flannery B. P., 1992, Numerical Recipes. Cambridge Univ. Press, Cambridge, 2nd ed 215, 218
Reid I. N., Gizis J. E., 1997, AJ, 113, 2246 251
Reid I. N., Gizis J. E., Hawley S. L., 2002, AJ, 124, 2721 224, 225
Reipurth B., Clarke C., 2001, AJ, 122, 432 232
Romano D., Chiappini C., Matteucci F., Tosi M., 2005, A&A, 430, 491 225, 234
Sacco G. G., Randich S., Franciosini E., Pallavicini R., Palla F., 2007, A&A, 462, L23 189
Salpeter E. E., 1955, ApJ, 121, 161 224
Scally A., Clarke C., 2002, MNRAS, 334, 156 184, 221
Scalo J. M., 1986, Fundamentals Cosmic. Phys., 11, 1 225, 226
Scalo J., 1998, in Gilmore G., Howell D., eds, ASP Conf. Ser. Vol. 142, The Stellar Initial Mass Function (38th Herstmonceux Conference). Astron. Soc. Pac., San Francisco, p. 201 228, 229
Shara M. M., Hurley J. R., 2002, ApJ, 571, 830 194
Spitzer L., 1987, Dynamical Evolution of Globular Clusters. Princeton Univ. Press, Princeton, NJ 183
Stamatellos D., Whitworth A. P., Bisbas T., Goodwin S., 2007, A&A, 475, 37 184
Šubr L., Kroupa P., Baumgardt H., 2008, MNRAS, 385, 1673 222
Testi L., Sargent A. I., Olmi L., Onello J. S., 2000, ApJ, 540, L53 184
Thies I., Kroupa P., 2007, ApJ, 671, 767 223, 232, 236, 238, 242
Tilley D. A., Pudritz R. E., 2007, MNRAS, 382, 73 184
Tinsley B. M., 1980, Fundamentals Cosmic. Phys., 5, 287 225
Tumlinson J., 2007, ApJ, 665, 1361 231
Tutukov A. V., 1978, A&A, 70, 57 192, 220
Vesperini E., 1998, MNRAS, 299, 1019 197
Vesperini E., 2001, MNRAS, 322, 247 197
Weidemann V., 1990, ARA&A, 28, 103 226
Weidemann V., 2000, A&A, 363, 647 226
Weidemann V., Jordan S., Iben I. J., Casertano S., 1992, AJ, 104, 1876 226
Weidner C., Kroupa, P., 2004, MNRAS, 348, 187 187
Weidner C., Kroupa P., 2005, ApJ, 625, 754 233

Weidner C., Kroupa P., 2006, MNRAS, 365, 1333 187, 188, 233
Weidner C., Kroupa P., Larsen S. S., 2004, MNRAS, 350, 1503 196, 198, 233
Weidner C., Kroupa P., Nürnberger D. E. A., Sterzik M. F., 2007, MNRAS, 376, 1879 193, 227
Woitas J., Leinert C., Koehler R., 2001, A&A, 376, 982 244
Wuchterl G., Tscharnuter W. M., 2003, A&A, 398, 1081 185, 227
Yasui C., Kobayashi N., Tokunaga A. T., Saito M., Tokoku C., 2008 (astro-ph/0801.0204) 230
Yasui C., Kobayashi N., Tokunaga A. T., Terada H., Saito M., 2006, ApJ, 649, 753 in Formation and Evolution of Galaxy Disks, ASP Conf. series, in press eds: J. G. Funes, E.M. Cossini (astro-ph/0801.0204) 230
Zhao H., 2004, MNRAS, 351, 891 189
Zinnecker H., 2003, in van der Hucht, K., Herrero A., Esteban C., eds, Proc. IAU Symp. 212, A Massive Star Odyssey: From Main Sequence to Supernova. Astron. Soc. Pacific, San Francisco, p. 80 224
Zinnecker H., Yorke H. W., 2007, ARA&A, 45, 481 184, 187, 222
Zoccali M., et al., 2006, A&A, 457, L1 230, 232
Zoccali M., Cassisi S., Frogel J. A., Gould A., Ortolani S., Renzini A., Rich R. M., Stephens A. W., 2000, ApJ, 530, 418 229, 230